Measurement Notes

Note 43

Loading Effect of Microfuse Sensors on Multipin Interfaces

September 18,1992

Walter L. Curtis
James P. Irwin
John R. Thomas

The Boeing Company
P.O. Box 3707
Seattle, WA 98125

Abstract

This paper presents measurements and calculations of the voltage reduction (loading) at a connector interface between a wire bundle and an electrical/electronic unit due to a class of resistive sensors. This class of sensors represents a microfuse threshold detector (TRW proprietary) proposed to be installed in shunt from each critical pin to ground in certain Mil Std (D38999 and Quad X) connectors. Section 2 formulates the mathematical model. Section 3 presents results of an experiment on a not-too-complex simulation. Section 4 reports results from EMPTAC #7 test at the Kirtland Air Force Base HPD simulator, where prototype microfuses were evaluated. Section 5 develops the model for computer calculation, shows results that correspond with data of previous sections, and presents calculations for other fuse resistances and other wire harness sizes.

Loading Effect of Microfuse Sensors on Multipin Interfaces

1.0 Introduction

In May of 1990 TRW [1,2] presented the idea of using integrated-circuit techniques to put microfuse sensors on a silicon wafer that could be inserted into a mated connector. The idea has promise for EMP testing of large electronic systems because, conceptually, fuse wafers might then be inserted in every LRU connector interface of importance in the system to provide a great deal more coverage of the system than could ever be obtained with conventional techniques. There were, however, serious technical concerns that needed resolution before acceptance of fuse wafers as a primary instrumentation technique. One of those concerns was the effect that using a large number of fuses might have on the voltages being measured. This report documents a study by Boeing to help evaluate that effect.

Additional background information is given in section 1.1, and a brief summary of results and a conclusion are presented in section 1.2. Section 2 gives a basic formulation of the problem for multi-terminal networks. Section 3 describes the results of laboratory measurements on a 50-wire cable, 10 meters long, with resistive type loads at each end to represent something typical of what might be found on a complex aircraft system. A detailed description of the test item and instrumentation are given along with a description of how the measurements were made. The data processing is described and test results are presented. Calibration procedures are detailed in Appendix A. Section 4 gives a brief description of high-level pulse tests on a full-size aircraft (EMPTAC) made at Kirtland AFB and gives a summary of the test results for fuse loading. Section 5 describes a theoretical model of the laboratory test configuration and shows computer calculated loading for many configurations not measured in the lab.

1.1 Background

Fuses are normally used to protect circuits from unexpected increases in current by melting and permanently changing their state. Thus, a fuse becomes a detector indicating that current through the fuse exceeded some threshold value. The application of this principle to EMP testing was studied by TRW in an IR&D program in the early 1980s [3]. That program was based on the use of small adapters that could be inserted at connector interfaces of interest to allow mounting of sensitive fuses with multipin IC sockets. A fuse could be connected in series to measure current or in shunt to ground to measure voltage to ground. In 1990 TRW [1,2] presented the idea of using integrated-circuit techniques to manufacture fuses on a silicon wafer thin enough (20 to 40 mils) to be inserted into a connector without an adapter. This wafer design could only put fuses in shunt, either between wires or from a wire to the connector case. TRW went a step farther and made the wafer more complex by making a network of different fuses for each pin to bin the voltage thresholds. The concept is excellent for EMP testing if the fuses have adequate sensitivity and the impedance of the fuses is large enough that placing them in shunt does not greatly change the circuit response. Fuse wafers might then be inserted in every LRU connector interface of importance in the system, and the system could be pulsed with simulated EMP at different angles of incidence and for different system configurations. This procedure would provide a great deal more coverage of the system than can ever be obtained with conventional techniques, but only relates to voltage, not current.

TRW proposed that the fuse wafer be used as part of a system level EMP test that was in the planning stage for testing at the Kirtland Air Force Base EMP test facilities. There were, however, serious technical concerns raised by the test working group (Northop, Boeing, Phillips Lab and other Air Force organizations) that needed resolution before acceptance of fuse wafers as a primary instrumentation

technique. TRW was funded to proceed with fuse development and to investigate the technical issues. At the same time, Boeing and Northrop conducted an independent evaluation of fuse performance. Specifically, Boeing studied the concern referred to as fuse loading, which is the effect (reduction of voltage) caused by the use of many fuses in shunt on multipin interfaces. Early in the program TRW proposed using fuses with a resistance of 5 to 10 ohms in a concept that the fuse wafer would then respond to the low-impedance, high-current circuits. The authors of this report objected because we knew that such low impedance in shunt on all wires would greatly change the circuit response and yield results not applicable to the system specification. As the fuse development continued, the achievable fuse resistance increased to about 100 ohms for prototype wafers used in a test on a modified 707-720B aircraft (EMPTAC) at the HPD facility, Kirtland AFB.

This report documents the results of the Boeing study and provides an independent evaluation of the applicability of the fuse wafer as an effective EMP test aid.

1.2 Summary and Conclusion

This study has shown that the application of shunt fuses, with a resistance on the order of 100 ohms, to a multiwire interface can load or greatly reduce the voltage at the interface. Laboratory measurements on a 10-meter test cable with 50 wires showed an average reduction at EMP frequencies of 19 dB. Calculations of the loading for 10-meter-long random-lay cables with 12 to 50 wires showed 13 dB to 21 dB average voltage reductions at EMP frequencies. Measurements from the EMPTAC # 7 tests showed average reduction of 5 dB for shielded cables and at least 13 dB for unshielded cables. Theoretically there is no limit to the amount of loading. However, the values found in this study are thought to be typical of the larger values expected on complex aircraft systems.

This large range of loading greatly limits the use of the fuse as a voltage indicator in an EMP test. If the fuse threshold or minimum threshold for a multi-step sensor is set low enough to detect the possible loaded case, then the sensor will also detect many cases that are not loaded (false indications—error of Type I). The usefulness of these indications (with Type I errors) depends on the system being tested. If the system has a large safety margin, such that there are few false indications, then the fuse wafer could be a useful adjunct to a system level EMP test. On the other hand, if the minimum fuse threshold is not set low enough, there will be high voltages that are missed—not effective when the purpose of the EMP test is to detect all the cases of voltage above a specification level.

The prototype fuse sensors used on the EMPTAC #7 tests had a minimum threshold of 1.5 volts. If these sensors were used in an EMP system level test and the result were that no fuses blew, then the only high-certainty conclusion is that the maximum voltage in the system is less than about 15 volts. This conclusion is not strong enough to provide verification of EMP hardness of the system being studied. Thus, fuse sensors like those used on EMPTAC #7 are not sensitive nor accurate enough to be a primary measurement tool for some System Level EMP tests. They could, however, be a useful adjunct to a test as a way of finding extreme values of voltage.

For the fuse sensor to be useful as a voltage sensing element in EMP testing it will need to have much greater resistance and somewhat better sensitivity.

2.0 The Effect of Shunt Resistance to Ground on Voltage at a Multiwire Interface

An ideal shunt fuse, one with high impedance and sufficient sensitivity, is a detector of peak voltage, one of the important norms used in EMP hardness varification. A general formulation of norms to multiwire interfaces is given by Baum [4]. Figure 2.1 shows a model for resistive loading due to application of TRW-type shunt fuses at the interface pins of an LRU connector. In the model an EMP source is connected to a passive load at pins that may be loaded with shunt microfuses. The Norton-equivalent source represents an entire system (e.g., a complete aircraft in a hypothetical EMP test) as seen at the connector pins of the LRU with the system excited by an EMP. The model consists of an admittance matrix and a current vector. In Figure 2.1 $\mathbf{Y}_L$ is the admittance matrix for the LRU connector to be measured by the shunt fuses. The term "fusing" as used here will mean connecting individual resistive fuse elements from each "fused" pin to ground at the connector interface. Installed fuses are also modeled by an equivalent admittance matrix. Because the TRW fuses are microcircuit elements

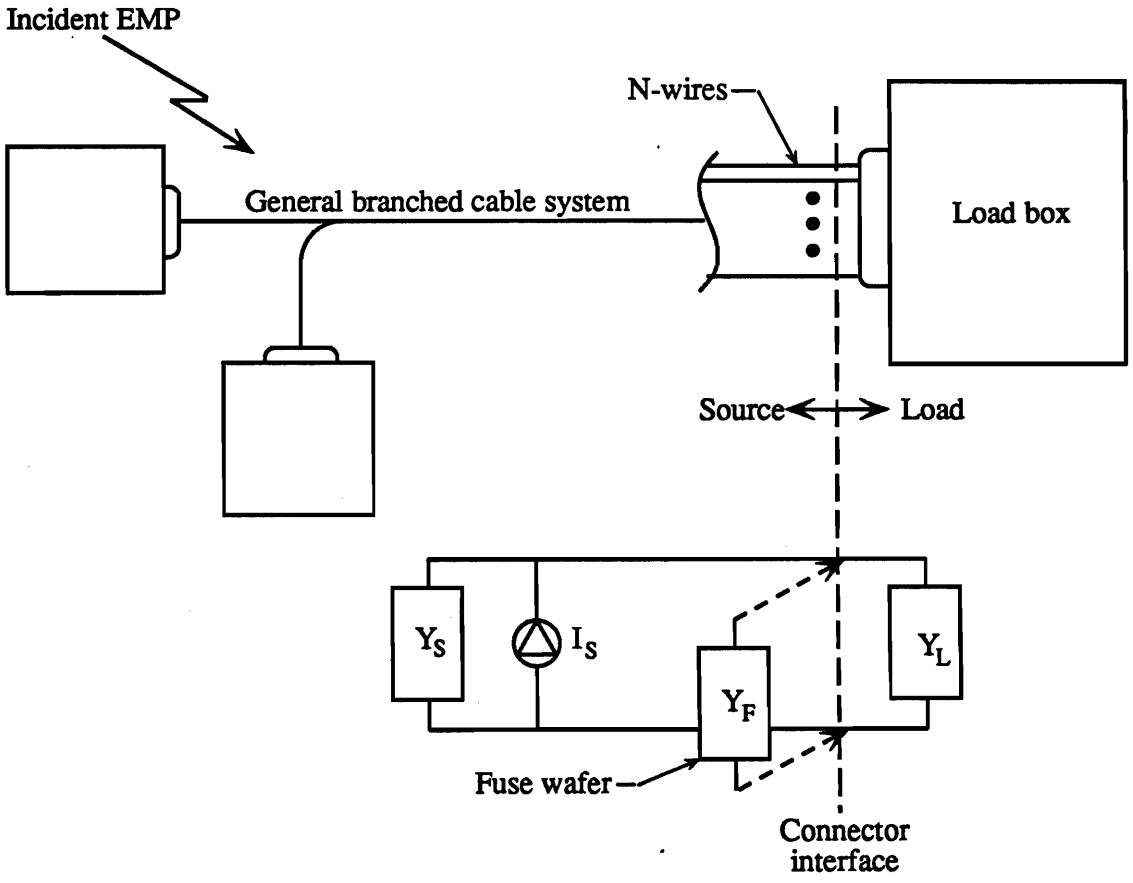

Figure 2.1. Schematic of general multiwire configuration and Norton equivalent circuit.

installed from pin to the immediately surrounding connector outer shield, they are modeled well as resistive circuit elements with no mutual coupling. Thus, the admittance matrix $\mathbf{Y}_F$ representing their load is diagonal.

In this model, voltage responses $\mathbf{V}_w$ and $\mathbf{V}_{w/o}$ at the LRU connector interface pins for configurations with and without fuses are related to the source current by

$$\mathbf{I}_S = (\mathbf{Y}_S + \mathbf{Y}_L)\mathbf{V}_{w/o} \tag{2.1}$$

$$\mathbf{I_S} = (\mathbf{Y_S} + \mathbf{Y_L} + \mathbf{Y_F})\mathbf{V_w} \tag{2.2}$$

where $\mathbf{I_S}$ is the EMP-induced source current vector, and the source admittance matrix $\mathbf{Y_s}$ represents the admittance looking into the wire harness.

From equations 2.1 and 2.2 the pin voltage responses for the fused and unfused configurations with the same source are related by

$$\mathbf{V_{w/o}} = \left(1 + \mathbf{Y_F}(\mathbf{Y_S} + \mathbf{Y_L})^{-1}\right)\mathbf{V_w} \tag{2.3}$$

Let $\mathbf{Z_{SL}} = (\mathbf{Y_S} + \mathbf{Y_L})^{-1}$ where $\mathbf{Z_{SL}}$ is an impedance matrix for the parallel combination of the source and load impedances. Then equation 2.3 can be reduced to

$$\mathbf{V_{w/o}} = (1 + \mathbf{Y_F}\mathbf{Z_{SL}})\mathbf{V_w} \tag{2.4}$$

Equation 2.4 is a complete matrix expression for voltage (i.e., N equations for N pins). The j^{th} equation gives the voltage on the j^{th} pin in the without-fuse condition as a linear function of pin voltages in the with-fuse condition. This linear function is the voltage (in the condition with fuses installed on whichever pins are chosen for fusing) on the j^{th} pin plus a sum of terms involving voltages on the pins that have a finite fuse resistance installed (i.e., pins that are fused).

Let the fuse resistance on pin i be denoted by R_{F_i} Then the j^{th} equation of the complete matrix relationship 2.4 may be written as

$$V_{w/o_j} = V_{w_j} + \sum_{i=1}^{N} \frac{Z_{SL_{ji}}}{R_{F_i}} V_{w_i} \tag{2.5}$$

where V_{w/o_j} is the voltage on pin j in the configuration without fuses, $Z_{SL_{ji}}$ is the i^{th} element in the j^{th} row of the source/load impedance matrix, and V_{w_j} and V_{w_i} are the voltages on the j^{th} and i^{th} pins after fusing. The N terms in the summation may be regarded as "correction" terms, one term for each fused pin.

2.1 Bounds for Voltage and Loading with Unblown Multiwire Fuses

In a "fuse" experiment, data is derived from the reading of resultant "blown" or "unblown" fuses. The data provide bounds or ranges for $|V_{w_i}|$ where i is contained in the set of pins with fuses. Equation 2.5 can be rewritten as

$$V_{w/o_j} = V_{w_j} A_{jj} + \sum_{\substack{i=1 \\ i \neq j}}^{N} \frac{Z_{SL_{ji}}}{R_{F_i}} V_{w_i} \tag{2.6}$$

where

$$A_{jj} = 1 + \frac{Z_{SL_{jj}}}{R_{F_j}}$$

If no fuse is installed on pin j, $R_{F_j} \to \infty$ and $A_{jj} = 1$.

A bound for V_{w/o_j} is obtained by taking the absolute value and applying the standard triangle inequality to equation 2.6, which results in

$$\left|V_{w/o_j}\right| \le \left|V_{w_j}\right|\left|A_{jj}\right| + \sum_{\substack{i=1 \\ i \neq j}}^{N} \frac{\left|Z_{SL_{ji}}\right|}{R_{F_i}}\left|V_{w_i}\right| \tag{2.7}$$

The summation extends only over fused pins.

In this study, loading from fuses is defined for an individual pin as the ratio of voltage with fuses to voltage without fuses. Thus, from equation 2.6 the loading ℓ_j on pin j due to fusing N interface pins is

$$\ell_j = \frac{V_{w_j}}{V_{w/o_j}} = \frac{1}{A_{jj} + \sum_{\substack{i=1 \\ i \neq j}}^{N} \frac{Z_{SL_{ji}} V_{w_i}}{R_{F_i} V_{w_j}}} \tag{2.8}$$

The lower bound L_j on loading is then

$$L_j = \frac{1}{\left|A_{jj}\right| + \sum_{\substack{i=1 \\ i \neq j}}^{N} \frac{\left|Z_{SL_{ji}}\right|}{R_{F_i}} \frac{\left|V_{w_i}\right|}{\left|V_{w_j}\right|}} \tag{2.9}$$

Since in a fuse experiment V_{w_j} can be less than V_{w_i}, the bound for loading does not have a lower limit distinct from zero for all possible values of $\mathbf{V}_w$. Therefore, this expression for loading in multiwire applications is only useful for special cases.

However, a finite bound does exist for the maximum possible voltage on a pin in an experiment where no fuses are blown. Equation 2.7 can be applied to a test situation where no fuses are observed to be blown. If all fuses are the same with voltage threshold V_F and resistance R_F, then the upper bound B_j for voltage on pin j in the without-fuse configuration for an experiment with no blown fuses is

$$B_j = V_F \left(|A_{jj}| + \frac{1}{R_F} \sum_{\substack{i=1 \\ i \neq j}}^{N} |Z_{SL_{ji}}| \right) \tag{2.10}$$

To produce a pin j voltage at the bound the following conditions must be met. In the with-fuse configuration, the voltage on all fused pins must be just below the threshold V_F and the source conditions must provide that each product $Z_{SL_{ji}} V_{w_i}$ be in phase with $V_{w_j} A_{jj}$.

In practice, the sensitivity of a fuse is rated by the peak current I_F at which it fuses. By Ohm's law, $V_F = I_F R_F$ and since

$$\left| 1 + \frac{Z_{SL_{ji}}}{R_F} \right| \leq 1 + \frac{|Z_{SL_{ji}}|}{R_F} \tag{2.11}$$

the upper bound can be restated as

$$B_j \leq I_F R_F \left(1 + \frac{1}{R_F} \sum_{i=1}^{N} |Z_{SL_{ji}}| \right) = \beta_j \tag{2.12}$$

where β_j is a less-precise bound for the largest voltage on pin j without fuses as determined from an experiment with no blown fuses. Also, the maximum of β_j relative to B_j is $\sqrt{2}B_j$ since the real part of $Z_{SL_{ji}}$ cannot be negative. Therefore, β_j is a realistic bound.

Figure 2.2 gives β_j as a function of $\sum_{i=1}^{N} |Z_{SL_{ji}}|$ for 10-mA fuses, the first being a 100-ohm device, the other being a 1000-ohm device. From $V_F = I_F R_F$ their voltage ratings are 1 volt and 10 volts, respectively. In the figure for low values of $\sum |Z_{SL_{ji}}|$ the bound for voltage on a pin j without fuses is very near to the rated fuse voltage. However, as $\sum |Z_{SL_{ji}}|$ increases, the bounds converge and increase linearly with $\sum |Z_{SL_{ji}}|$. At $\sum |Z_{SL_{ji}}| = 10^4$ even the 10-volt fuse has lost 20 dB of sensitivity with respect to the upper bound. Also, large values for $\sum |Z_{SL_{ji}}|$ are possible in a multiwire situation.

This result is demonstrated in Section 2.3 where this summation is shown to approach the number of wires times the cable characteristic impedance.

2.2 Voltage for Single-Wire Fusing

Until now we have viewed the loading effect issue from the multi-terminal perspective. However, there is a potential advantage to installing a single fuse in a multi-wire connector because a single-fuse application should not in general perturb the measurement as much as a multiple-fuse application. Certainly, the upper bound for a single-fuse measurement is less than or equal to the upper bound for a multiple-fuse measurement when the pin of interest is fused. From equation 2.5 the

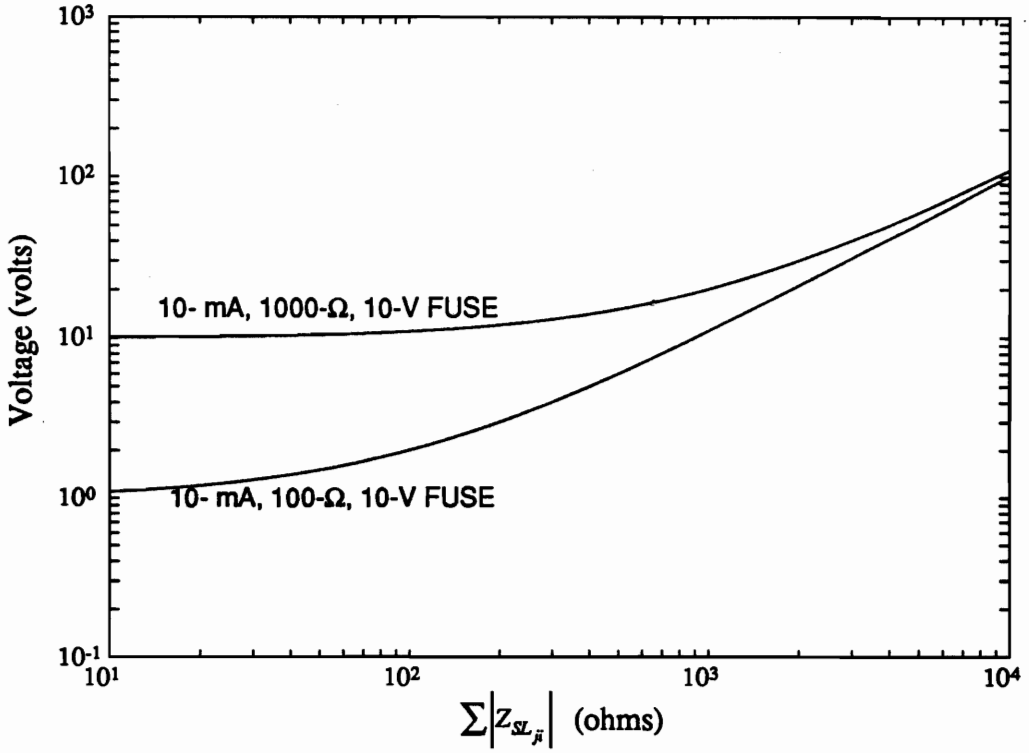

Figure 2.2. Upper-bound voltage without fuse from an experiment with no blown fuses.

voltage on this pin in the without-fuse condition as a function of the voltage with fuse installed is

$$V_{w/o_j} = V_{w_j}\left(1+\frac{Z_{SL_{ji}}}{R_{F_j}}\right) \tag{2.13}$$

Now, for pin j the largest possible voltage without fuse that would not blow a fuse occurs when the voltage with fuse installed is slightly less than the fuse threshold. Hence, the upper bound B_j^1 for voltage on a single fused pin with no other pins in the connector fused is the magnitude of equation 2.11 with $\left|V_{w_j}\right| = V_F$.

$$B_j^1 = V_F\left|1+\frac{Z_{SL_{ji}}}{R_F}\right| \tag{2.14}$$

Equation 2.14 can be used to simplify equation 2.10 as

$$B_j = B_j^1 + \frac{1}{R_F}V_F\sum_{\substack{i=1\\ i\neq j}}^{N}\left|Z_{SL_{ji}}\right| \tag{2.15}$$

Equation 2.15 expresses the multiple-fuse bound for voltage in terms of the single-fuse bound. In 2.15, for pin j, since B_j^1 is positive real, if a term exists in the j^{th} row of Z_{SL} for any other fused pin,

then B_j is greater than B_j^1. If such a term does not exist then B_j equals B_j^1. Therefore, B_j is greater than or equal to B_j^1. Also when the latter condition exists (when $\mathbf{Z}_{SL}$ has no off-diagonal terms), then by definition the solution at pin j is a single-terminal solution.

2.3 Example of Extreme Loading from Multiwire Fusing

The following example illustrates the potential severity of loading from multi-wire fusing. In this example, a basic interface configuration shown in Figure 2.3 is assumed. The configuration consists of a multi-wire cable source connected to an LRU at an interface with N terminals. To demonstrate severe loading from fusing, all N interface pins are fused. Also, all loads are assumed open circuit and the source cable bundle is unshielded and high above ground. For simplicity, the source cable length is infinite (i.e., a high-frequency example). In this configuration, with the LRU load open circuit ($\mathbf{Y}_L = 0$), $\mathbf{Z}_{SL}$ is merely the surge impedance looking into the source cable from the interface. With the cable high above ground all of the elements of $\mathbf{Z}_{SL}$ are comparable to the characteristic impedance of the source cable. This is shown below for a typical diagonal and off-diagonal term of $\mathbf{Z}_{SL}$.

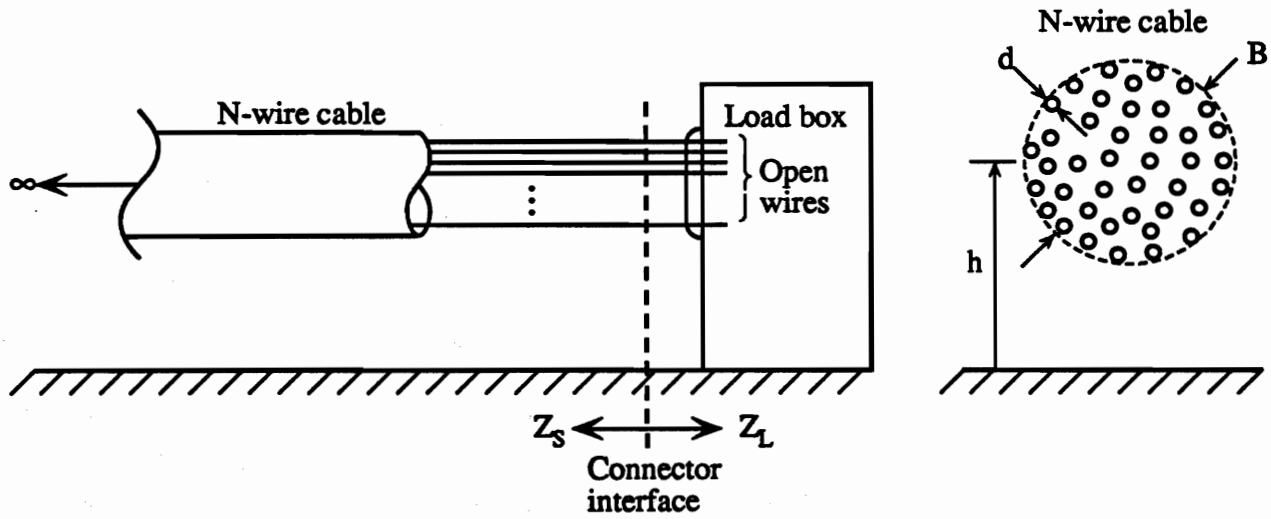

Figure 2.3. Notation for example of long unshielded cable above a ground plane.

For a cable of infinite length, the diagonal or self impedance $Z_{SL_{jj}}$ of a single wire in the source cable is approximately

$$Z_{SL_{jj}} \cong \frac{1}{2\pi}\sqrt{\frac{\mu}{\varepsilon}}\ln\left(\frac{4h}{d}\right) \tag{2.16}$$

where h is the average wire height in the cable and d is the wire diameter.

In terms of the source cable characteristic impedance Z_{SL_0}, $Z_{SL_{jj}}$ is

$$Z_{SL_{ij}} \cong \frac{1}{2\pi}\sqrt{\frac{\mu}{\varepsilon}}\ln\left(\frac{4h}{B}\right)+\frac{1}{2\pi}\sqrt{\frac{\mu}{\varepsilon}}\ln\left(\frac{B}{d}\right)=Z_{SL_0}+\varepsilon_1 \tag{2.17}$$

where $Z_{SL_0}=\frac{1}{2\pi}\sqrt{\frac{\mu}{\varepsilon}}\ln\left(\frac{4h}{B}\right)$, B is the bundle diameter and ε_1, is a difference term for the diagonal expression relative to Z_{SL_0}.

For large h, Z_{SL_0} dominates ε_1., i.e.:

$$\lim_{h\to\infty} Z_{SL_0} >> \varepsilon_1 \tag{2.18}$$

and $Z_{SL_{ij}}$ is approximated by Z_{SL_0}.

The off-diagonal impedances are estimated similarly, except that an average wire spacing is used instead of the cable diameter. The off-diagonal impedance $Z_{SL_{\mu}}$ can be approximated by

$$Z_{SL_{\mu}} \cong \frac{1}{2\pi}\sqrt{\frac{\mu}{\varepsilon}}\ln\left(\frac{2h}{S}\right)=\frac{1}{2\pi}\sqrt{\frac{\mu}{\varepsilon}}\ln\left(\frac{4h}{B}\right) \tag{2.19}$$

where S is the average wire spacing.

Again in terms of Z_{SL_0}, $Z_{SL_{\mu}}$ is approximately

$$Z_{SL_{\mu}} \cong \frac{1}{2\pi}\sqrt{\frac{\mu}{\varepsilon}}\ln\left(\frac{4h}{B}\right)+\frac{1}{2\pi}\sqrt{\frac{\mu}{\varepsilon}}\ln\left(\frac{B}{S}\right)=Z_{SL_0}+\varepsilon_2 \tag{2.20}$$

where ε_2 is a difference term for the off-diagonal expression relative to Z_{SL_0}.

Now, as before, for large h, Z_{SL_0} dominates the difference term, which in this case is ε_2, i.e.,

$$\lim_{h\to\infty} Z_{SL_0} >> \varepsilon_2 \tag{2.21}$$

and $Z_{SL_{\mu}}$ is approximated by Z_{SL_0}.

The approximate impedance matrix for $\mathbf{Z}_{SL}$ is then a full matrix with each term equal to Z_{SL_0}. In actuality the diagonal terms always differ from the off-diagonal by an amount that prevents singularity. Despite its analytical limitations, this approximate $\mathbf{Z}_{SL}$ can be used to estimate bounding. From equation 2.10 the upper bound for voltage in this without-fuse configuration for no blown fuses is

$$B_j \cong V_F\left(1+\frac{N\cdot Z_{SL_0}}{R_F}\right) \tag{2.22}$$

In this case for fuse resistances in the rough neighborhood of Z_{SL_0}, the voltage upper bound tends to

be linearly dependent on the number of wires; i.e., $B_j \approx NV_F$. For the TRW microfuse where $R_F \cong 100\Omega$ the characteristic impedances of wire bundles well above the ground plane are in the rough neighborhood of 100 ohms.

In the example where $R_F \approx Z_{SL_e}$ the loading is proportional to $1/N$. Hence, for large harnesses with many wires the maximum voltage and loading can be extreme.

3.0 Laboratory measurements

A small laboratory test program was carried out in Boeing facilities to determine the loading effects of shunt fuses on a multiwire system. The tests were planned and started after considerable preliminary discussion motivated by the fuse development for system level EMP test. The general analytic formulation of the problem given in Section 2 had been formulated, but no quantitative calculations were available for large multiwire cases.

Hence, a simulated wire harness with simulated load boxes was designed and built to provide a relatively simple but realistic evaluation. The wire harness is a 10-meter-long 50-wire bundle. This choice was made partly to provide a test bed somewhat comparable to the TRW Fuse Sensor Testbed, although without branching. Also, our simulation had an objective to provide impedances (characteristic and load impedances) that represent a fairly high-impedance situation characteristic of crew compartment unshielded wiring to LRUs.

The harness is routed down one side of a Boeing-built screen room, across the top of the screen room and back to the other end of the screen room as shown in Figure 3.1. The wire-harness center line is spaced approximately 2 inches off the screen room exterior ground plane. The 50-wire harness is connected to the response-end load box with a 79-pin D38999 B-2 plug designated MS27467T21B35P. The load box has the mating receptacle MS27605T21B35S.

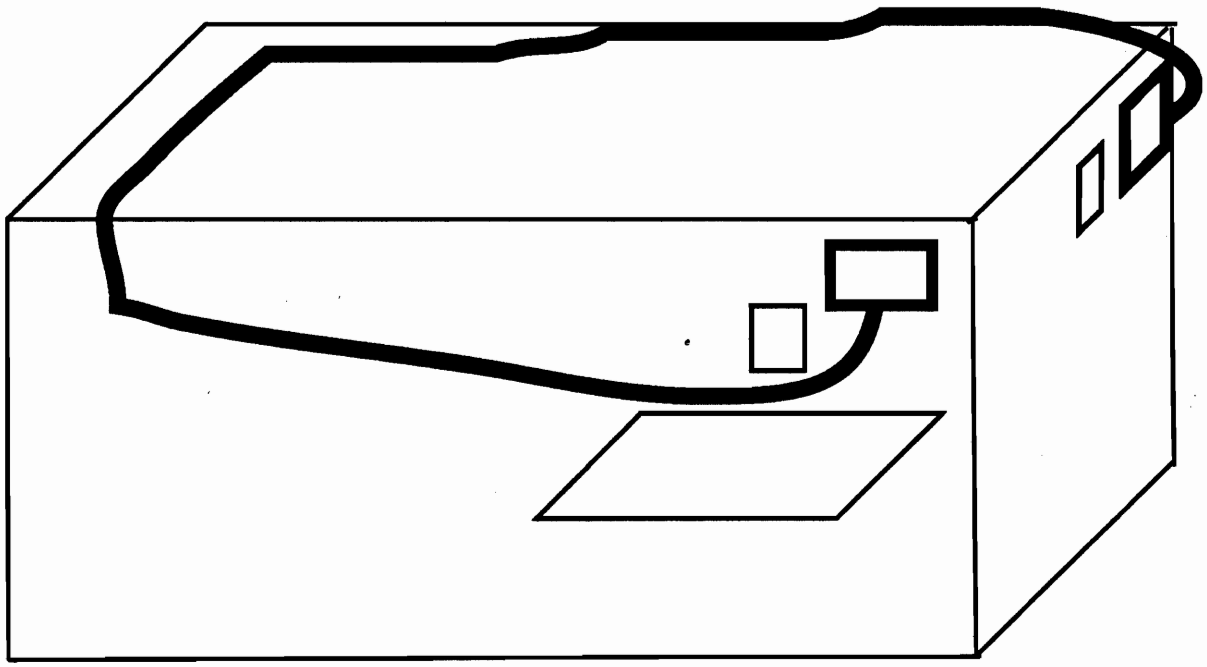

Figure 3.1. Test bed built on copper screen room.

In this evaluation of loading effects, the simulated EMP coupling source was established as a reference relative to which voltage or currents are measured. The reference level needs to be stable and well above the noise level of the measurement. A Stoddart 91550-2 current probe used as a drive coupler provides wide-band coupling at a fairly low level. To obtain adequate signal in the reference channel, a small parallel loop loaded with 100 ohms is strung through the coupler aperture and through a small 5-ohm current probe (Tektronix CT-1). This CT-1 output is then fed to the reference channel input of the

network analyzer.

A somewhat schematic representation of the measurement set up is shown in Figure 3.2.

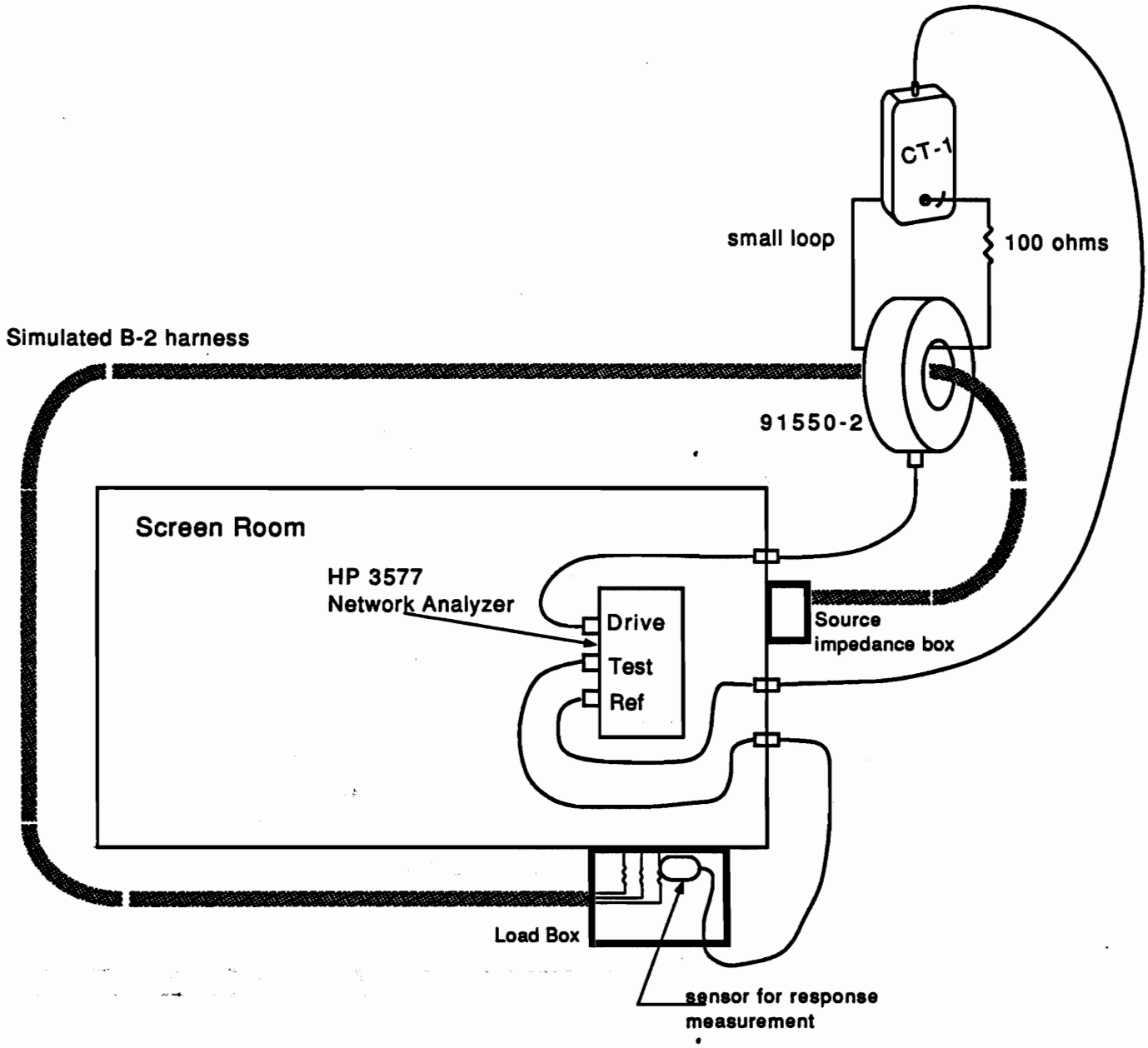

Figure 3.2. Drive coupler with test and reference sensors on test wire harness.

The 91550-2 coupler induces a voltage V_{loop} in the 10-meter harness and the same voltage in the small loop. The resulting loop current of $I_l = V_{loop} / (100 + j\omega L) = V_{loop} / Z_{loop}$ in turn causes an output from the CT-1 of

$$V_{CT-1} = Z'_{CT-1} I_l = \frac{Z'_{CT-1}}{Z_{loop}} V_{loop} \qquad (3.1)$$

The test channel sensor measures current or voltage by providing a proportional voltage

$$V_{sensor} = T_s R_w$$

where R_w is the response (voltage or current) on a wire in the load box and T_s is the sensor transfer function. A voltage probe measurement in the load box is shown in Figure 3.3. In these equations Z^t_{CT-1} denotes the transfer impedance of the CT-1 probe.

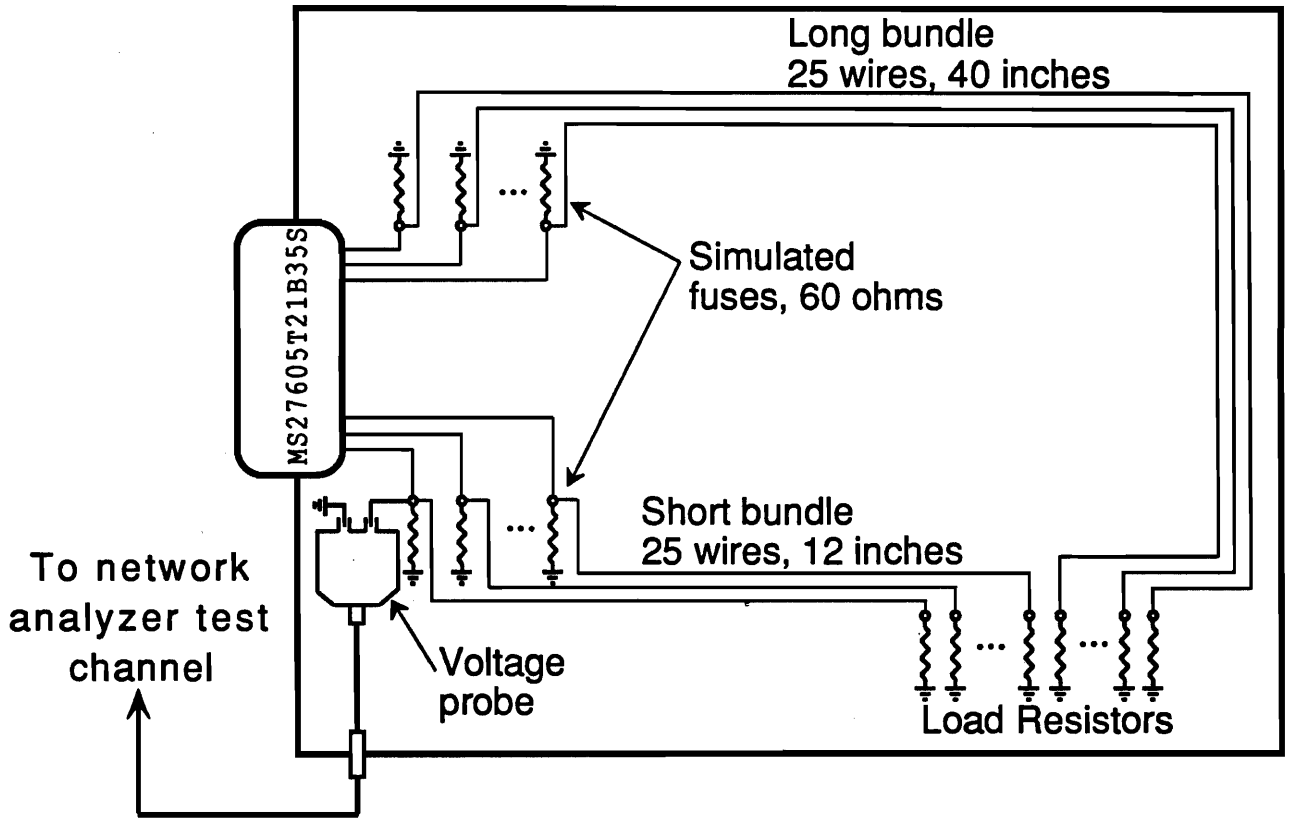

Figure 3.3. Load box configuration with voltage probe measurement.

These signals are carried to the network analyzer via coaxes dedicated to the particular channels (test and reference). Let the attenuation in these two coax channels be denoted by A_{test} and A_{ref}, respectively. Then the signals input to the network analyzer are

$$V_{test} = A_{test} V_{sensor} = A_{test} T_s R_w \tag{3.2}$$

and

$$V_{ref} = A_{ref} V_{CT-1} = A_{ref} \frac{Z^t_{CT-1}}{Z_{loop}} V_{loop} \tag{3.3}$$

The desired quantity to be obtained from the measurement is R_w / V_{loop}. The network analyzer output is

$$M = 20 \log\left(\frac{V_{test}}{V_{ref}}\right) + \Delta_{NA} \tag{3.4}$$

where Δ_{NA} is the offset (error) of the network analyzer. This offset can be measured by a calibration run referred to as CAL0.

Other calibration steps are required to relate the desired circuit response R_w to the voltage at the test channel input and the loop voltage to the reference channel input. From Equations 3.2 and 3.3

$$R_w = \frac{V_{test}}{A_{test} T_s} \tag{3.5}$$

and

$$V_{loop} = \frac{V_{ref}}{A_{ref}\left(\frac{Z^t_{CT-1}}{Z_{loop}}\right)} \tag{3.6}$$

Thus,

$$\frac{R_w}{V_{loop}} = \frac{V_{test}/V_{ref}}{\left[A_{test} T_s \Big/ \left(A_{ref}\frac{Z^t_{CT-1}}{Z_{loop}}\right)\right]} \tag{3.7}$$

Network analyzer measurements are conventionally expressed in the dB domain. Hence, let $20\log A_{test} = B_{test}$ and $20\log A_{ref} = B_{ref}$. Then

$$\begin{aligned} 20\log\frac{R_w}{V_{test}} &= 20\log\frac{V_{test}}{V_{ref}} - \left[20\log T_s + B_{test} - 20\log\frac{Z^t_{CT-1}}{Z_{loop}} - B_{ref}\right] \\ &= M - \left[20\log T_s + B_{test} - 20\log\frac{Z^t_{CT-1}}{Z_{loop}} - B_{ref} + \Delta_{NA}\right] \end{aligned} \tag{3.8}$$

where $M - \Delta_{NA}$ was substituted from equation 3.4. The quantity in square brackets is the calibration function to be applied to the measurement with the specific probe and coaxes that correspond to T_s, A_{test}, and A_{ref}. All measurements were corrected with the appropriate calibrations stored on floppy disks. The measurements were later transferred from HP floppy format to HP magnetic cartridge to DOS floppy to Macintosh computer. Details of the sequence of calibrations are given in Appendix C. This appendix also contains several figures that illustrate details of instrumentation practice.

3.1 Measurements

The 50 wires of the test harness are terminated at the source end with 3 treatments:

(1) shorted to the source-end load box (Load Box 1), which is in turn shorted directly to the screen room copper surface
(2) connected to 100-ohm resistors that are connected to ground in this box
(3) left open (unconnected) in the close vicinity of the other connections in this source-end box.

The load for each wire, specified by its interface pin at the load box (Load Box 2) is given in Table 3-1.

Table 3-1. Test Configuration

Pin Number	Load in Load Box 1	Load in Load Box 2
1	short	open
2	short	100
3	short	open
4	short	100
5	short	open
9	short	open
10	short	100
11	short	open
12	short	100
13	short	open
17	short	open
18	short	100
19	short	open
20	short	100
21	short	open
25	short	100
26	short	open
27	short	100
28	short	open
29	short	100
33	short	open
34	short	100
35	short	open
36	short	100
37	short	open
41	100	open
42	100	100
43	100	open
44	100	100
45	100	open
49	100	open
50	100	100
51	100	open
52	100	100
53	100	open
57	100	open
58	100	100
59	100	open
60	100	100
61	100	open
65	100	open
66	open	100
67	open	open
68	open	100
69	open	open
73	open	open
74	open	100
75	open	open
76	open	100
77	open	open

The load boxes were constructed with small printed circuit panels and pin/jack arrangements inserted so that the loads could be changed fairly easily and any pin could be instrumented. A photo of the load box is shown in Figure 3.4. However, the fairly simple combinations of Table 3-1 led to reasonable complexity (See results in Section 3.2) in the response functions and no additional variations were tried. The load-box pins selected for response measurements were

#1, #10, #45, #50, #66, and #77.

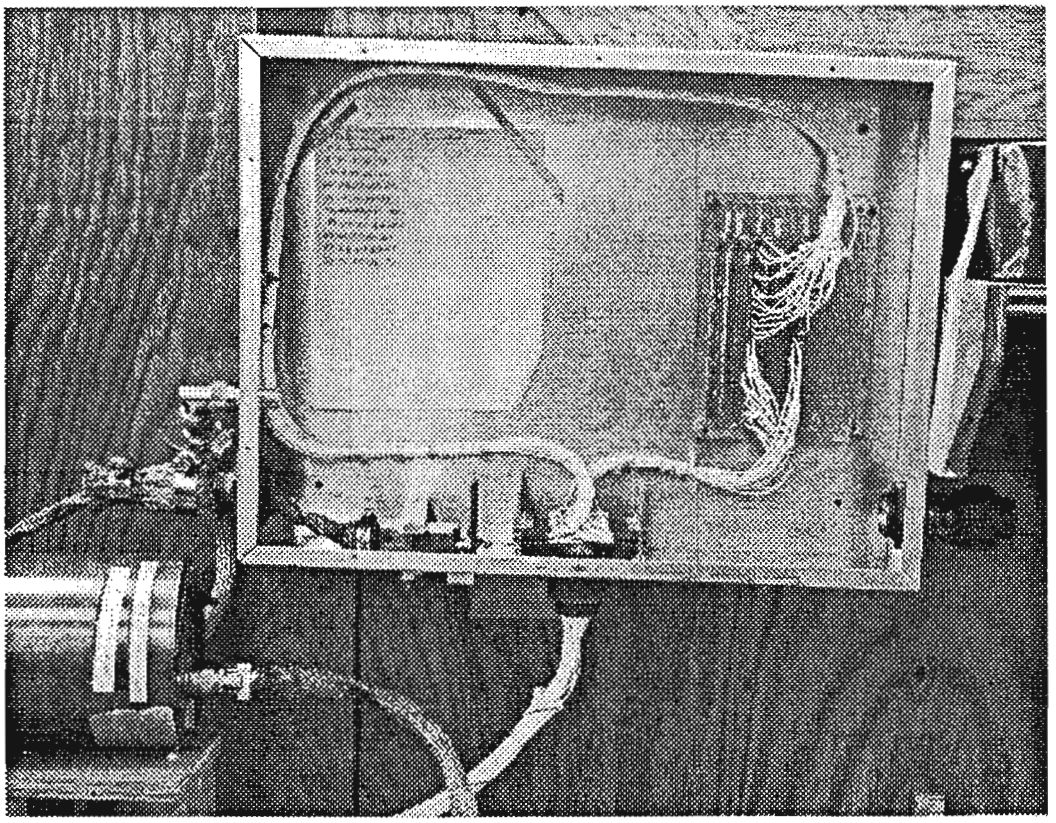

Figure 3.4. Photo of Miletus probe in load box.

These pins provide measurements to represent all the combinations of source-end terminations and load box 2 terminations. (3 x 2 = 6 conditions.) Further, half of the pins are in the long-bundle (40-inch) group and half in the short-bundle (12-inch) group in the load box (Load Box 2). See Figure 3.3.

The simulated fuse resistors were 60-ohm 1/8-watt metal-film resistors installed on the printed circuit board to load each of the wired pins relative to ground at this measurement interface.

At low frequency (10 kHz to about 50 kHz) the coaxial shielding becomes thin (less than a skin depth) and thus voltages leak in or out of the lines. This effect is minimized by keeping coaxes as short as possible. In particular, inside the screen room the network analyzer is placed right next to the feed through panel for the test channel measurement, and the load box is near this panel on the outside. The voltage probe balun is mounted to the feed through connector with one barrel adapter—no coax. The leakage noise level for voltage measurement with these techniques is shown in Figure 3.5. The leakage due to coax and fittings dominates the noise in the frequency range below about 50 kHz. The noise approaches the resistor or amplifier random noise level from about 10^5 to 10^7 Hz. At frequencies above 10 MHz the noise is mainly due to stray coupling to the loop needed to connect the voltage probe to the test point.

The active probe head is grounded by bracket mounting to minimize current flow over the probe tips because this current causes leakage around the joints of the tips to the case head. The probe tips have as short a wiring connection to the test pins as is possible.

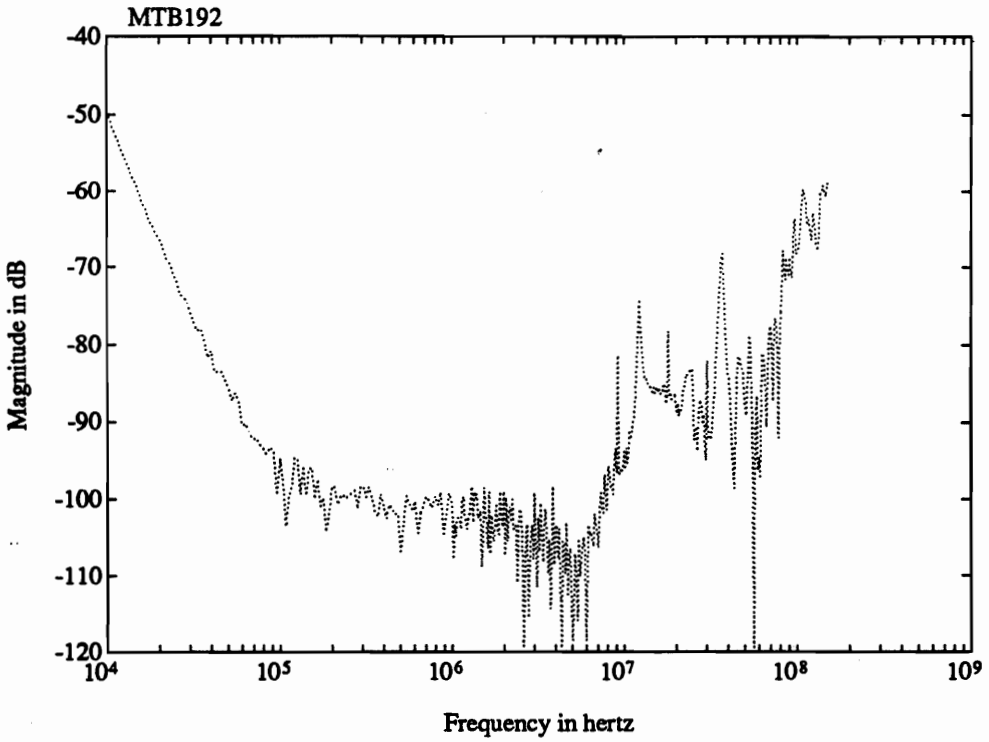

Figure 3.5. Noise for voltage measurement, long-wire side.

Noise measurements that apply to specific measurements are shown as dotted lines with the accompanying measurement plot. Three examples of voltage transfer functions for circuits without simulated fuse loading are shown in Figures 3.6 through 3.8.

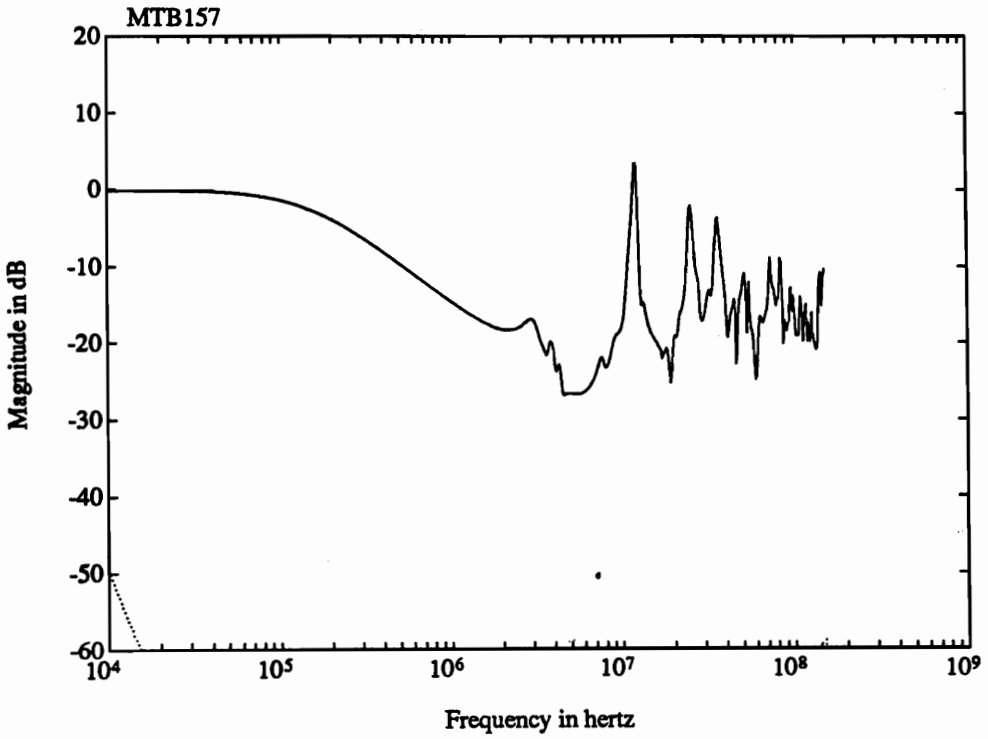

Figure 3.6. Ideal Voltage Transfer Function on pin 1.

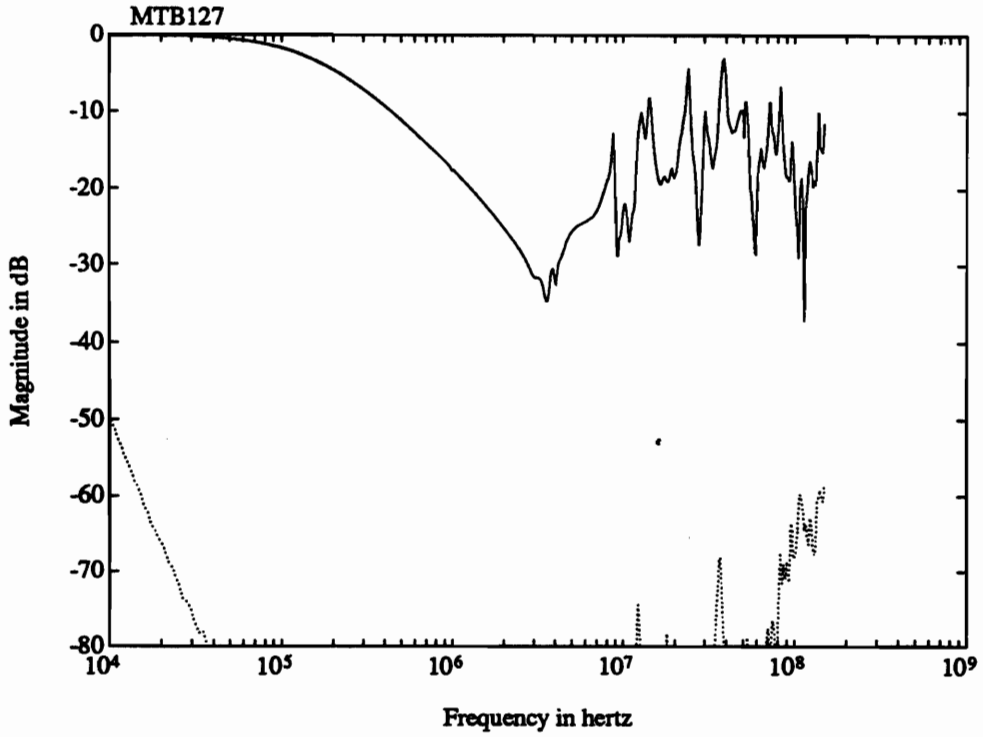

Figure 3.7. Ideal Voltage Transfer Function on pin 10.

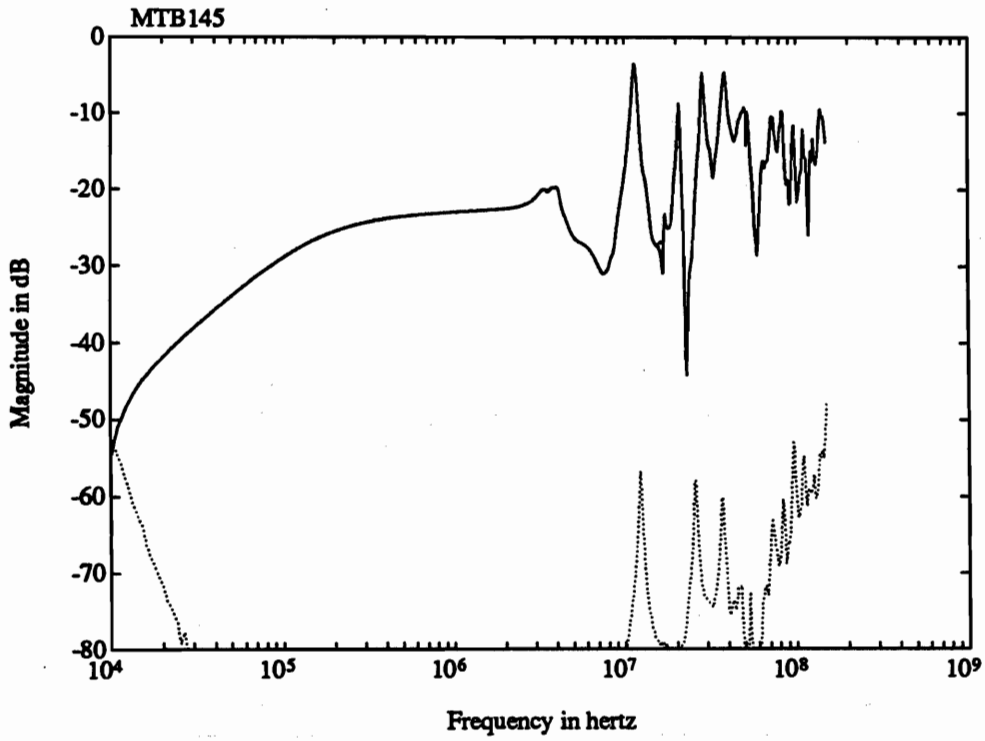

Figure 3.8. Ideal Voltage Transfer Function on pin 66.

Table 3-1 provides information that the wire on pin 1 is shorted in Load Box 1 (i.e., at the end next to the drive) and is open in the measurement load box (Load Box 2). Therefore, the voltages measured on pin 1 should be equal to the coupled voltage at low frequency (transfer function = 0 dB) as shown in Figure 3.6. Also, the general level of coupling is highest at high frequencies on pin 1 as shown by comparison with Figures 3.7 and 3.8. Pin 10 differs only moderately from pin 1. The pin 10 load in Load Box 2 is 100 ohms—high compared to the short in Load Box 1 and the resistance of the wire. Thus, the low-frequency transfer functions are essentially the same for pins 1 and 10, but pin 10 has slightly lower transfer function magnitudes over the high-frequency range (>10 MHz).

Pin 66 represents a case where the drive-end load is open (more precisely, a small capacitance) and the measurement end is terminated in 100 ohms. Thus, the curve as shown in Figure 3.8 rises linearly with frequency at low frequency. The curvature below about 15 kHz in Figure 3.8 is due to interference from a leakage (noise) signal. However, the range of transfer function values at high frequencies is not greatly different from the other two pins. These high-impedance results illustrate the homogeneity introduced by the strong mutual coupling of all wires in the harness, as discussed in Sections 2 and 5.

For pin 1, the same pin as presented in Figure 3.6, Figure 3.9 gives an example of a transfer function after simulated fuse loading (60 ohms to ground) was installed on all the wired pins. The reduction of the transfer function is significant for essentially all frequencies above 100 kHz.

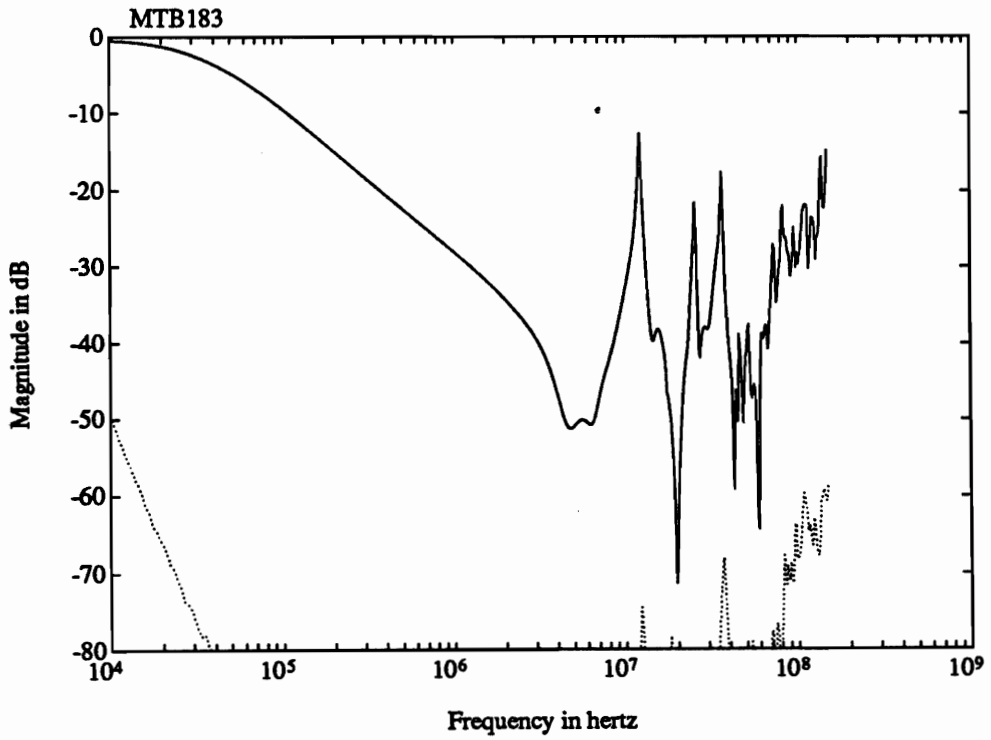

Figure 3.9. Fused (loaded) Voltage Transfer Function on pin 1.

3.2 Data Processing and Results

The calibrated measurements have been analyzed with the MATLAB program on a Macintosh computer. The analysis determines the response (current and voltage) on the measured pins that would be produced by a damped sine voltage (normalized to unit scale factor) injected at the same localized position as that of the drive coupler in the test. In other words, the measured transfer functions are multiplied by transforms of damped sine functions with unit scale factor A and then inverse transformed to get time domain results.

Specifically in equations, the calculations were formulated as follows. A damped sine function with unit scale factor is given by

$$f_{DS} = Ae^{-\alpha t}\sin(\omega_o t)U(t) \qquad (3.9)$$

where

A = scale factor of the damped sine = 1

$\omega_o = 2\pi f_o$ is the center frequency of the undamped oscillator

$\alpha = \omega_o / (2Q)$ with Q being the damping factor of this function.

The analysis was performed for the case of Q = 6, a specification value. The damped sine function for center frequency f_0 = 10 MHz is shown in Figure 3.10. For the specified Q=6, this plot represents any of the damped sine drives by adjustment of the time scale in inverse proportion to f_0.

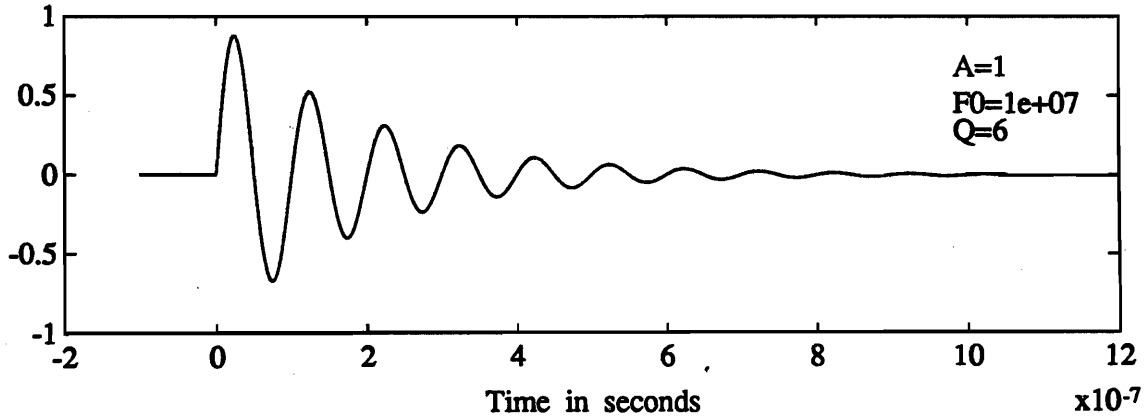

Figure 3.10. The damped sine function used as voltage source.

The Fourier transform of equation 3.9 is

$$F_{DS}(\omega) = \frac{\omega_o}{(j\omega + \alpha)^2 + \omega_o^2} \qquad (3.10)$$

where ω is the Fourier transform variable equal to $2\pi f$.

Let $V_m(\omega)$ = the measured transfer function as illustrated in Figures 3.6 through 3.8. Then the voltage

response at the measured test point to the damped sine drive of equation 3.9 is given by

$$f_m(t) = \frac{1}{2\pi} \int_{-\infty}^{\infty} F_{DS}(\omega) V_m(\omega) e^{j\omega t} d\omega \qquad (3.11)$$

This result is just the inverse transform of the product of the damped sine and the measured transfer function.

Pin voltage responses to the 10-MHz damped sine drive, as calculated from the example measurements, are shown in Figure 3.11. The four separate plots in Figure 3.11 are labeled by the file name of the particular measurement to which the calculation of equation 3.11 was applied. Table 3-2 gives the correspondence between file name and the pin and fuse condition of the test point for the measurements presented in this section.

Table 3-2

File name	Pin (See Table 3-1.)	Fuse condition
MTB125	77	no fuse simulation
MTB127	10	no fuse simulation
MTB145	66	no fuse simulation
MTB157	1	no fuse simulation
MTB183	1	all 50 pins loaded with simulated fuses

The 10-MHz damped sine used for Figure 3.11 drives the harness strongly in a band near the primary resonances of the test bed. The resultant waveforms shown in Figure 3.11 are reasonably symmetric (positive and negative) and three of the four look rather like damped cosines.

Figures 3.12 through 3.14 present the calculated responses on the same four pins (i.e., for the same measurements) at center frequencies of 100 MHz, 2 MHz, and 20 MHz, respectively. The responses for f_0 = 100 MHz in Figure 3.12 show two interesting properties:

(1) A small precursor oscillation before t = 0 illustrates the accuracy limitations of the measurements (especially phase values) and of the Fourier transform sampling. In this case, the measured data, which are sampled to only 150 MHz, give surprisingly good results for a 100-MHz damped sine.

(2) A ring with a period of slightly less than 10^{-7} seconds occurs at the round-trip propagation time on the 10-meter harness.

The responses for f_0 = 2 MHz in Figure 3.13 exhibit strongly asymmetric behavior in three of the four cases. However, this appearance is similar to many EMP responses measured in system level test in large simulator facilities. The responses for f_0 = 20 MHz in Figure 3.14 have a fairly wide variety of ringing and damping that are also characteristic of full-scale EMP tests. Thus, Figures 3.11 through 3.14 support the deduction that the calculated responses are correct and realistic.

For every measurement, computer calculations of the response were run for damped-sine excitation with 60 center frequencies f_0 spaced uniformly on a logarithmic scale from 1 MHz through 100 MHz. For

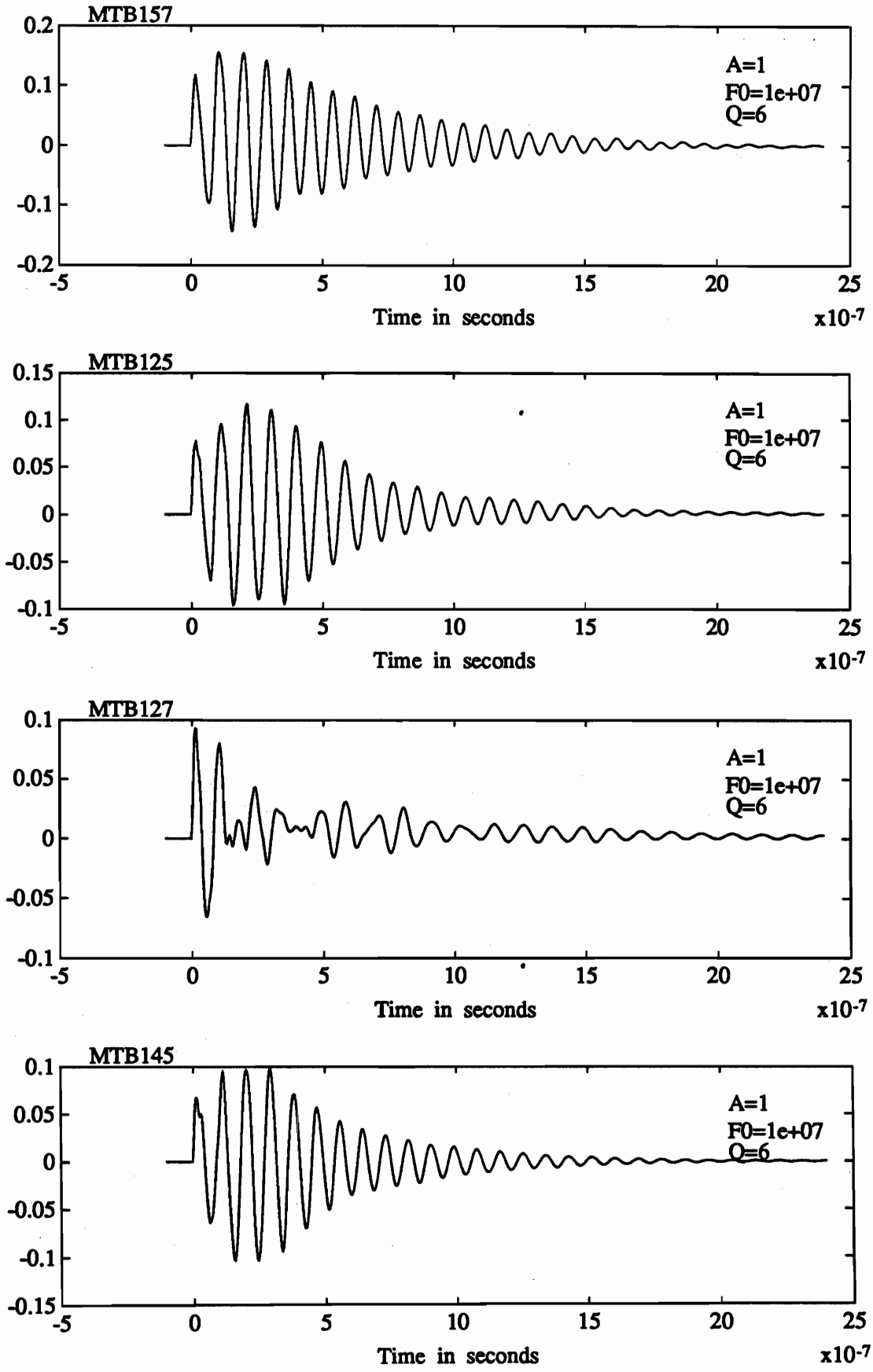

Figure 3.11. Unloaded responses at four pins to the 10-MHz damped sine.

each damped-sine center frequency the peak value of the calculated response was recorded. For example, on measurement MTB157 for f_0 = 10 MHz, the peak value may be read from Figure 3.11 as approximately 0.16 volts (for A = 1 volt). These 60 values, plotted on a scale of dBV (dB_{Volts}) as a function of frequency, show the smoothing effect of damped-sine response in comparison to the cw transfer functions (cf., Figures 3.6 through 3.8).

Figure 3.15 shows dB plots of these damped-sine responses on pin 1 for the measurement without fuses (MTB157, solid line) and for the measurement with shunt fuses on all pins (MTB158, dashed line). Note, for example, that 20log(0.16) = –16 dB is the value on the solid curve at 10 MHz.

The effect of shunt fuse loading is defined as the reduction in voltage as measured by the ratio of voltage with fuses to voltage without fuses. On a dB scale this loading ratio for pin 1 is given by the difference of the two curves (dashed curve – solid curve) in Figure 3.15. This difference curve along with five others is plotted in Figure 3.16. Figure 3.16 summarizes the loading effect on all six of the measured pins of this test. At frequencies above about 4 MHz the loading ratios of all pins track moderately well with a spread (maximum to minimum) of about 10 dB. When all 360 loading values in dB (60 points per pin x 6 pins) were averaged, the mean was –18.86 dB with a standard deviation of 4.6 dB.

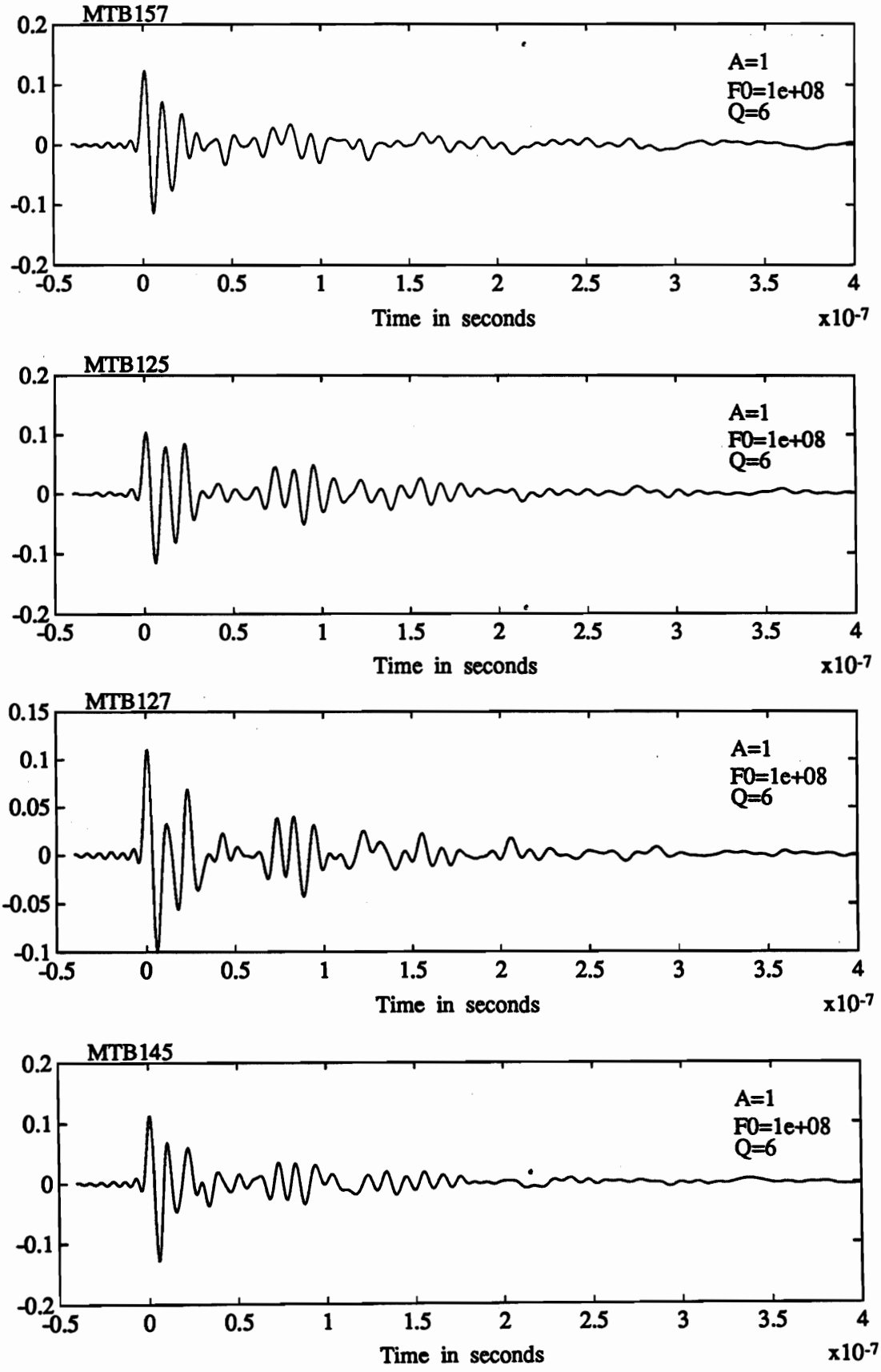

Figure 3.12. Unloaded responses at four pins to the 100-MHz damped sine.

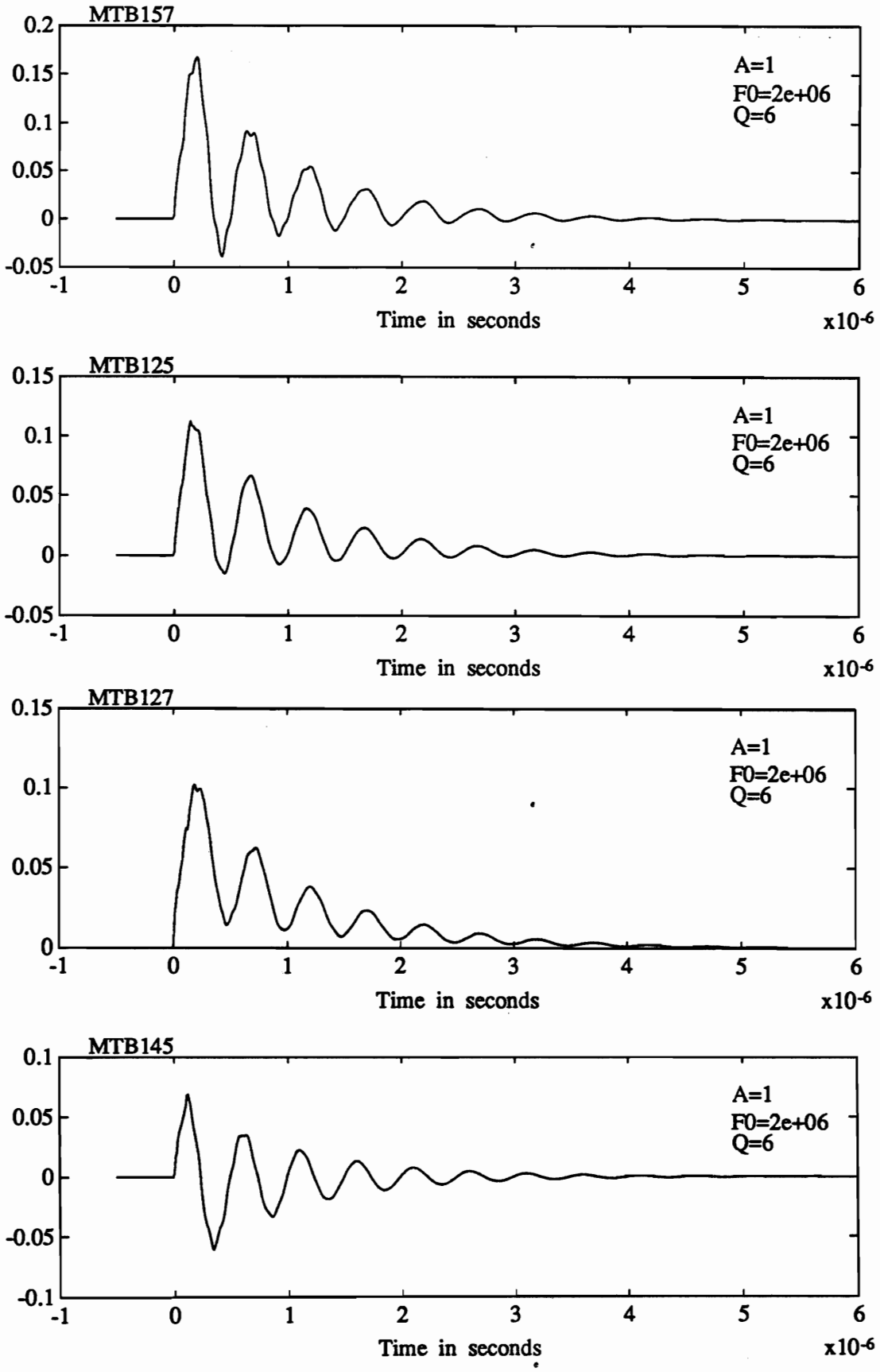

Figure 3.13. Unloaded responses at four pins to the 2-MHz damped sine.

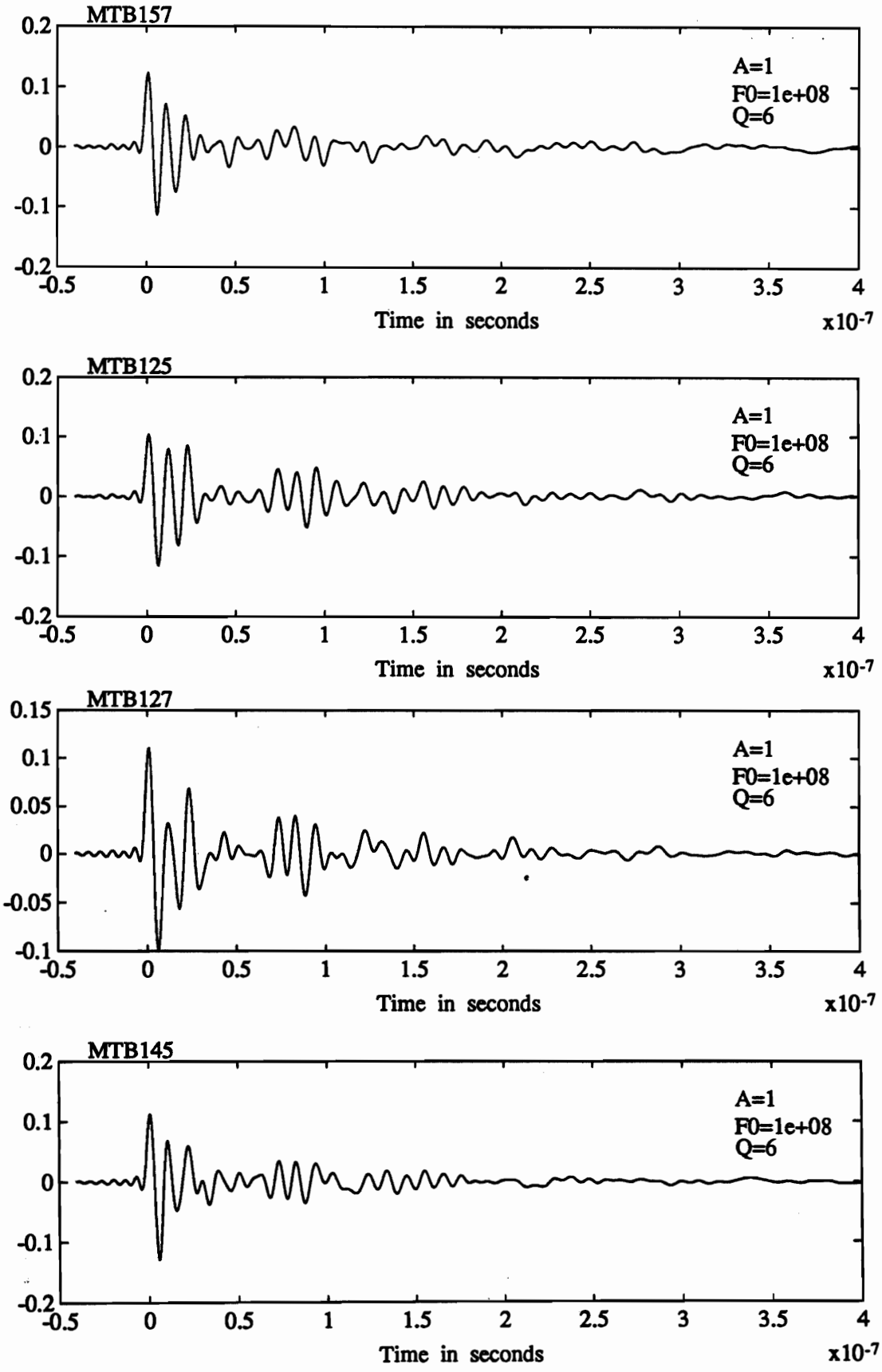

Figure 3.14. Unloaded responses at four pins to the 20-MHz damped sine.

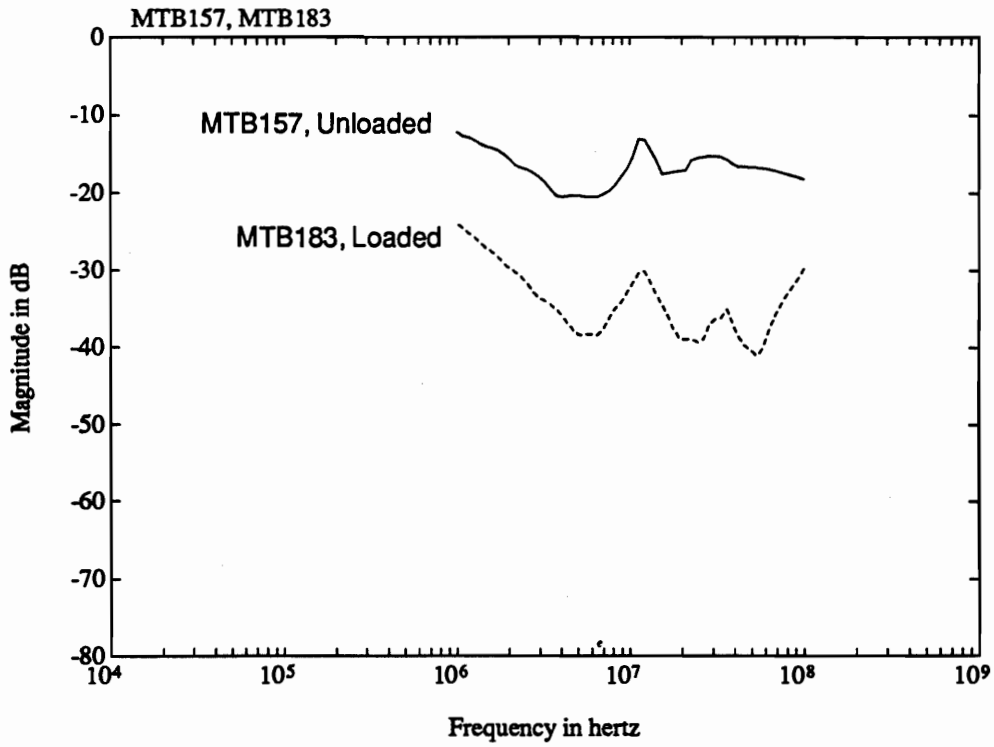

Figure 3.15. Envelope of damped sine responses on pin 1.

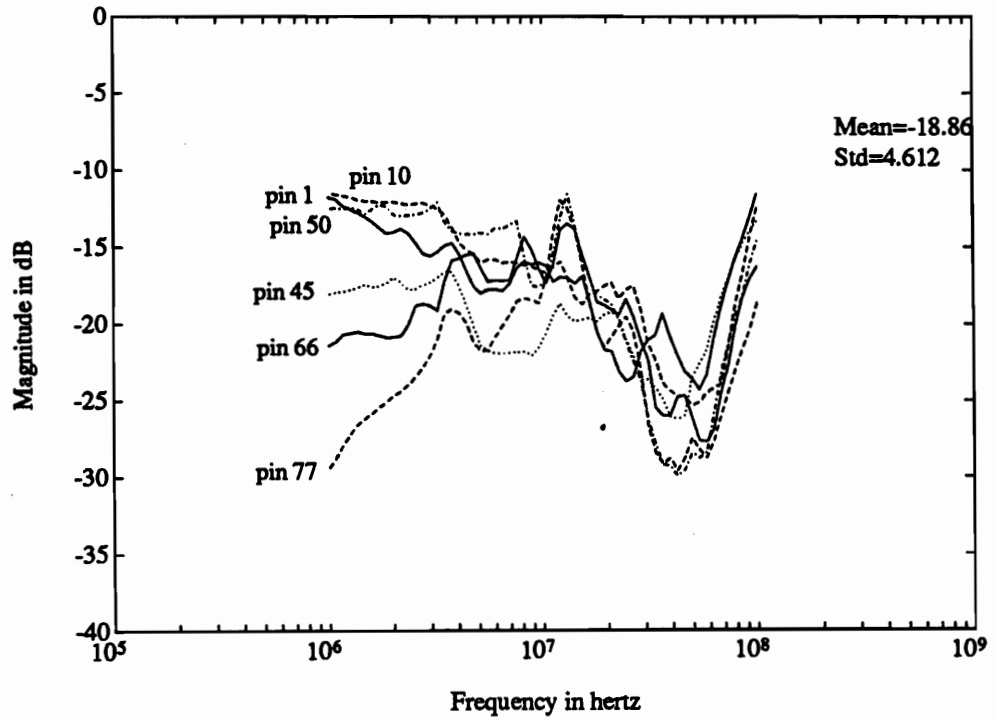

Figure 3.16. Summary of loading ratios on all measured pins.

Section 4.0 EMPTAC #7 Measurements

The development effort for fuses included their use in a near-threat EMP test carried out on the EMPTAC aircraft at the HPD test facility, Kirtland AFB. The EMPTAC is a modified 707-720B maintained at the Phillips Laboratory as a test bed. This test to evaluate the fuse sensors is named EMPTAC #7. A sketch of the aircraft is shown in Figure 4.1.

As part of the fuse evaluation effort, TRW put together a Fuse Sensor Testbed (FST) which was made up of three simulated LRUs, a junction box, three unshielded cables and three shielded cables. The FST assembly consists of three cables, and those three were chosen as all the unshielded ones or all the shielded ones in different test configurations. Two shielded and two unshielded cables each contained 50 wires, ten of which were twisted shielded pairs (TSP). The remaining cables had six wires each. The FST was used in the laboratory by TRW to make measurements similar to those described in section 3. The FST configuration shown in Figure 4.2 was used on the EMPTAC as shown in Figure 4.1. The load boxes and junction box were set on the floor of the main cabin and the cables to boxes 2 and 3 were routed along the walls of the cabin for some tests and on the floor of the cabin for other tests. Tests were made using both shielded and unshielded cables. Also shown in Figure 4.1 are two other load boxes with cables, box #6 and box #19, already existing on the EMPTAC, which were also used for fuse wafer evaluation. Box #6 was part of a shielded system and was located in the cockpit area of the EMPTAC. Box #19 was connected to three unshielded cables and located in the aft section of the EMPTAC.

All FST load boxes were constructed and instrumented so voltage or current could be measured inside the load box at points close to the connector on the load box. This allowed measurements to be as close as possible (within 3 inches) of the fuse wafer location. However, modifications were needed on load

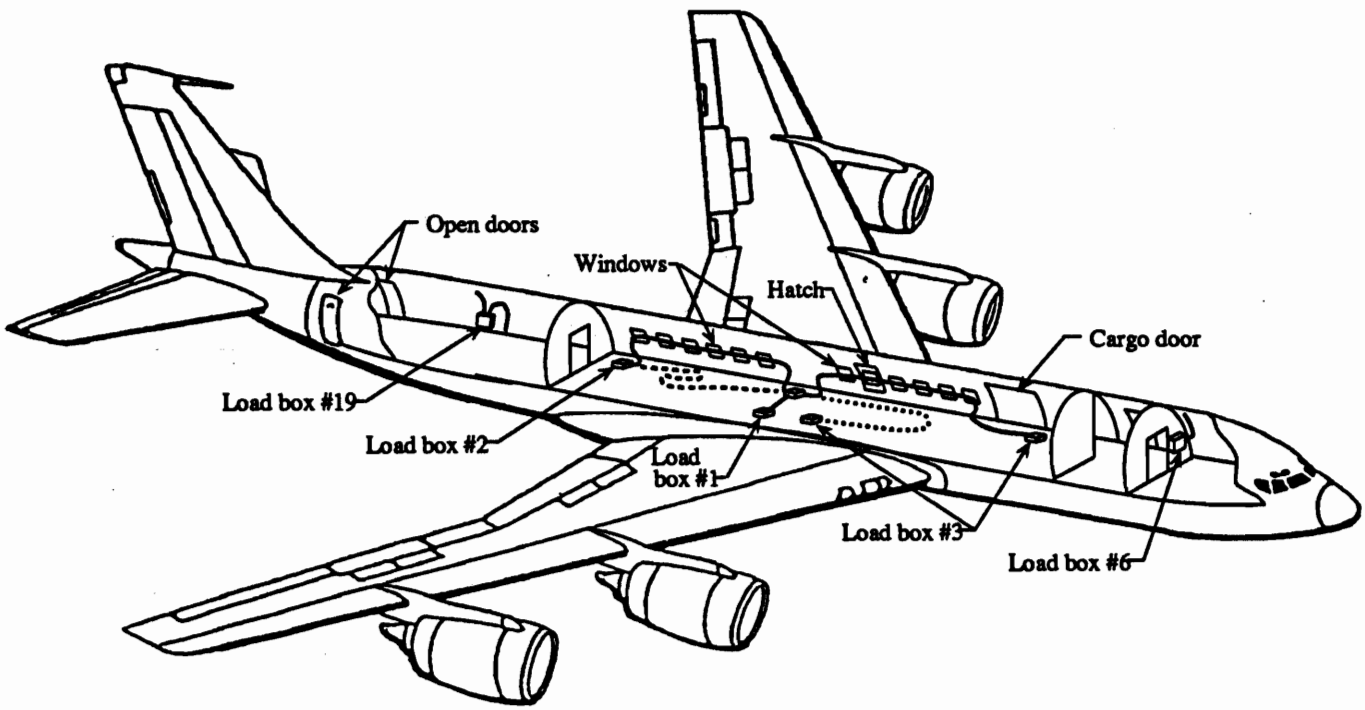

Figure 4.1 EMPTAC and load box locations.

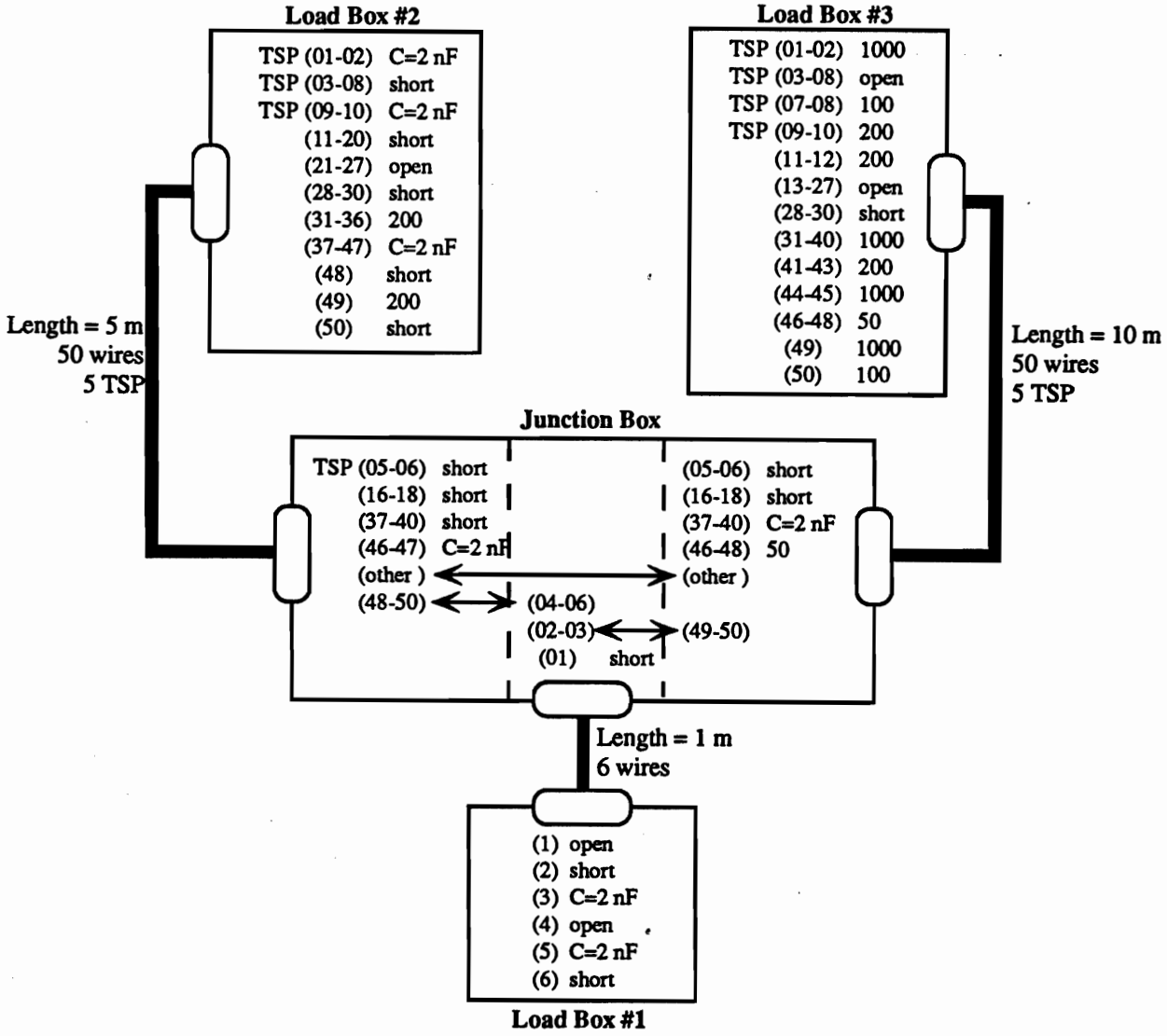

Figure 4.2 Fuse sensor testbed (FST) configuration as used on the EMPTAC.

boxes #6 and #19 because they did not have connectors that matched the prototype fuse wafers. For box #6 a short length of shielded cable and a small shielded box with a short length of cable attached were constructed so they could be inserted between load box #6 and the existing cable on the EMPTAC. The connector on the small shielded box was matched to the prototype wafers and the box was constructed to allow measurements to be made close to the fuse wafer. Load box #19 was modified by inserting two short lengths of cable between box 19 and one of the existing cables on the EMPTAC with the intermediate connector pair matching the prototype wafers. Hence, the measurements taken inside load box #19 were not close to the fuse wafer but about 10 to 12 inches away. In addition, the inserted cables connected to box 19 were located where sufficient EMP coupling occurred between where they were fused and where they were measured to change the result. For these reasons the measurements on box #19 are not a good indicator of fuse loading.

The EMPTAC tests were conducted by recording the voltage on a selected set of wires, usually one or two per connector, with fuse wafers in place and then, without changing the instrumentation, the voltages

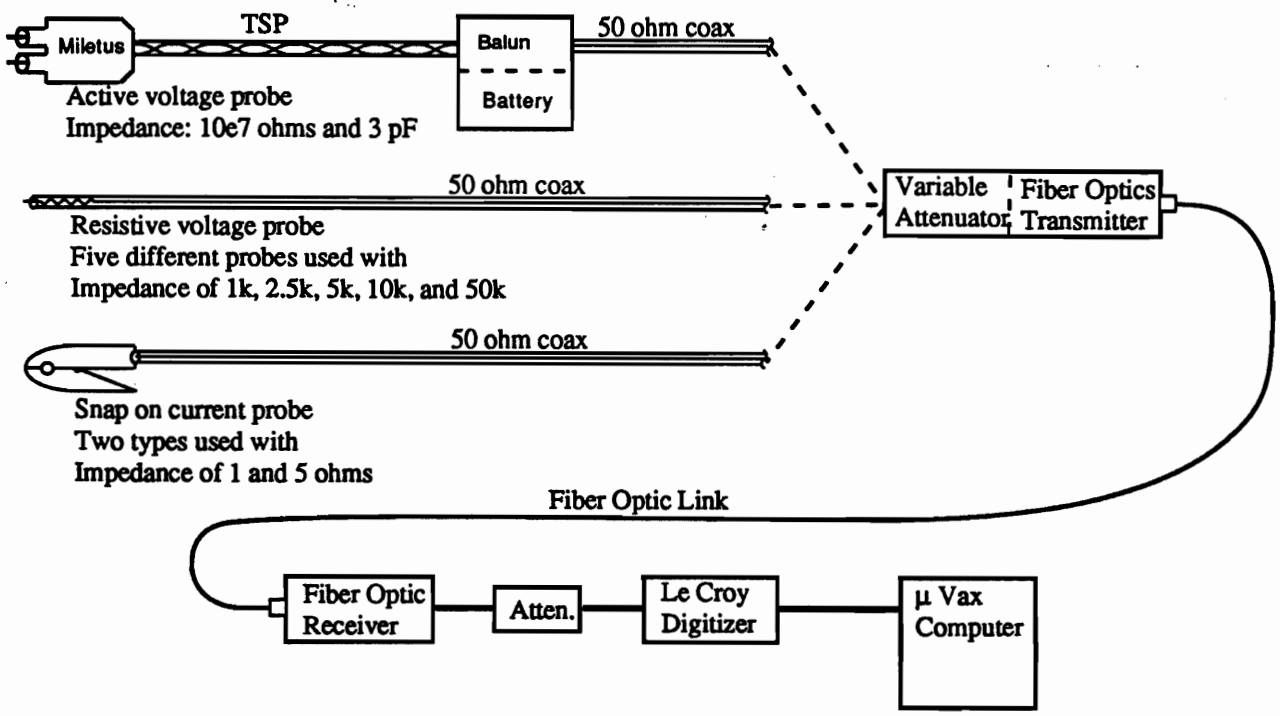

Figure 4.3 Instrumentation for EMPTAC tests.

were recorded with the fuse wafers removed. The instrumentation used to record the voltage and current measurements is shown in Figure 4.3. All measurements were taken in the EMPTAC position with fuselage parallel to and centered directly under the HPD antenna as shown in Figure 4.4.

To measure the maximum fuse loading it is necessary that no fuses blow when recording the response with fuses. As each level or step in a fuse sensor blows, the resistance of the remaining sensor goes up, and the increased resistance reduces the loading effect. In EMPTAC #7 tests the response level for the FST was controlled by covering windows in the main cabin with aluminum foil, by changing the routing of the FST cables from the walls alongside windows to the floor and by relocating box #3 close to box #1.

4.1 Analysis of EMPTAC #7 data

All of the data recorded during the EMPTAC #7 test were processed by Fourier transforming the digitized waveform recorded from the LeCroy digitizers, folding in the frequency domain calibration for probes, attenuators and fiber optics link and then transforming the result back to the time domain. Two examples of typical time and frequency domain results are shown in Figures 4.5 and 4.6. This data is typical of almost all data, both voltage and current, taken at pin/wire interfaces in that the peak value in the time domain is determined primarily by frequencies from 50 MHz to 100 MHz. Loading effects were determined by comparing the peak value of voltage when fused to the peak value of voltage when not fused. The data were carefully screened to eliminate errors such as wrong calibration factors and malfunction of voltage probes and to eliminate inappropriate data such as high-excitation cases where all fuses blew and cases where the fuse wafer was found broken into separate pieces. In addition, for reasons previously stated, no load box #19 data could be used to determine loading effects. In fact, some voltages inside box #19 were increased by adding fuses to the connector external to box #19.

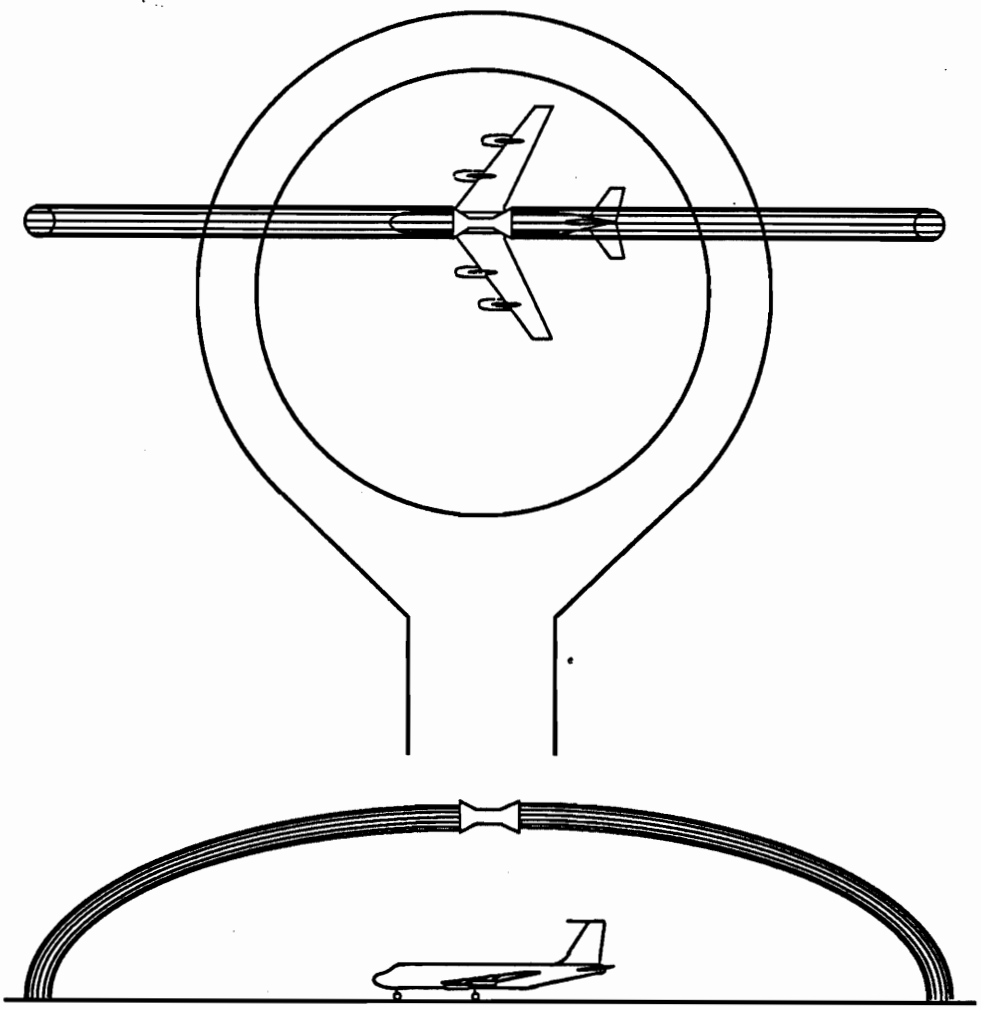

Figure 4.4 Location of the EMPTAC under the HPD antenna.

A summary of the final loading results is given in Table 4-1. The statistics given in Table 4-1 are the mean and standard deviation of the loading effects when the loading effect is expressed in dB. The loading indicated in Table 4-1 is probably biased low for several reasons. The first reason is that the data includes many cases where the first step of one or more sensors at a connector interface was blown. The prototype sensors had a resistance of about 100 ohms with no steps blown and jumped to an average of 400 ohms with one step blown. The data is included here because there is not much data left if it is excluded. The second reason is that the data includes results for which wafers were found to be cracked. A cracked wafer, in effect, disconnects or opens the fuse sensors that intersect the crack. It is not known whether the crack was generated on insertion, extraction, or post test handling. The third reason is that the contact between the fuse sensors and the pins of a connector was found to be unreliable. TRW felt that the contact was good with the first insertion of a wafer but was unreliable with subsequent insertions.

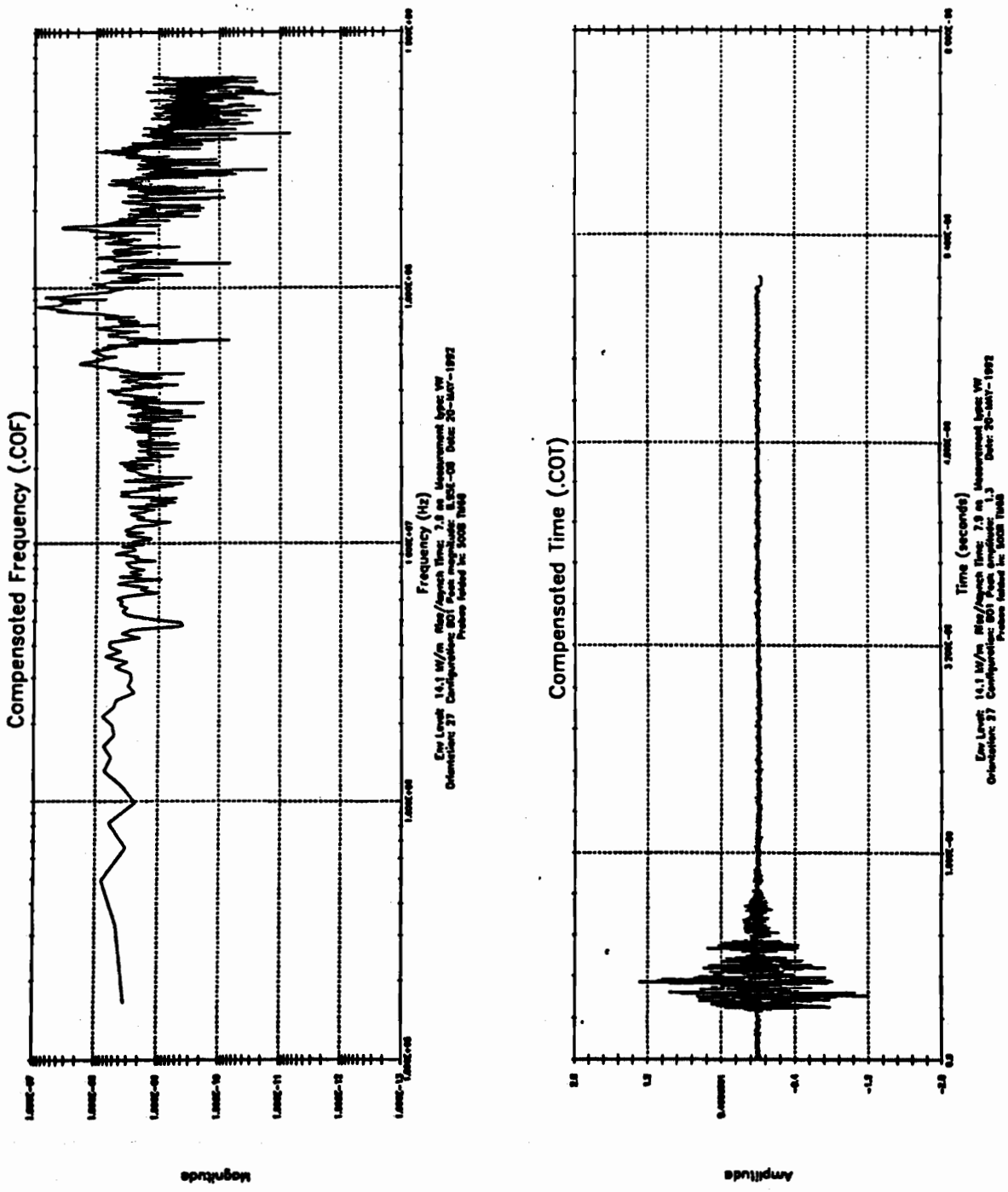

Figure 4.5 Time and frequency domain results for voltage on pin 42 on load box #2 with unshielded cables on FST.

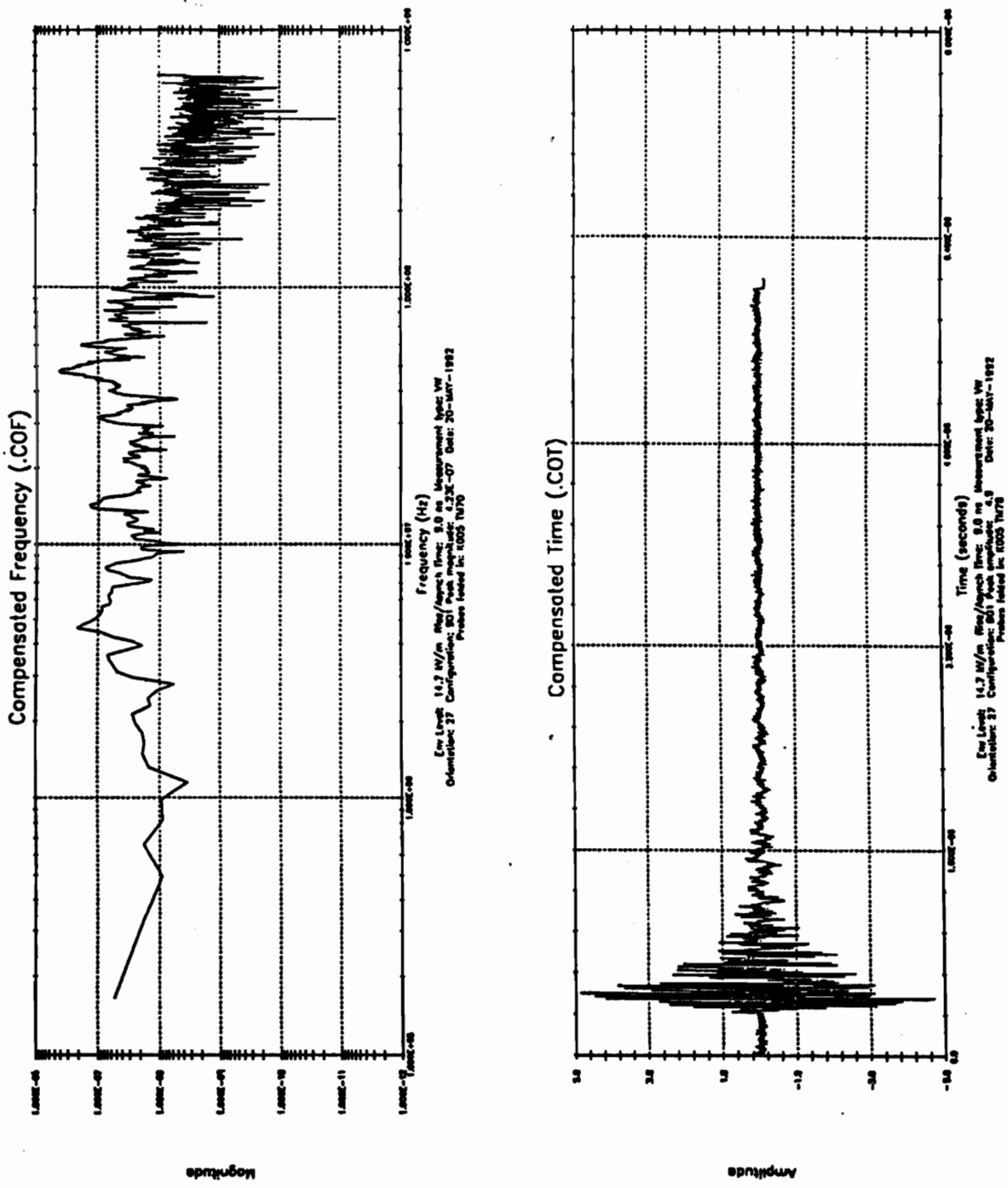

Figure 4.6 Time and frequency domain results for voltage on pin 49 on load box #3 with unshielded cables on FST.

Table 4-1 Summary of loading effects from EMPTAC #7 tests.

Configuration		Number of data points	Mean (dB)	Std Dev (dB)
Unshielded	6 wire Load Box #1	6	-9.0	2.5
	50 wire Load Box #2, #3	20	-12.5	2.1
Shielded	50 wire Load Box #2, #3 23 wire Load Box #6	26	-4.6	2.1

5.0 Theoretical Model Calculations

A theoretical model that predicts the loading from fuse wafers is important because it is much easier and quicker to calculate the effects of configuration changes than it is to make the same changes to a physical model and measure the effects in the lab. The rest of this section shows how the simple physical models being measured in the lab can be modeled using multi-wire transmission line equations. Calculations are then made assuming random-lay cables with suitable parameter values. Comparisons are made with lab measurements, and then results are calculated to show the loading effects of fuse resistance, variation of load impedance and number of wires in a bundle.

The notation used to model a multi-wire transmission line is shown in Figure 5.1 and is based on the work of Strawe [5]. Assuming the existence of N independent eigenmodes, we can write the solution in terms of an incident and reflected traveling wave for each eigenmode. A convenient way of expressing the solution for this study is also shown in figure 5.1 where the cascade matrix representation for a section of multi-wire line is written out. The bracketed terms used in the expressions for A, B, C and D are diagonal matrices defined as

$$[f(\gamma)] \equiv \text{Diagonal}[f(\gamma_1), f(\gamma_2), \cdots f(\gamma_N)]. \tag{5.1}$$

Once the per-unit-length parameters **Z** and **Y** of a section of transmission line are given, the equations in Figure 5.1 are easily solved on desktop computers. The calculations for this report were all done on a Macintosh using a program called MATLAB. The **Z** and **Y** matrices are NxN, complex, symmetric and, in general, the values are difficult to obtain with the exception of a few special wire geometries. One such geometry, used in this study, is called random lay. A random-lay cable is defined as a wire bundle where, over the length of the cable, the wires are assumed to be in different positions relative to each other in such a way that the mutual impedance between the conductors is on the average the same for all conductors in the bundle. Then, both **Z** and **Y** can be specified with only two values, a diagonal term and an off diagonal term. Real wire bundles made up in the lab or on form boards have a component of randomness but also tend to have some controlled lay of the wires. Thus, real cables would be expected to show greater differences in response on each wire. The random-lay cable does keep track of each wire and thus will show the effects of coupling between the wires, the number of wires, different loads and sources on individual wires and branching in the cable.

The notation and equations used to obtain the per-unit-length parameters for a random-lay cable are shown in Figure 5.2. The inductive terms are the easiest to understand. The self or diagonal inductive term is taken to be the inductance of a thin wire with diameter d, at a height h above a ground plane where h is the average height for every wire in a random lay cable. In other words, the self inductance is proportional to ln(4h/d). The mutual or off diagonal inductive term is assumed to be the same as the mutual inductance of two wires, both a height h above a ground plane and separated from each other by half the bundle diameter B. In other words, the mutual inductance is proportional to $.5\ln(1+(4h/B)^2)$. Real wire cables also have a small amount of resistance in each wire. This is approximated in this study by using a complex permeability for the self inductance term, i.e., $\mu_c=\mu_0(1-jL_{tm})$ where L_{tm} is like a magnetic loss tangent. In this study, L_{tm} is set at a small fixed value which is equivalent to assuming a small wire resistance that is proportional to frequency. This differs from the resistance of real wires which, at high frequency, is proportional to the square root of frequency. The approximation used in this study was made because it is numerically

Uniform N-wire transmission line

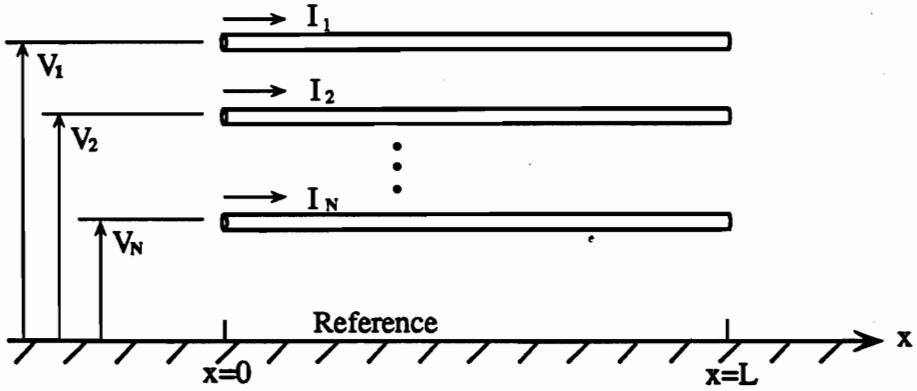

$$\text{Voltage vector} = \mathbf{V}(x) = \begin{bmatrix} V_1 \\ V_2 \\ \vdots \\ V_N \end{bmatrix} \qquad \text{Current vector} = \mathbf{I}(x) = \begin{bmatrix} I_1 \\ I_2 \\ \vdots \\ I_N \end{bmatrix}$$

A solution depends on the diagonalization of ZY, expressed as $\mathbf{X}^{-1}\mathbf{ZYX} = \gamma^2$

where: $\mathbf{Z}$ = NxN complex matrix of per-unit-length impedance parameters of the line,

$\mathbf{Y}$ = NxN complex matrix of per-unit-length admittance parameters of the line,

$\mathbf{X}$ = NxN complex matrix of eigenvectors,

γ^2 = NxN complex diagonal matrix of corresponding eigenvalues.

Section of N-wire line as a circuit element

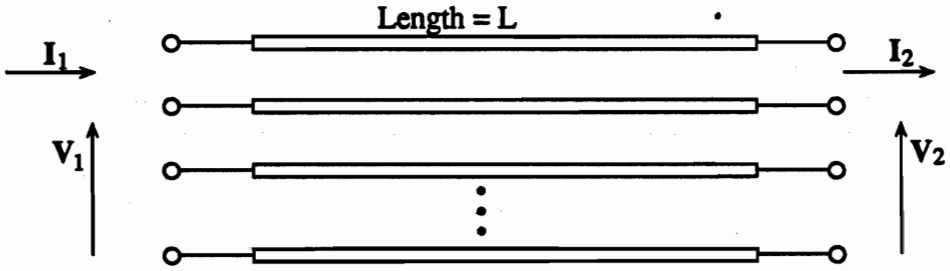

Cascade matrix representation

$$\begin{bmatrix} \mathbf{V}_1 \\ \mathbf{I}_1 \end{bmatrix} = \left[\begin{array}{c|c} \mathbf{A} & \mathbf{B} \\ \hline \mathbf{C} & \mathbf{D} \end{array}\right] \begin{bmatrix} \mathbf{V}_2 \\ \mathbf{I}_2 \end{bmatrix}$$

$$\mathbf{A} = \mathbf{X}\,[\cosh(\gamma L)]\,\mathbf{X}^{-1}$$

$$\mathbf{B} = \mathbf{X}\left[\frac{\sinh(\gamma L)}{\gamma}\right]\mathbf{X}^{-1}\mathbf{Z}$$

$$\mathbf{C} = \mathbf{YX}\left[\frac{\sinh(\gamma L)}{\gamma}\right]\mathbf{X}^{-1}$$

$$\mathbf{D} = \mathbf{A}^{T}$$

Figure 5.1 Notation used to model a multiwire transmission line.

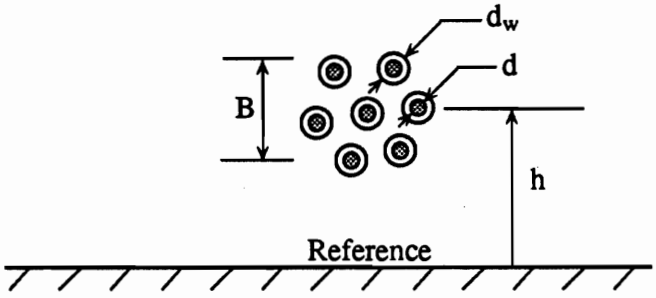

n = number of wires in bundle
h = height to center of bundle
d = diameter of wires (metal part only)
d_w = diameter of wires including dielectric
B = bundle diameter
B_t = diameter of tightly packed bundle, i.e. $B \geq B_t = d_w\sqrt{\frac{4n}{\pi}}$
ε_r = relative dielectric constant of dielectric around each wire
ε_{rc} = effective relative dielectric constant between bundle and reference
ε_{rd} = effective relative dielectric constant between wires in the bundle
$= \varepsilon_r / (B_t/B + (1 - B_t/B)\,\varepsilon_r)$
$\varepsilon_0 = 10^{-9}/(36\pi)$ = free space dielectric constant
$\mu_0 = 4\pi 10^{-7}$ = free space permeability
L_{te} = electric loss tangent (to account for loss in dielectric)
L_{tm} = magnetic loss tangent (to account for resistive loss in wires)
$\varepsilon_{cc} = \varepsilon_0\,\varepsilon_{rc}\,(1\text{-}j\,L_{te})$ = complex dielectric constant, bundle to reference
$\varepsilon_{cd} = \varepsilon_0\,\varepsilon_{cd}\,(1\text{-}jL_{tm})$ = complex dielectric constant, between wires
$\mu_c = \mu_0\,(1\text{-}j\,L_{tm})$ = complex permeability (for resistance terms only)
Z = impedance per unit length parameters
Y = admittance per unit length parameters

For random lay bundle:

$$\mathbf{Z}=\begin{bmatrix} z_s & z_m & \cdots & z_m \\ z_m & \ddots & \ddots & \vdots \\ \vdots & \ddots & \ddots & z_m \\ z_m & \cdots & z_m & z_s \end{bmatrix} \qquad \mathbf{Y}=\begin{bmatrix} y_s & y_m & \cdots & y_m \\ y_m & \ddots & \ddots & \vdots \\ \vdots & \ddots & \ddots & y_m \\ y_m & \cdots & y_m & y_s \end{bmatrix}$$

$z_s = j\,f\,\mu_c \ln(4h/d)$
$z_m = j\,f\,\mu_0 .5 \ln(1+(4h/B)^2)$
$y_s = j\,f\,4\,\pi^2\,(\varepsilon_{cc}\,C_c + (n\text{-}1)\,\varepsilon_{cd}\,C_m)$
$y_m = -\,j\,f\,4\,\pi^2\,\varepsilon_{cd}\,C_m$
$C_m = 1\,/(\,n \ln(B/d)\,(C_c \ln(B/d) + 1))$
$C_c = 1/(n \operatorname{acosh}(2h/B))$
f = frequency

Figure 5.2 Notation and equations for obtaining the per-unit-length parameters for a random lay bundle of wires over a ground plane.

expedient that all terms of the per-unit-length parameters be directly proportional to frequency.

The per-unit-length admittance parameters are more difficult to obtain than the impedance parameters because of the dielectric material used in the construction of the cable. If there were no insulating materials used, only air, then the admittance parameters could be obtained directly from the impedance parameters because all modes have the same free space propagation constant. In this study the wires were covered with a dielectric and the laboratory configuration had a layer of 3/4" plywood on the reference ground plane. This combination means that the capacitance between wires is proportional to a different relative dielectric constant, ε_{rd}, from the relative dielectric constant, ε_{rc}, used for the capacitance between wires and the reference ground plane. The capacitance of a wire to the reference plane is assumed to be the capacitance of the whole wire bundle to the reference plane divided equally to each wire. In other words, the self capacitance is proportional to C_c (note that C_c is not capacitance) where

$$C_c = 1/(n \operatorname{acosh}(2\,h / B)). \tag{5.2}$$

The capacitance between wires is assumed to be the capacitance between two wires with the average spacing of wires in the bundle divided equally to each wire in the bundle. In other words, the mutual capacitance is proportional to C_m where

$$C_m \approx 1/(n \ln(B / d)). \tag{5.3}$$

A slightly more accurate expression for C_m that includes the effect of the bundle being close to the reference plane is given by

$$C_m = 1/(n \ln(B / d)(C_c \ln(B / d) + 1)). \tag{5.4}$$

The per-unit-length admittance parameters are related to the capacitance terms as shown in Figure 5.2. The diagonal term is the sum of the self and mutual capacitive admittance to all other wires. The off diagonal term is the negative of the mutual capacitive admittance between each wire. A dielectric loss tangent L_{te} was included in this study even though dielectric losses are small for insulation used on common aircraft wiring. The loss tangent makes little or no difference in this study, but was included to allow for the possibility of modeling effective losses caused by the scattering from discontinuities in non-smooth ground planes. The effective relative dielectric constant between wires in a bundle depends on how tightly the wires are grouped together. Most wire bundles are tied tightly together so that the effective dielectric constant is almost equal to the dielectric constant of the insulation around each wire. In this study we wanted to include the LRU back plane wiring, which sometimes is not tightly tied over the full run of the wiring. The latter condition was especially true in our laboratory test configuration. The following expression was used to approximate the reduction in dielectric constant for a non tightly grouped bundle

$$\varepsilon_{rd} = \varepsilon_r / (B_t / B + (1 - B_t / B)\,\varepsilon_r) \tag{5.5}$$

where B is the bundle diameter and B_t is the diameter of the same bundle when tightly grouped.

A simple multi-wire configuration, useful for building up more complicated configurations, is shown in Figure 5.3.

The configuration consists of a length of multi-wire transmission line with arbitrary loads at each end and a voltage source at one end. The voltage V_1 and current I_1 at end one are found starting with the definition of the cascade matrix which is given as

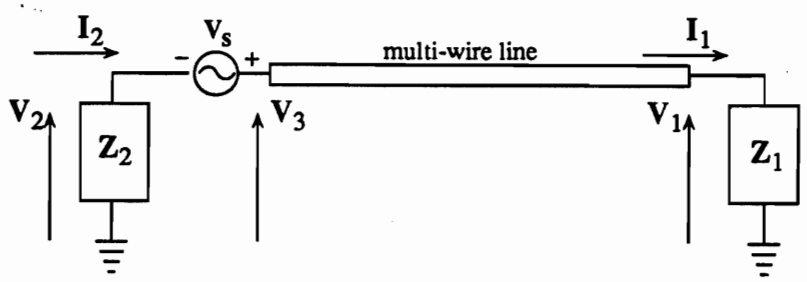

Figure 5.3 Basic multi-wire circuit used to build up more complicated circuits.

$$\begin{bmatrix} V_3 \\ I_2 \end{bmatrix} = \begin{bmatrix} A & B \\ C & D \end{bmatrix} \begin{bmatrix} V_1 \\ I_1 \end{bmatrix}, \tag{5.6}$$

Substituting

$$I_1 = Y_1 V_1 \tag{5.7}$$

and

$$V_3 = V_s - Z_2 I_2 \tag{5.8}$$

into (5.6) and solving for V_1 results in

$$(Z_2(C + DY_1) + A + BY_1)V_1 = V_s \tag{5.9}$$

where **A, B, C** and **D** are the cascade matrix parameters for the multiwire line and Y_1 is the inverse of Z_1. The only additional equations needed are those for impedance and admittance at the input to a multi-wire line. The following 4 equations for input impedance and admittance follow directly from the definition of the cascade matrix and the notation in Figure 5.4.

$$Z_{in} = (AZ + B)(CZ + D)^{-1} \tag{5.10}$$

$$= (A + BY)(C + DY)^{-1} \tag{5.11}$$

$$Y_{in} = (CZ + D)(AZ + B)^{-1} \tag{5.12}$$

$$= (C + DY)(A + BY)^{-1} \tag{5.13}$$

With the above equations it is easy to get solutions for more complex configurations.

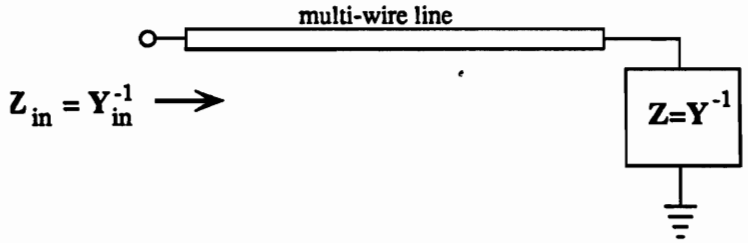

Figure 5.4 Notation for input impedance and admittance of a section of multiwire transmission line.

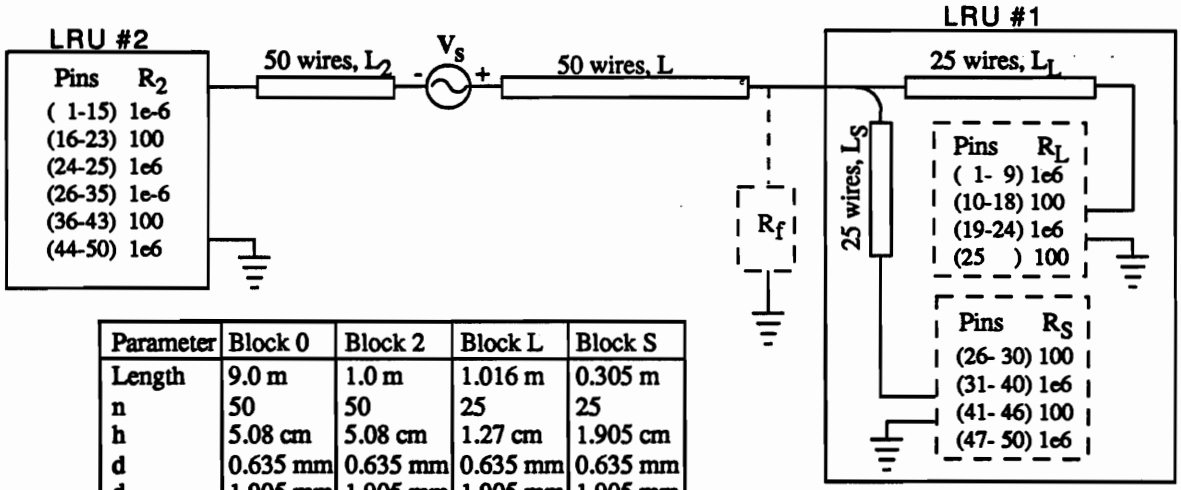

Parameter	Block 0	Block 2	Block L	Block S
Length	9.0 m	1.0 m	1.016 m	0.305 m
n	50	50	25	25
h	5.08 cm	5.08 cm	1.27 cm	1.905 cm
d	0.635 mm	0.635 mm	0.635 mm	0.635 mm
d_w	1.905 mm	1.905 mm	1.905 mm	1.905 mm
B	1.52 cm	1.52 cm	1.27 cm	1.27 cm
ε_{rc}	1.6	1.6	1.0	1.0
ε_{rd}	2.4	2.4	2.4	2.4
L_{te}	0.02	0.02	0.02	0.02
L_{tm}	0.02	0.02	0.02	0.02

Figure 5.5 Random-lay cable model of configuration used in the laboratory.

Figure 5.5 shows the basic model used in this study. The parameter values shown in Figure 5.5 are those used to match the laboratory configuration described in section 3. Load box #1 was modeled with two separate bundles (Block L and S) of 25 wires each. One bundle had a length L_L of 40 inches and the other was shorter with a length L_S of 12 inches. Both bundles are modeled over a ground plane with no wood or other dielectric between the ground plane and bundle. In addition, the shorter bundle was set a little higher above the ground to better match the test configuration. The input admittances for each block in LRU #1, using (5.12), are given as

$$\mathbf{Y_L} = (\mathbf{C_L R_L} + \mathbf{D_L})(\mathbf{A_L R_L} + \mathbf{B_L})^{-1} \tag{5.14}$$

$$\mathbf{Y_S} = (\mathbf{C_S R_S} + \mathbf{D_S})(\mathbf{A_S R_S} + \mathbf{B_S})^{-1} \tag{5.15}$$

where $\mathbf{R_L}$ and $\mathbf{R_S}$ are diagonal matrices with the values on the diagonal as listed in Figure 5.5. The admittance for load box #1 is thus given by

$$\mathbf{Y_1} = \begin{bmatrix} \mathbf{Y_L} & \mathbf{0} \\ \mathbf{0} & \mathbf{Y_S} \end{bmatrix}. \tag{5.16}$$

When fuses are put on the interface at load box #1, then the admittance at the interface becomes

$$\mathbf{Y_{1f}} = \mathbf{Y_1} + \mathbf{Y_f} \tag{5.17}$$

where $\mathbf{Y_f}$ is a diagonal matrix of fuse admittance values. The impedance for the source end of the line, using (5.10), is given by

$$\mathbf{Z_2} = (\mathbf{A_2 R_2} + \mathbf{B_2})(\mathbf{C_2 R_2} + \mathbf{D_2})^{-1}. \tag{5.18}$$

Using the above values of $\mathbf{Y_1}$ and $\mathbf{Z_2}$ in (5.9) and (5.7) results in values of voltage and current at LRU #1 for any given source voltage $\mathbf{V_s}$. Calculations were made for the case of a common mode drive

of one volt on each wire in the bundle to match the condition for lab data shown in section 3. Results for 6 different wires are shown in Figure 5.6 for voltage and Figure 5.7 for current. For comparison the laboratory measurements are shown in the same figures as dotted curves. Even though the random lay model is not expected to match any particular wire in the physical lab model, there is a surprising number of similar properties in the two results.

1. As expected, the random-lay model exactly matches the lab results at low frequency for wires with a finite resistance at the source end of the cable. The two cases that do not match are those with an open circuit in load box #2. They do not match because the responses in the open-cirucit case depend more on the relative wire-lay positions. The random-lay model differs in detail from the lay in the lab cable.
2. The random-lay model does an excellent job of showing the reduction in response as frequency is increased starting at about 0.1 MHz. This reduction does not occur in single-wire transmission lines.
3. A single-wire transmission line has a strong resonance (increase in response) when its length is .25 wavelengths (4 to 5 MHz for cable in this study) but, as shown in Figures 5.6 and 5.7 for both the lab measurements and the random-lay model, that resonance is suppressed in the multi-wire line.
4. Both lab and random-lay models show a strong half-wavelength resonance (approximately 10 MHz) for all 6 wires.
5. A general reduction in response at about 60 MHz is also predicted by the random lay model.

The random-lay model calculations differ from the lab measurements at frequencies above 80 MHz, probably because the random-lay model does not include details of box grounding, connector wiring and load resistances. The above comparisons show that the random-lay model contains all the necessary relationships to show the effects of fusing all the wires at a connector interface to an LRU.

As explained in section 3 it is useful to determine peak response when the source is a damped sine pulse. This procedure serves as a filter that tends to smooth out the wide variations seen in the frequency domain data and produce results more closely related to an EMP response. Figure 5.8 shows the peak damped sine response for damped sine frequencies between 1 MHz and 100 MHz for the same transfer function shown in Figure 5.6.

The process for determining fuse loading from the random-lay model is the same as described in section 3 for lab measurements. The transfer voltage and peak damped sine response are calculated for a LRU interface without fuses and then with fuses. The loading is defined as the ratio of peak damped sine response with fuses to the peak damped sine response without fuses. As an example the response calculations for the lab configuration model shown in Figure 5.5 are shown in Figures 5.9 – 5.18. The voltage transfer function and peak damped sine responses are shown in Figures 5.9 and 5.10. The voltage transfer function and damped sine loading for 50-ohm, 100-ohm, 200-ohm and 400-ohm fuses are shown in Figures 5.11 – 5.18. To summarize the large amount of data shown in the above figures, the mean and standard deviation of the loading data were calculated and are listed on the figures showing the damped sine loading. The statistical moments were calculated using the dB values of all the data shown on each graph, i.e., each curve is made from 60 frequency points distributed logarithmically from 1 MHz to 100 MHz. There are 6 curves for a total of 360 points. The loading for this configuration is further summarized in Figure 5.19, which shows a plot of the mean loading values and the mean plus and minus one standard deviation as a function of fuse resistance. The mean and standard deviation data should be used with caution because they tend to hide the

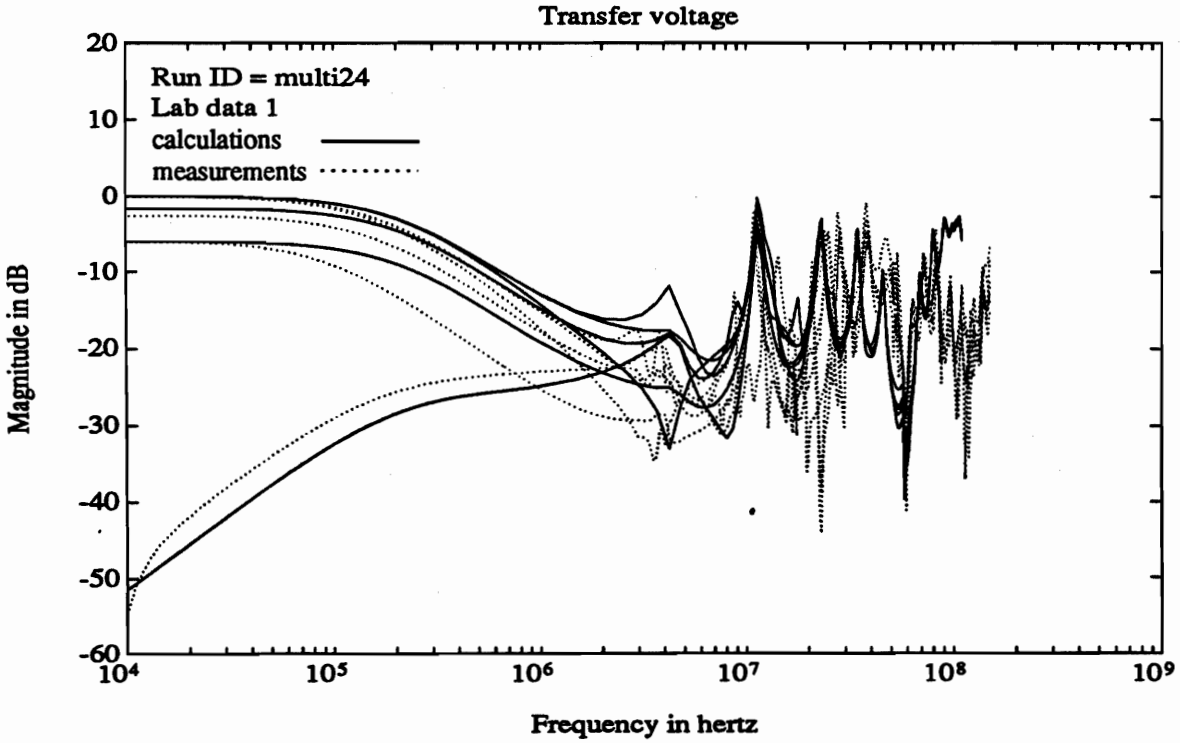

Figure 5.6 Comparison of voltage transfer functions for data measured in the lab (dotted curves) and calculations on a random-lay model (solid curves).

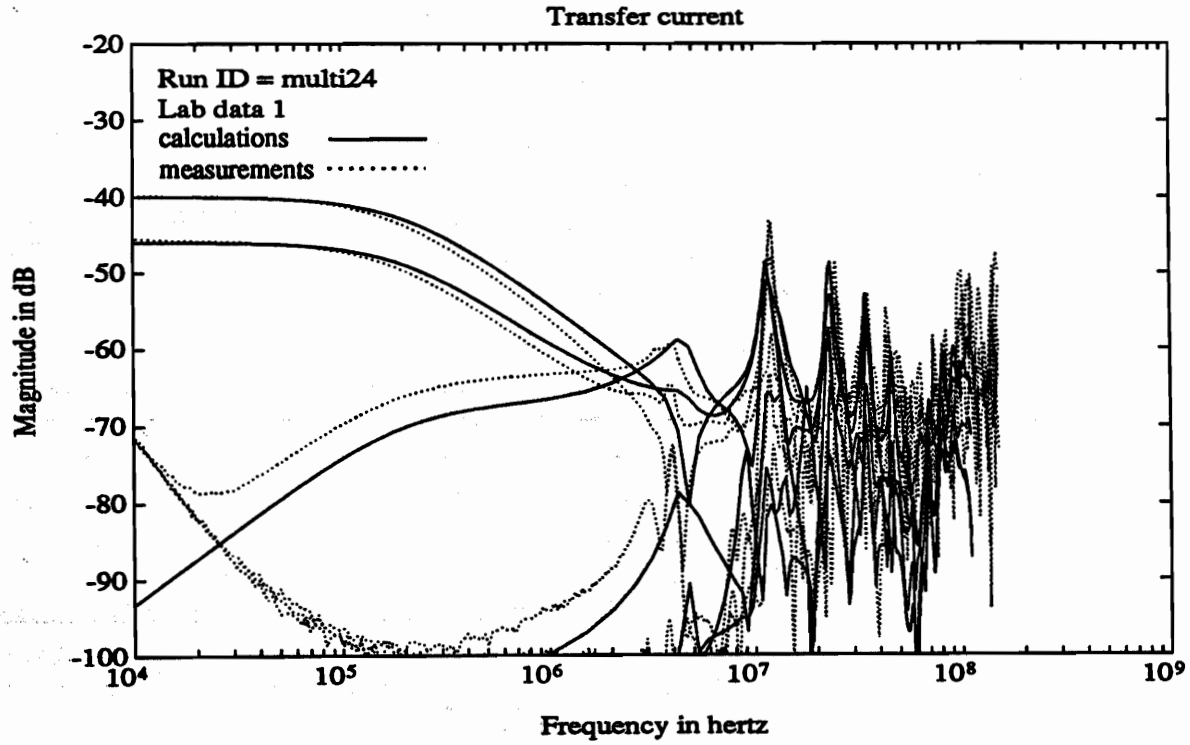

Figure 5.7 Comparison of current transfer functions for data measured in the lab (dotted curves) and calculations on a random-lay model (solid curves).

variations with frequency. Most of the results show greater variation at the lower frequencies. Even so, the above mean is a reasonable value to use to compare various configuration changes. Similar calculations have been made on several different configurations. Models used for 25-wire cables are shown in Figure 5.20 and for 12-wire cables in Figure 5.21. A code (Run ID) that relates calculated results to a particular configuration is listed in Table 5.1. Representative calculations for various models are shown in Figures 5.22 through 5.73. A summary of the results is shown in Table 5.2, which lists the mean values of loading for a 100-ohm fuse for each model calculated.

Table 5.1 Code for calculated results

Run ID	Model Description		
multi24	Figure 5.5	L = 9.0 m	L_2 = 1.0 m
multi22	Figure 5.5	L = 5.0 m	L_2 = 5.0 m
multi23	Figure 5.5	L = 0.1 m	L_2 = 9.1 m
multi25	Figure 5.20	L = 9.0 m	L_2 = 1.0 m
multi26	Figure 5.20	L = 5.0 m	L_2 = 5.0 m
multi27	Figure 5.20	L = 0.1 m	L_2 = 9.1 m
multi28	Figure 5.5	L = 9.0 m	L_2 = 1.0 m

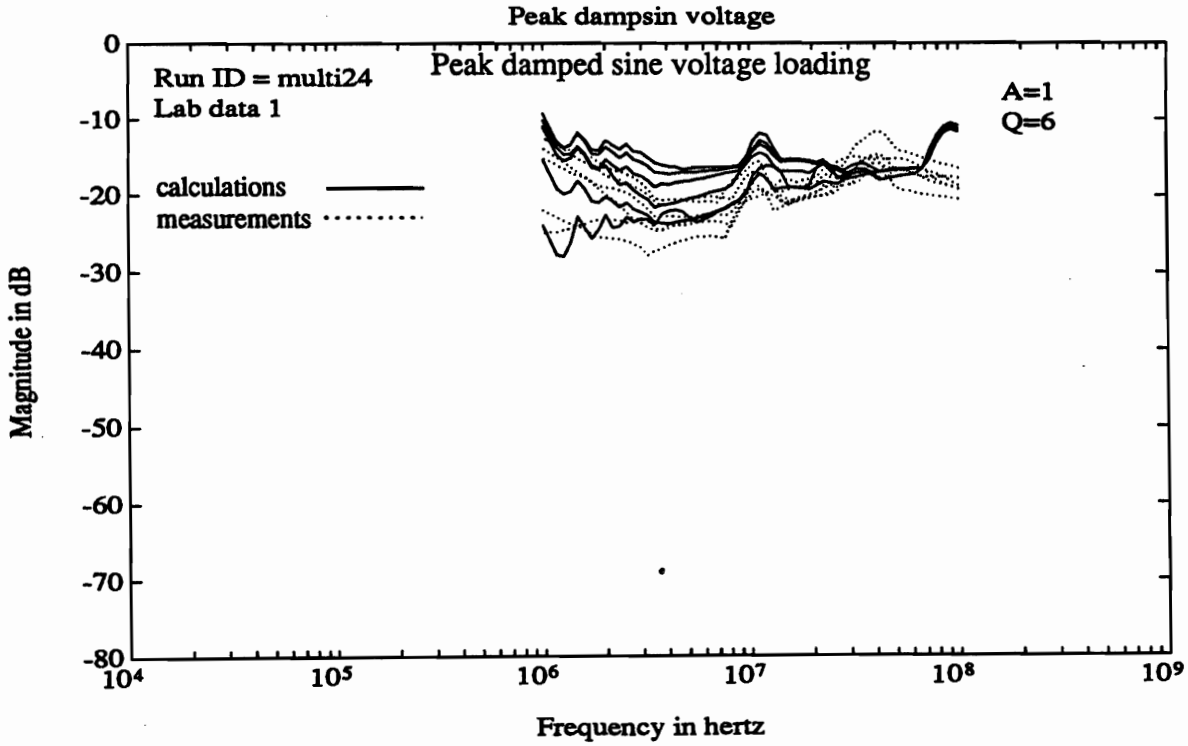

Figure 5.8 Comparison of peak damped-sine voltage responses for measurements from the lab (dotted curves) and calculations on a random-lay model (solid curves).

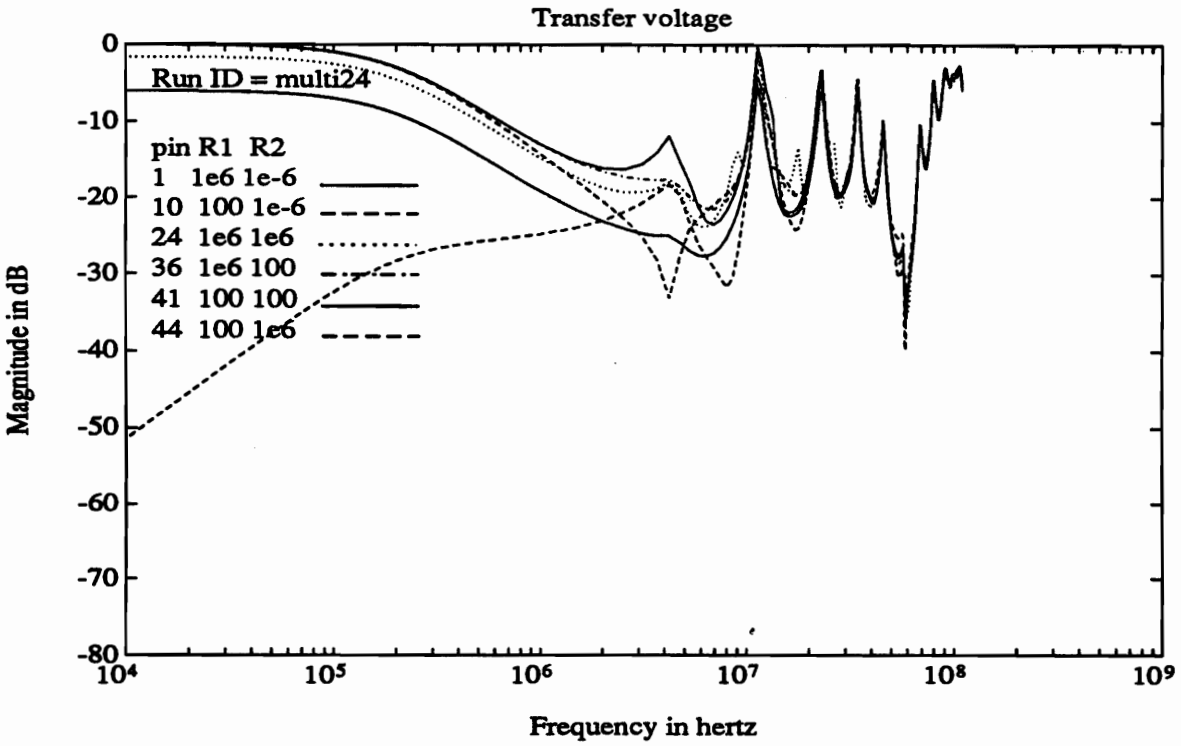

Figure 5.9 Transfer voltage for 50-wire cable with no fuses.

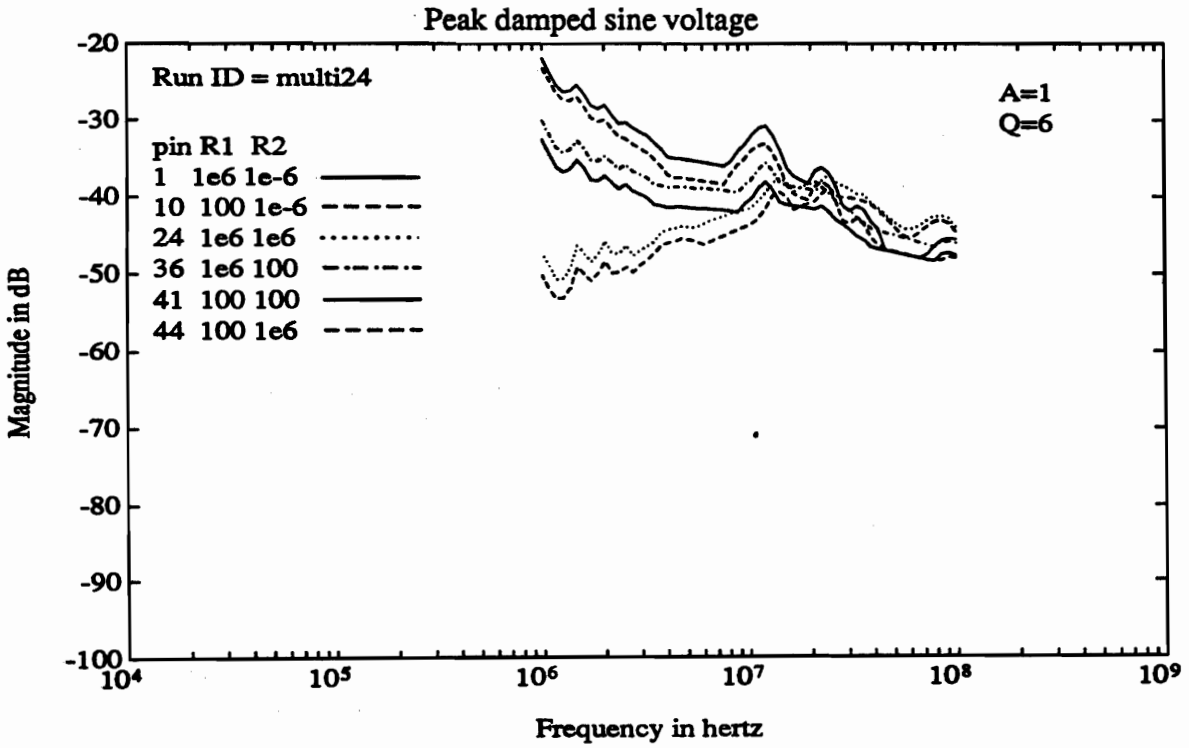

Figure 5.10 Peak damped-sine voltage response for 50-wire cable with no fuses.

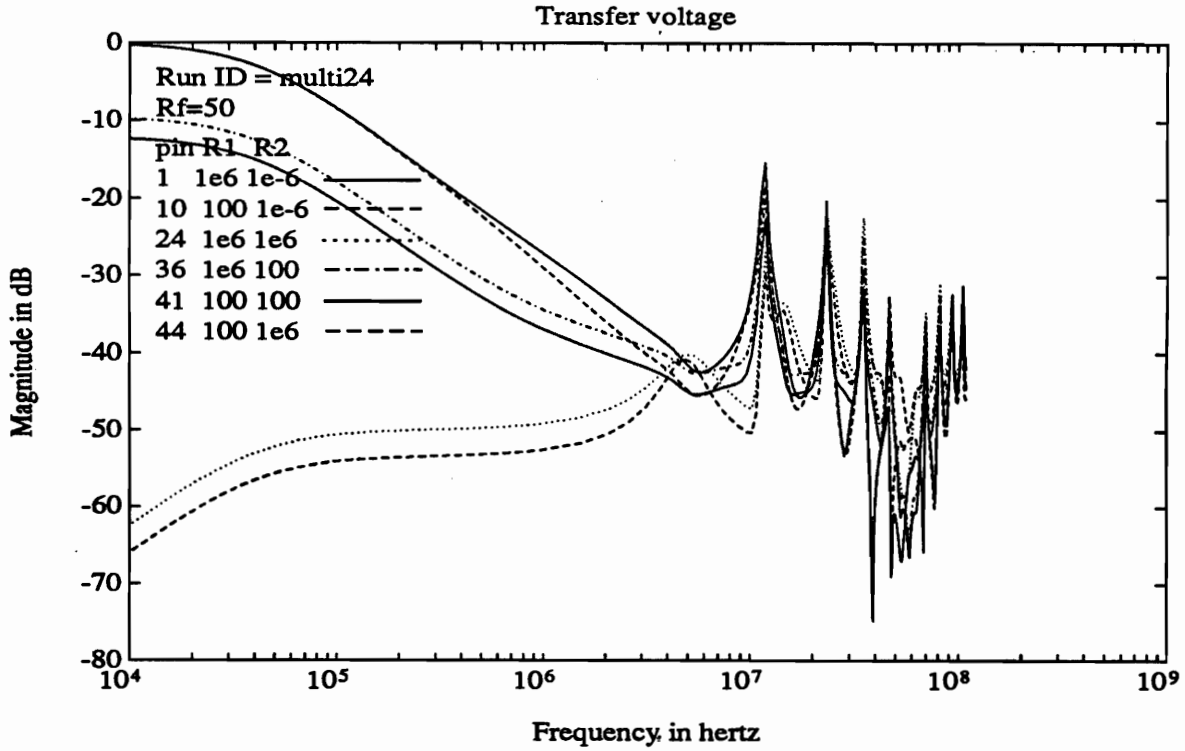

Figure 5.11 Transfer voltage for 50-wire cable with 50-ohm fuses.

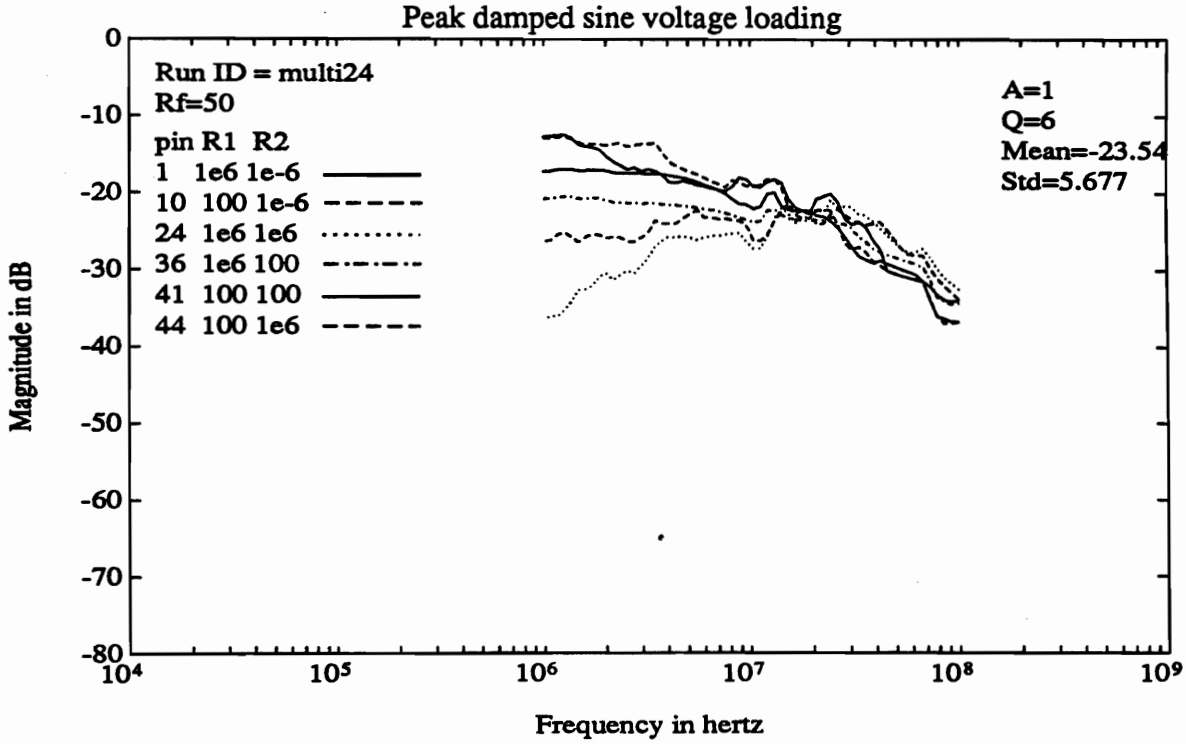

Figure 5.12 Peak damped-sine loading for 50-wire cable with 50-ohm fuses.

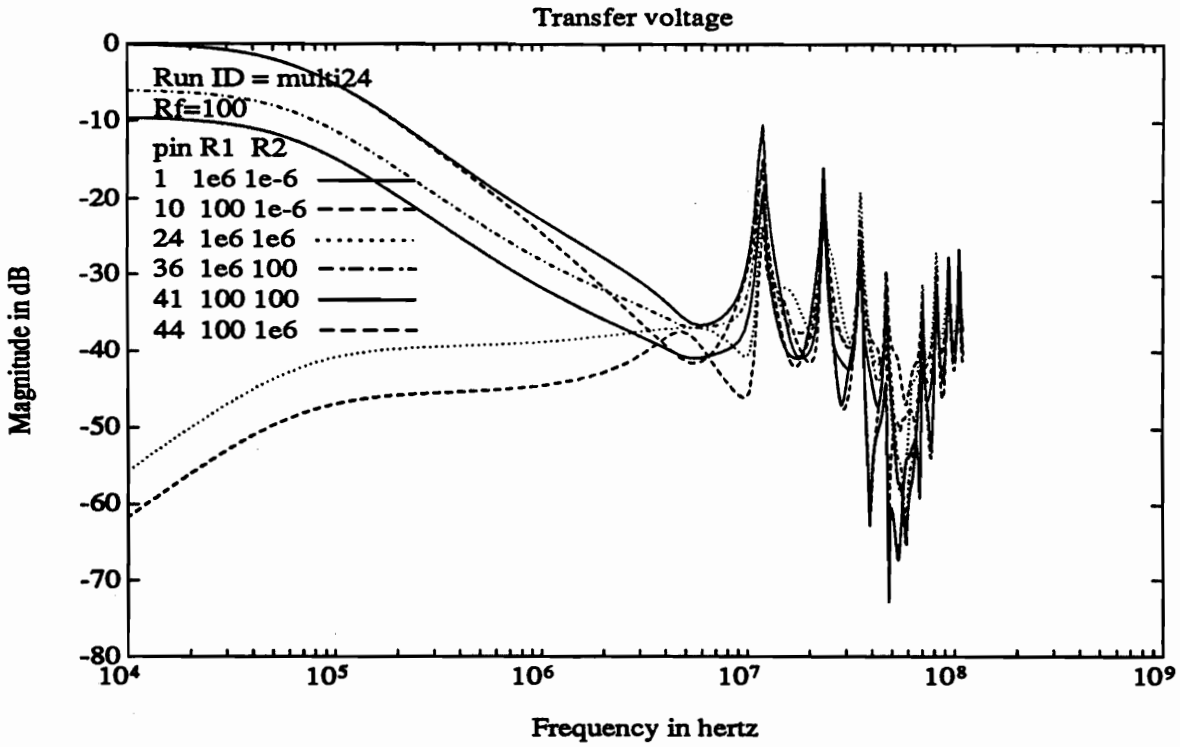

Figure 5.13 Transfer voltage for 50-wire cable with 100-ohm fuses.

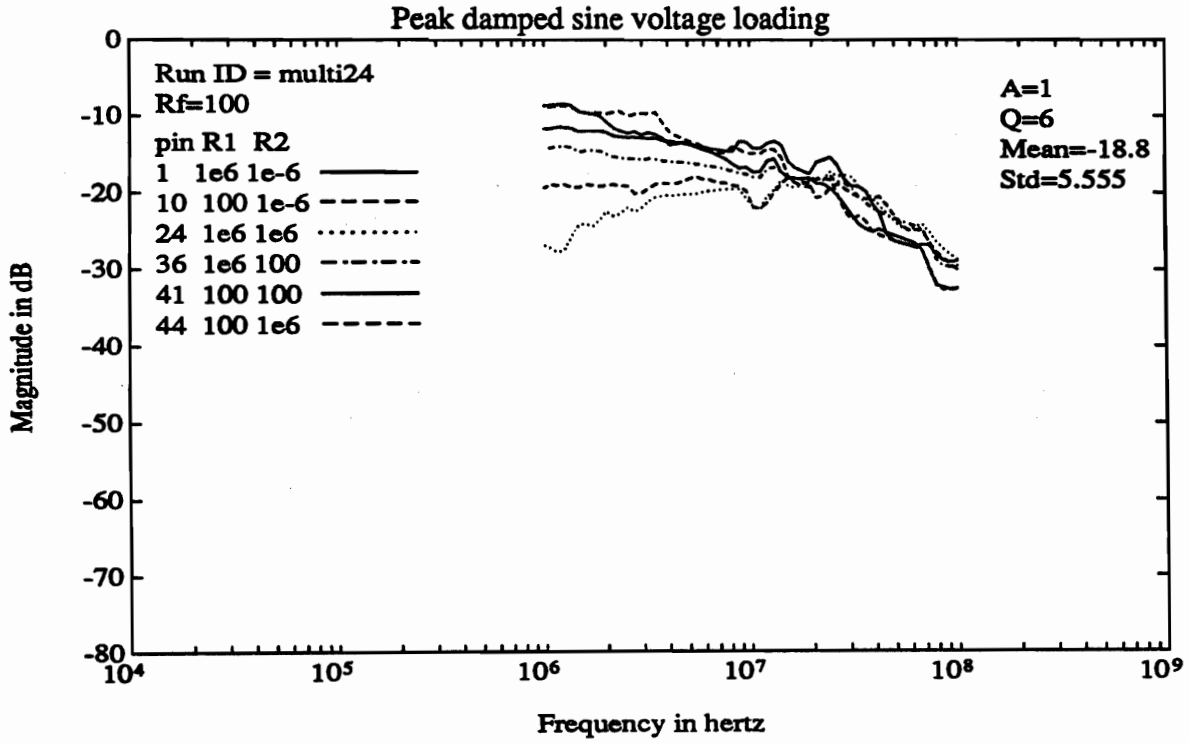

Figure 5.14 Peak damped-sine loading for 50-wire cable with 100-ohm fuses.

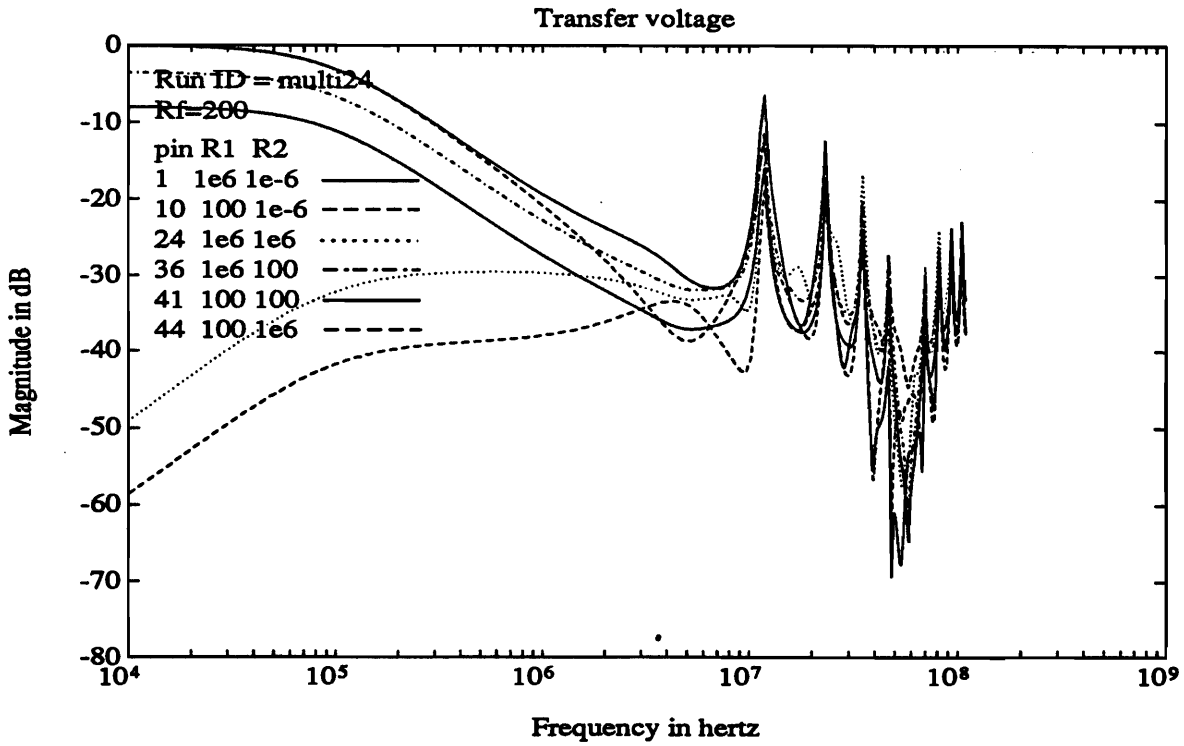

Figure 5.15 Transfer voltage for 50-wire cable with 200-ohm fuses.

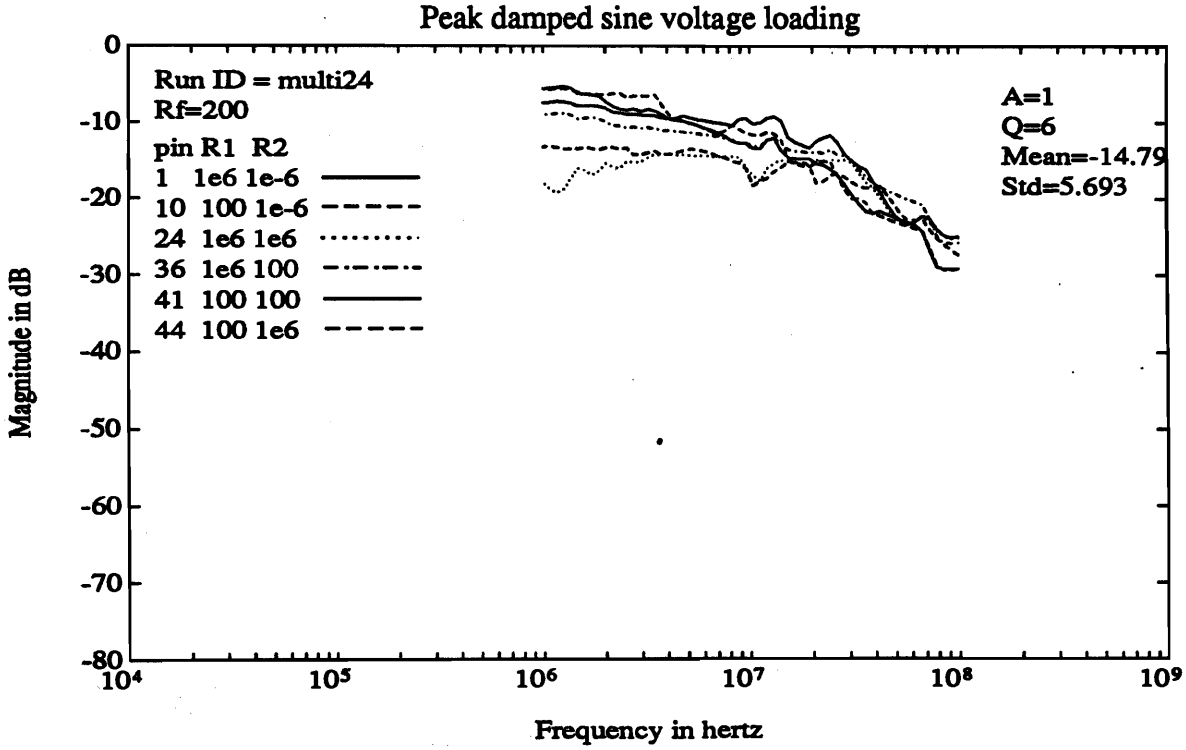

Figure 5.16 Peak damped-sine loading for 50-wire cable with 200-ohm fuses.

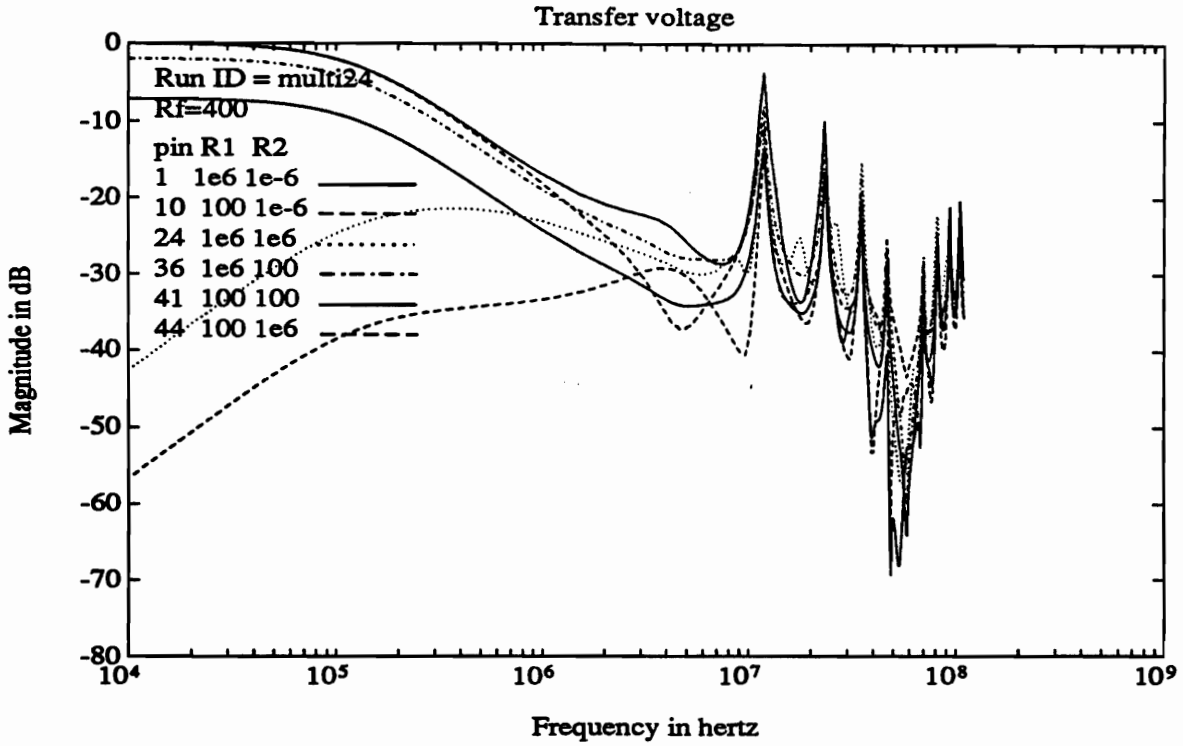

Figure 5.17 Transfer voltage for 50-wire cable with 400-ohm fuses.

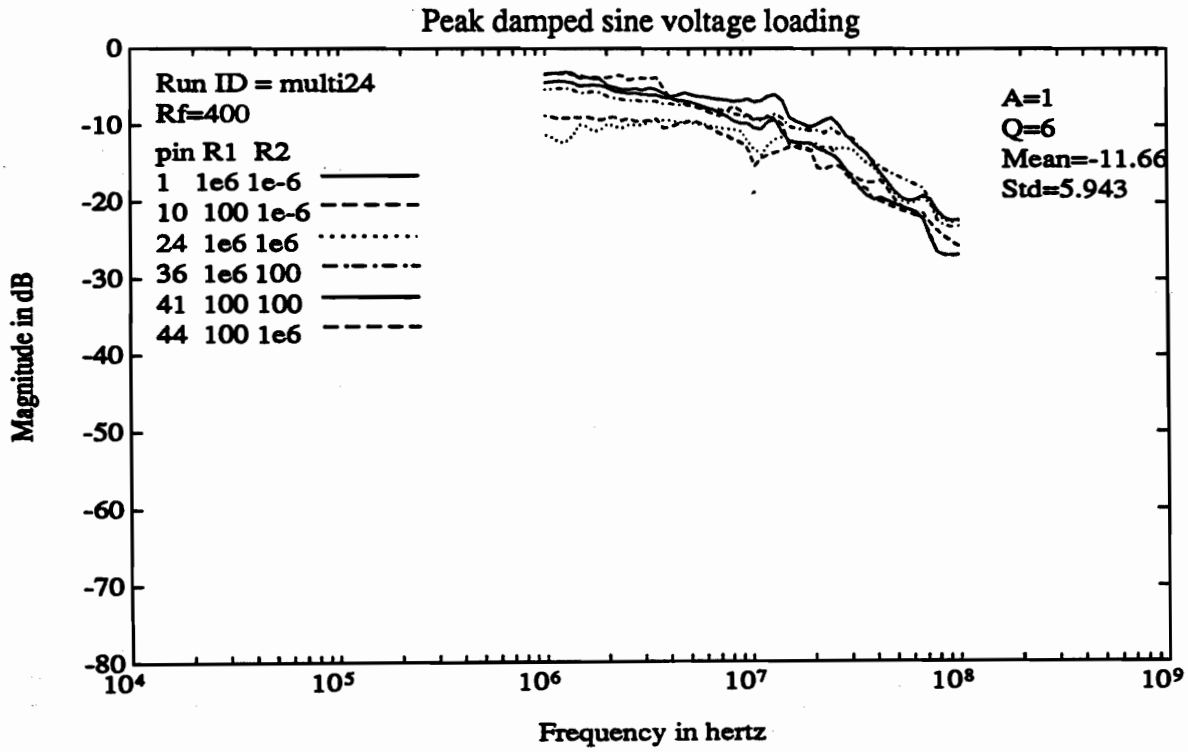

Figure 5.18 Peak damped-sine loading for 50-wire cable with 400-ohm fuses.

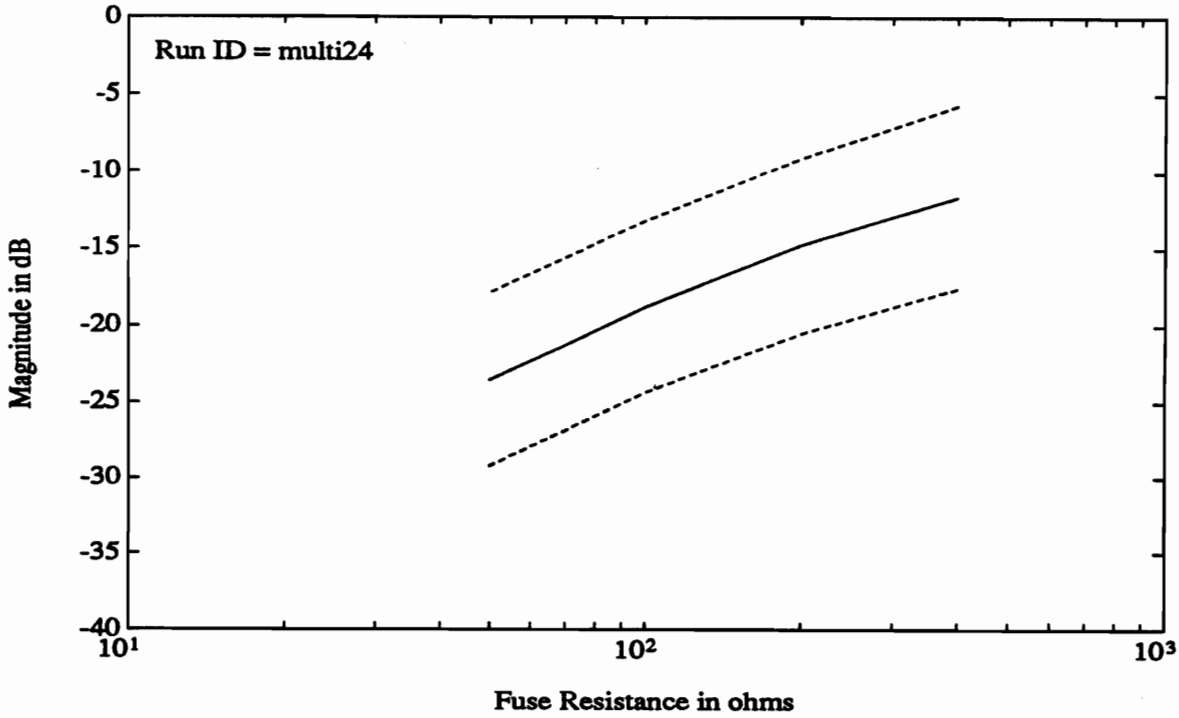

Figure 5.19 Mean and standard deviation of fuse loading for 50-wire cable.

Table 5.2 Summary of fuse loading.

Model	Number of Wires	Drive Location	Mean Loading 100 ohm Fuse
multi24	50	LRU #2	-18.8 dB
multi22	50	Middle	-19.0 dB
multi23	50	LRU #1	-18.0 dB
multi25 case L	25	LRU #2	-20.1 dB
multi25 case S	25	LRU #2	-15.7 dB
multi26 case L	25	Middle	-20.9 dB
multi26 case S	25	Middle	-15.8 dB
multi27 case L	25	LRU #1	-19.6 dB
multi27 case S	25	LRU #1	-14.8 dB
multi28 case L	12	LRU #2	-16.3 dB
multi28 case S	12	LRU #2	-13.2 dB

It was shown in Section 2 that the loading is dependent on the voltage across every fuse at an interface. This means that loading is dependent on the location of the voltage source. To check out the importance of source location the same model was used with the source at three different locations as indicated in Table 5.1. Comparison of the transfer voltage without fuses shown in Figures 5.9, 5.22 and 5.33 show that there are large differences with location of the source. For example, when the cable is driven at its middle, the 10-MHz and 30-MHz resonances are missing and the null at 60 MHz is missing. Even so, the peak damped sine loading is almost the same for all three locations. The mean value for the loading by a 100-ohm fuse is within 1 dB for the three locations. The same is true for the L and S case of the 25-wire models. This is an indication that fuse loading might be insensitive of source location for common mode drives. Further investigation would be needed to make a statement about differential drives.

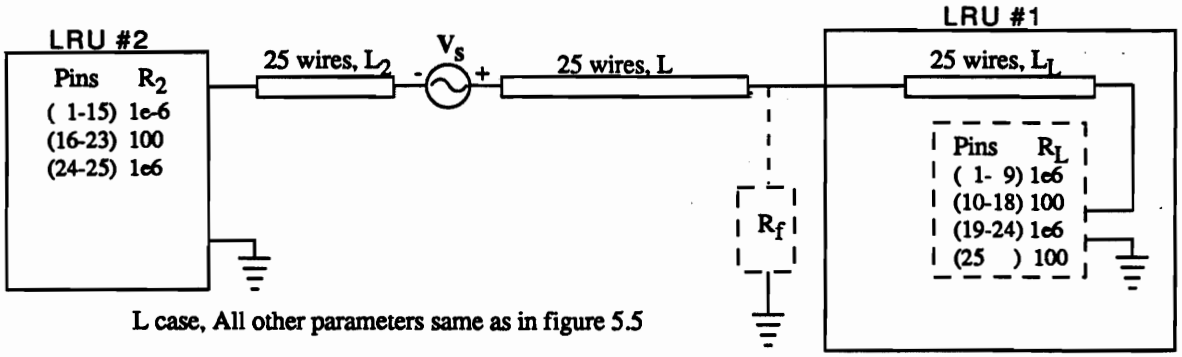

L case, All other parameters same as in figure 5.5

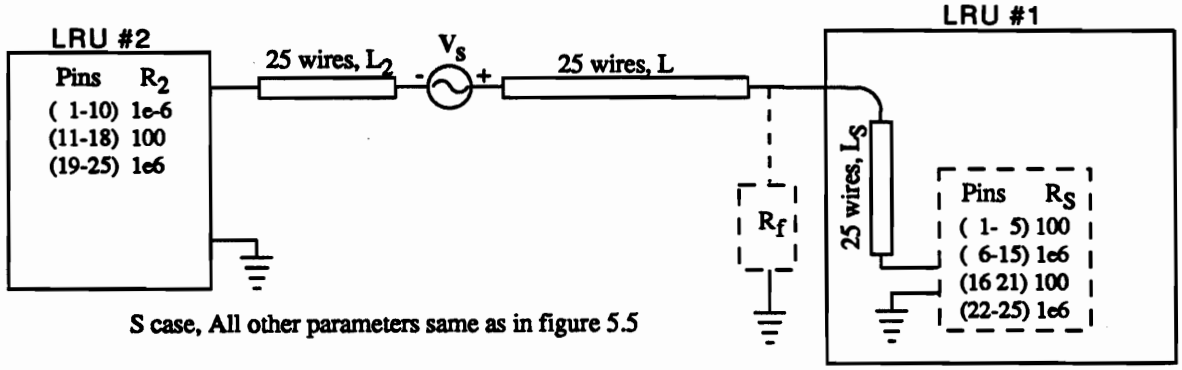

S case, All other parameters same as in figure 5.5

Figure 5.20 Random lay models for cables with 25 wires.

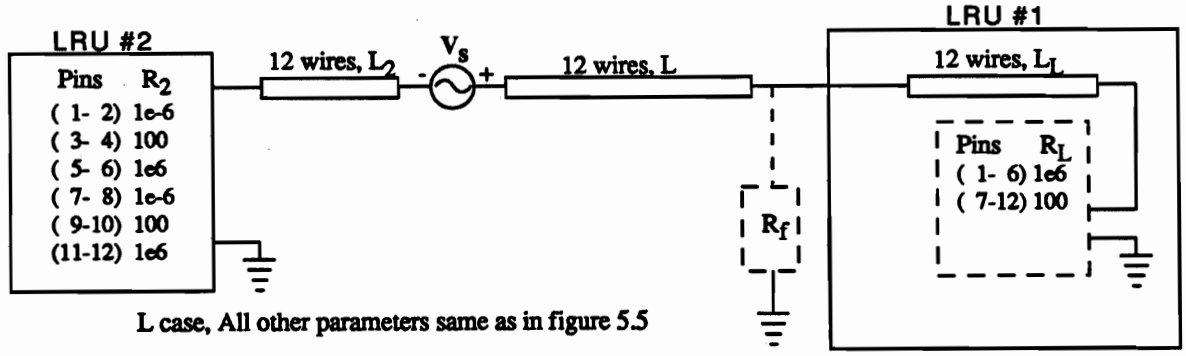

L case, All other parameters same as in figure 5.5

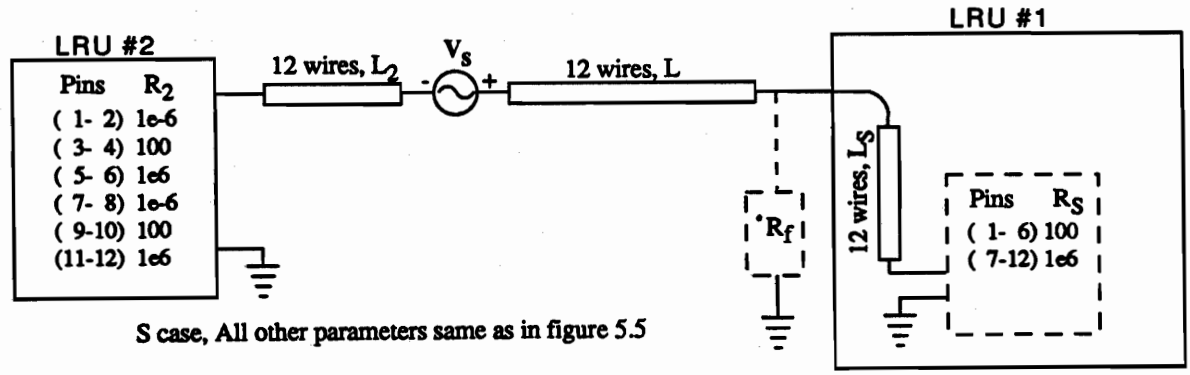

S case, All other parameters same as in figure 5.5

Figure 5.21 Random-lay models for cables with 12 wires.

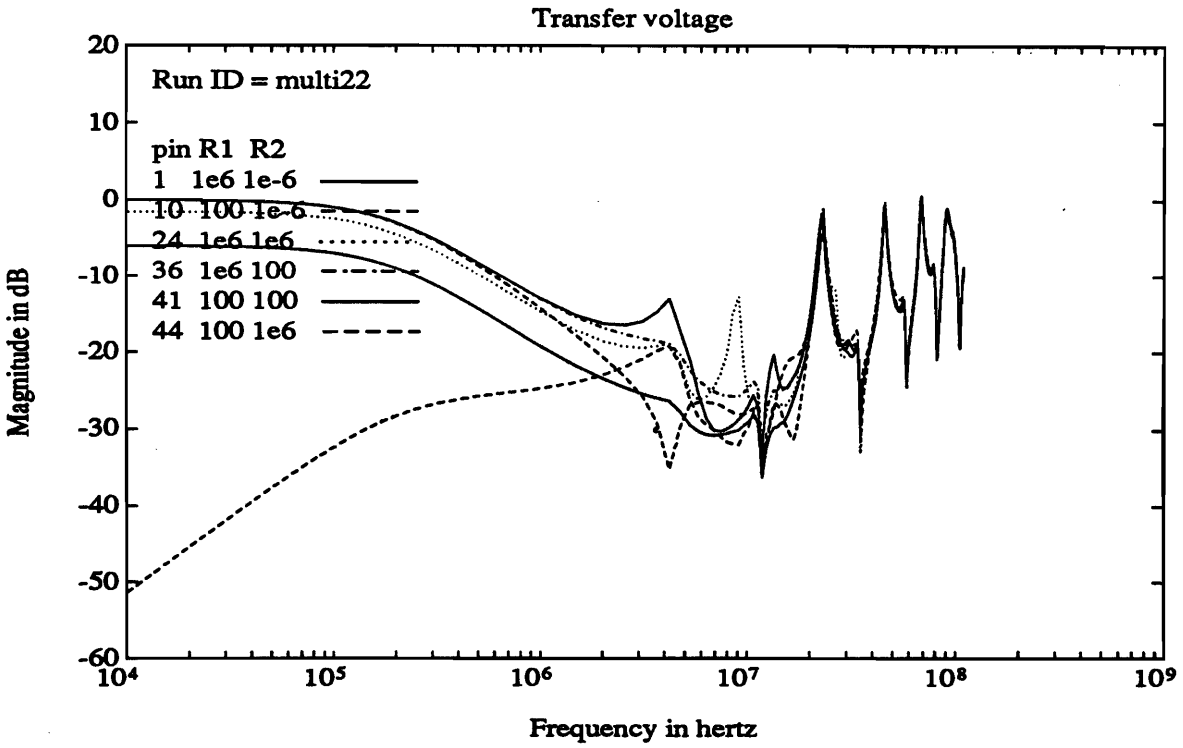

Figure 5.22 Transfer voltage for 50-wire cable with no fuses.

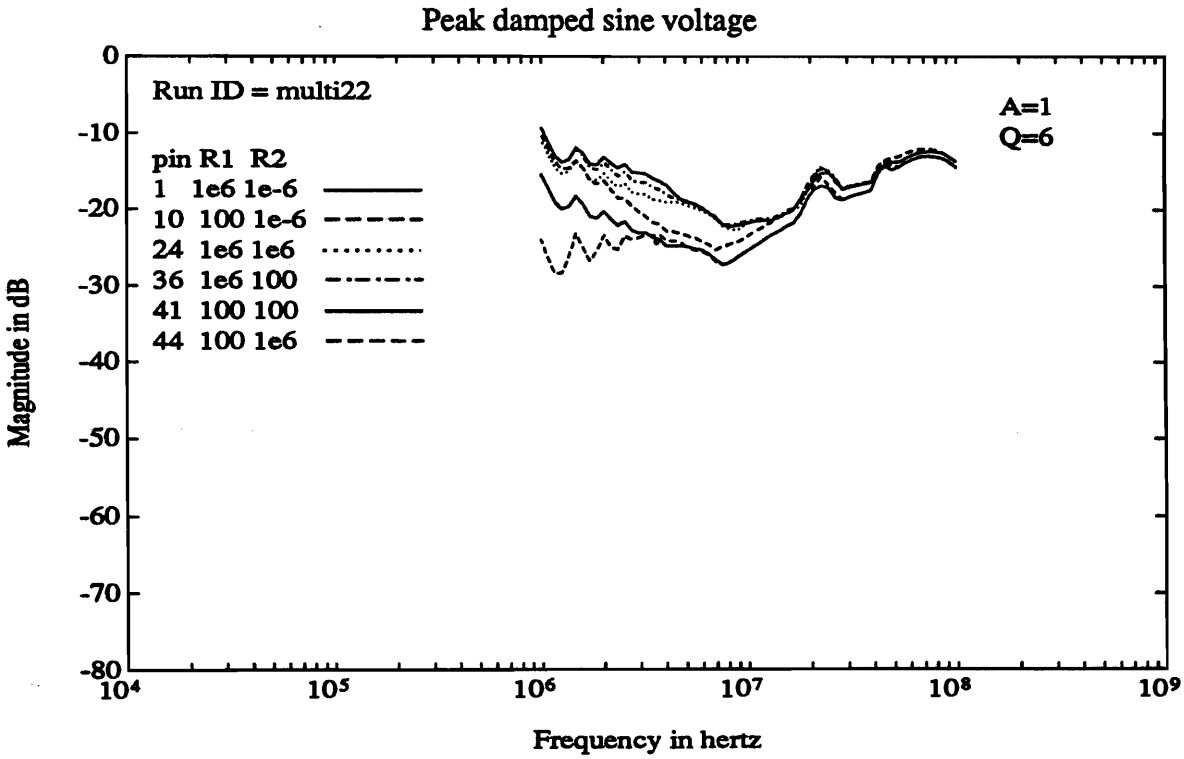

Figure 5.23 Peak damped-sine voltage response for 50-wire cable with no fuses.

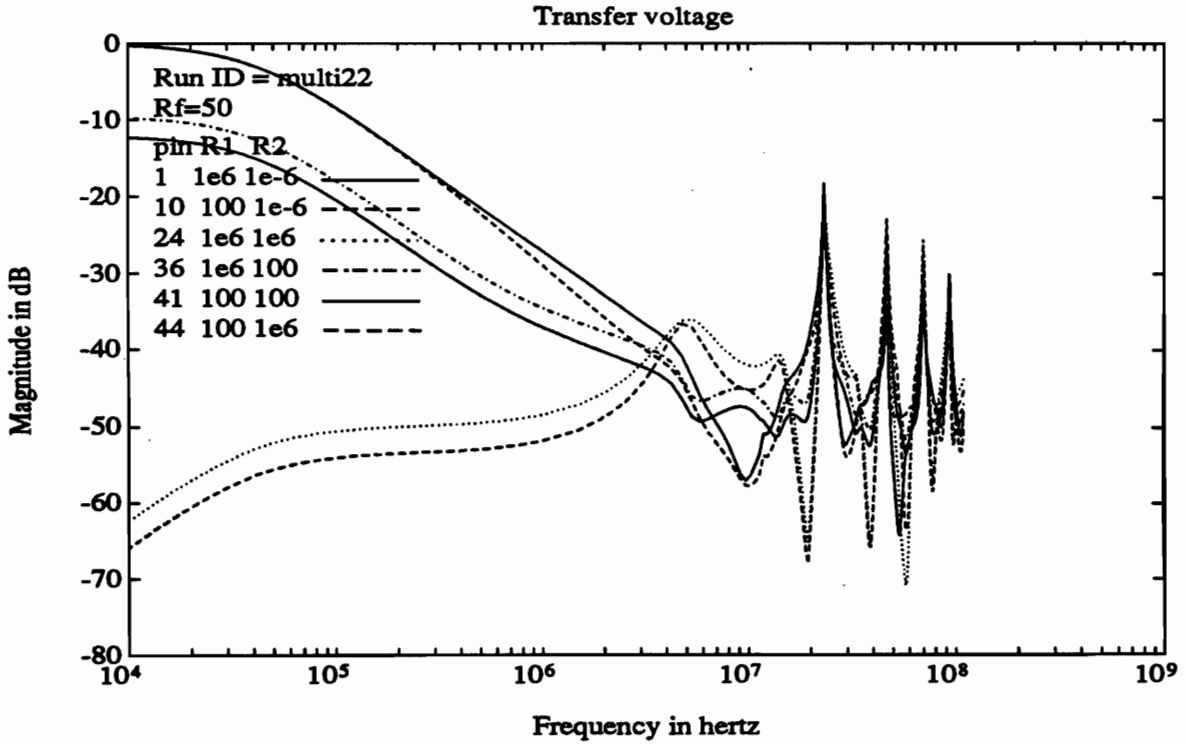

Figure 5.24 Transfer voltage for 50-wire cable with 50-ohm fuses.

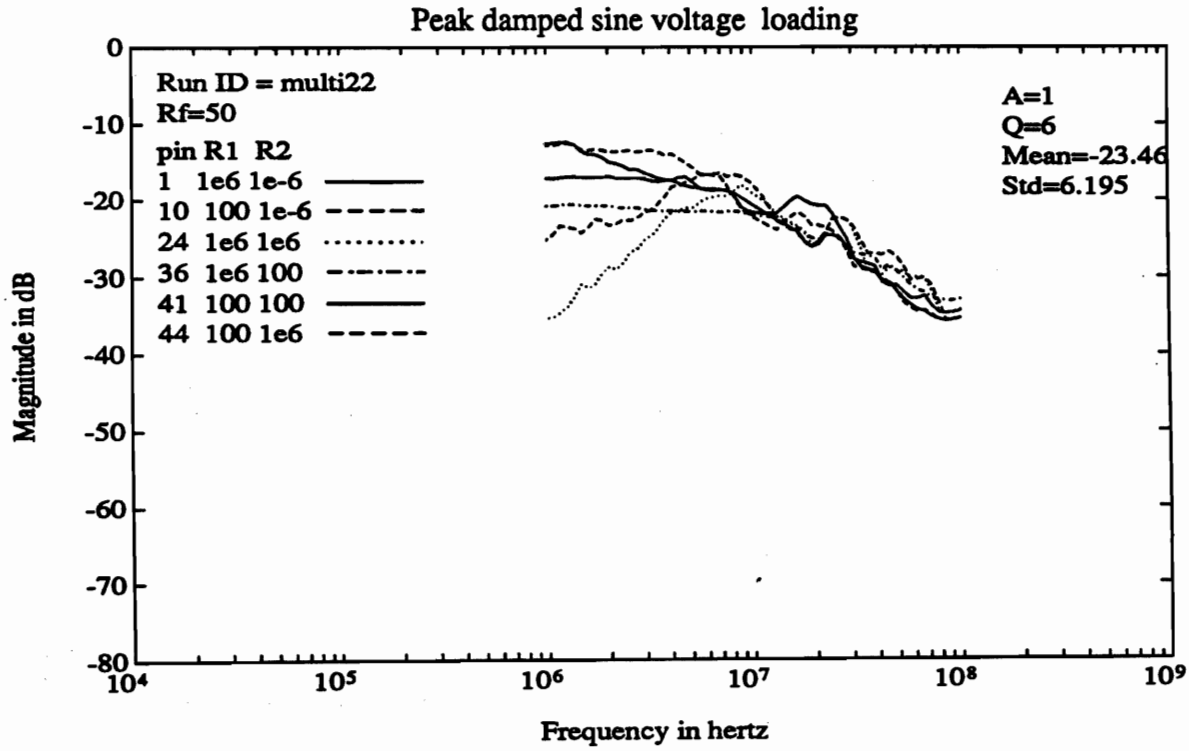

Figure 5.25 Peak damped-sine loading for 50-wire cable with 50-ohm fuses.

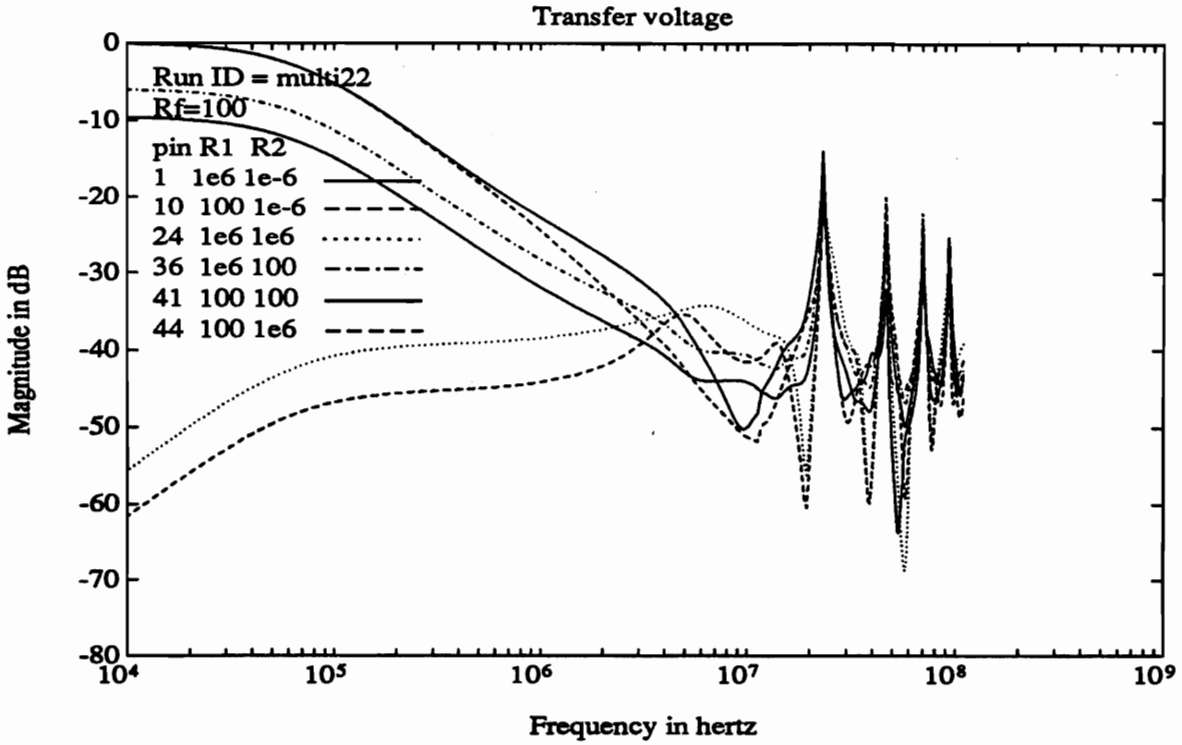

Figure 5.26 Transfer voltage for 50-wire cable with 100-ohm fuses.

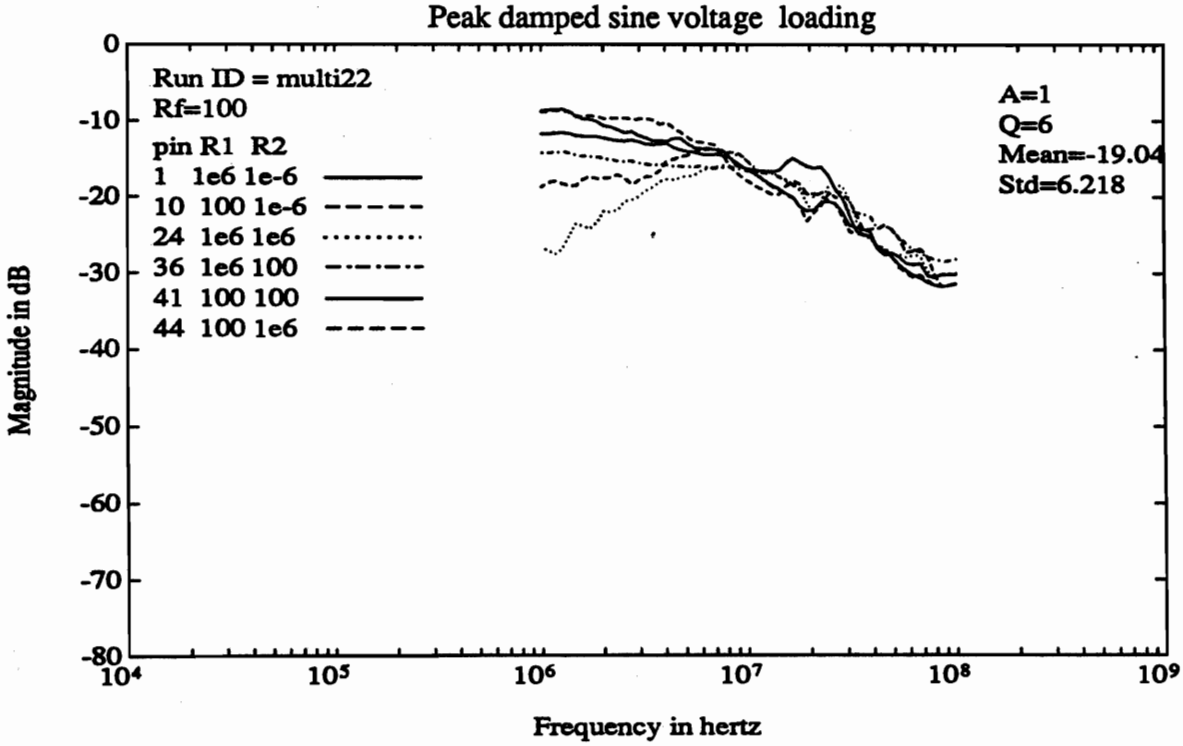

Figure 5.27 Peak damped-sine loading for 50-wire cable with 100-ohm fuses.

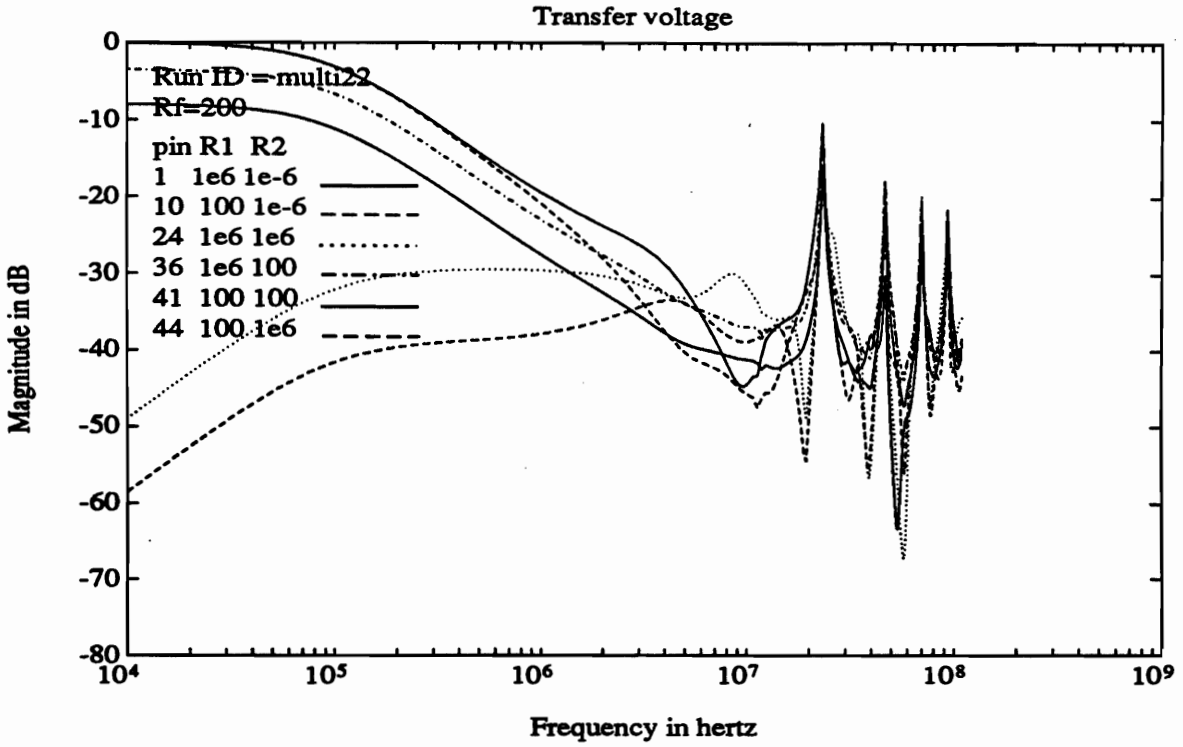

Figure 5.28 Transfer voltage for 50-wire cable with 200-ohm fuses.

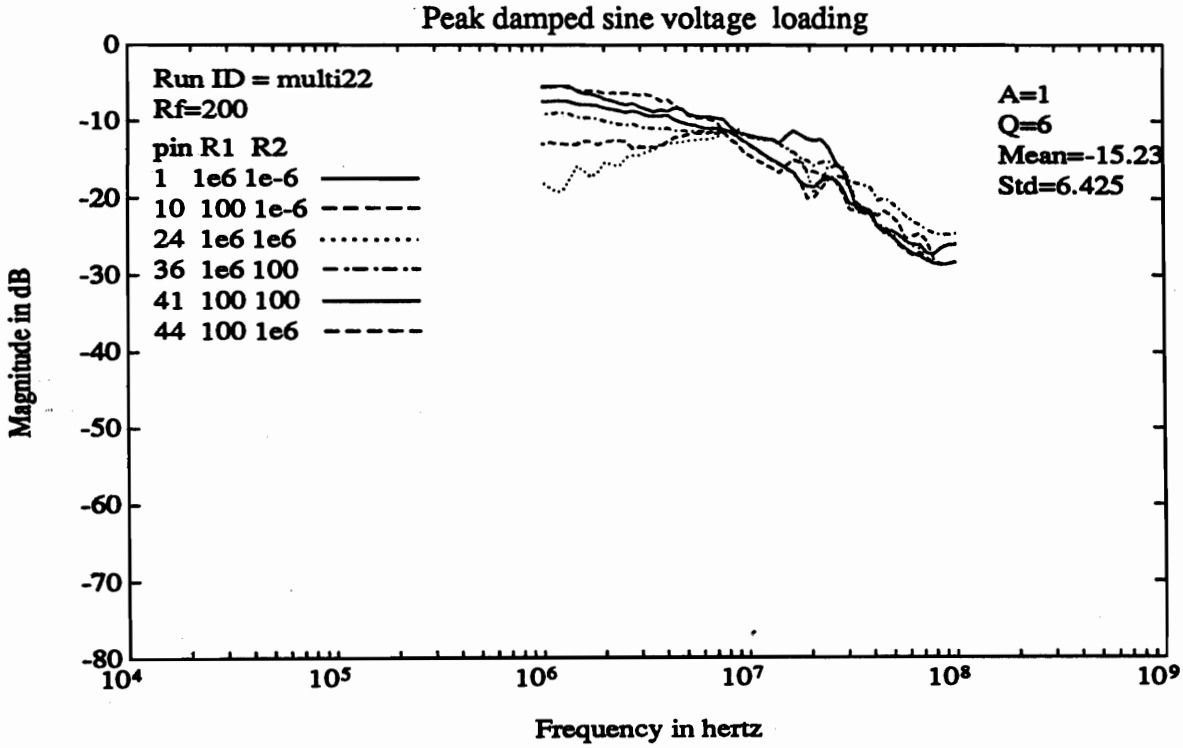

Figure 5.29 Peak damped-sine loading for 50-wire cable with 200-ohm fuses.

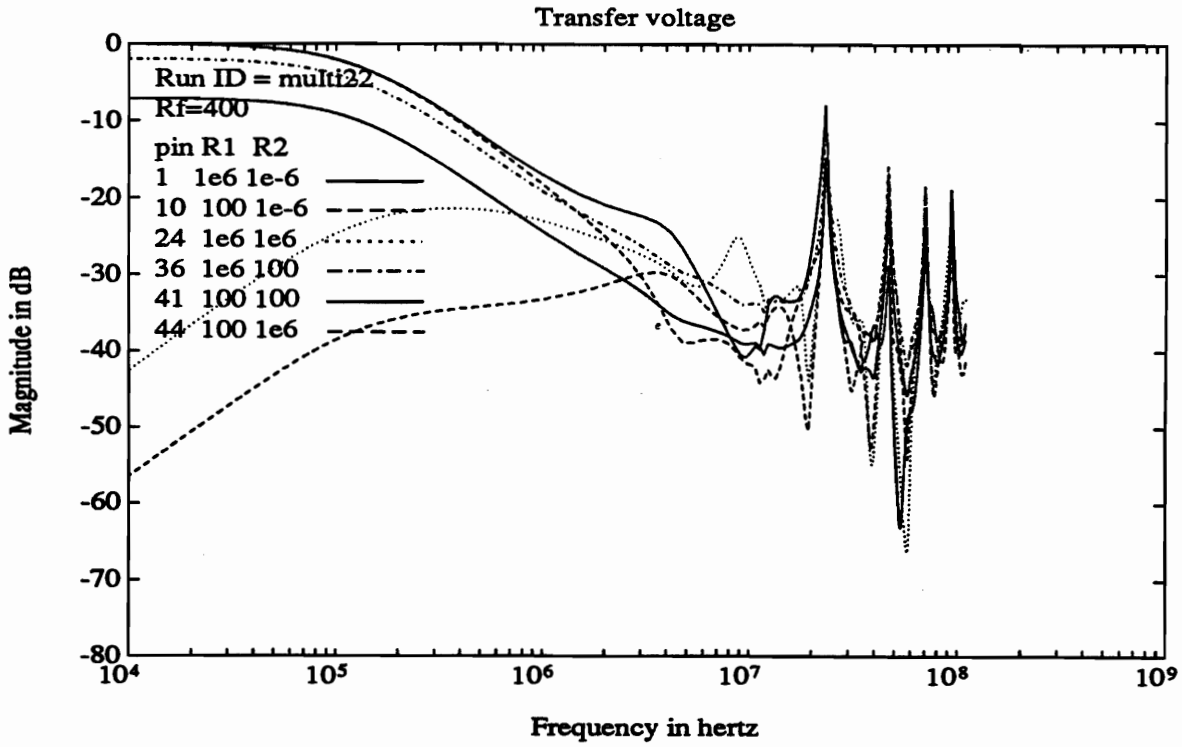

Figure 5.30 Transfer voltage for 50-wire cable with 400-ohm fuses.

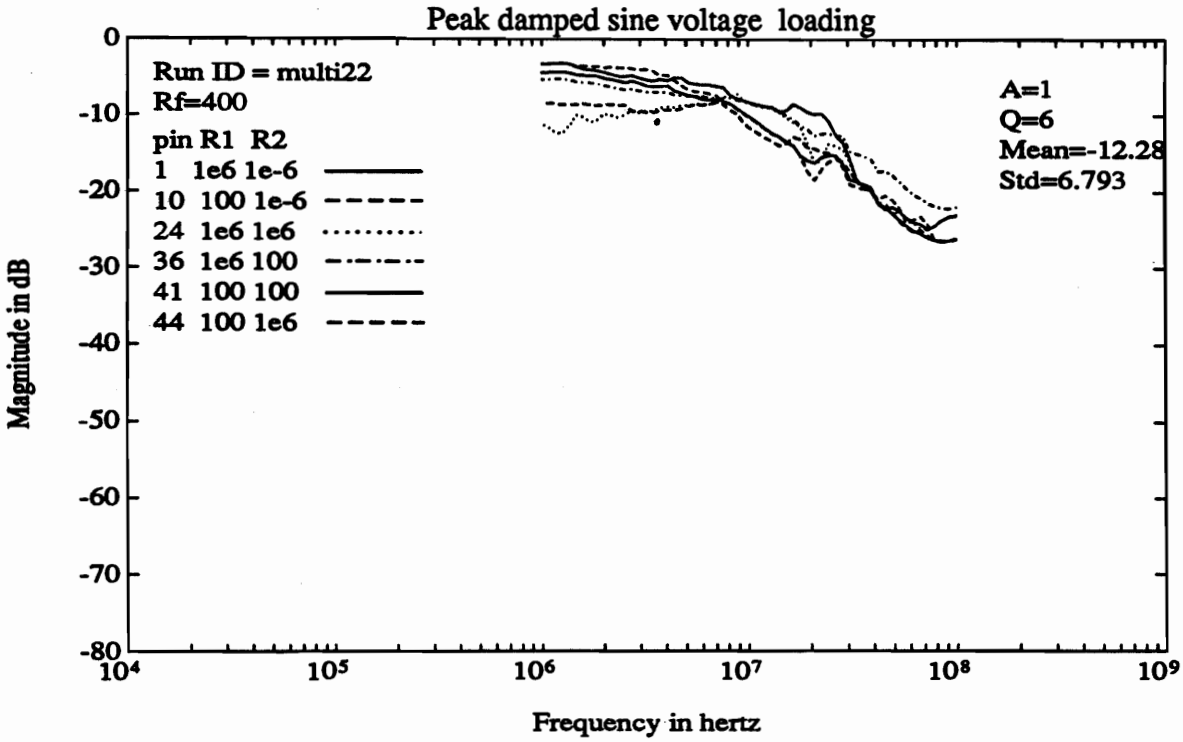

Figure 5.31 Peak damped-sine loading for 50-wire cable with 400-ohm fuses.

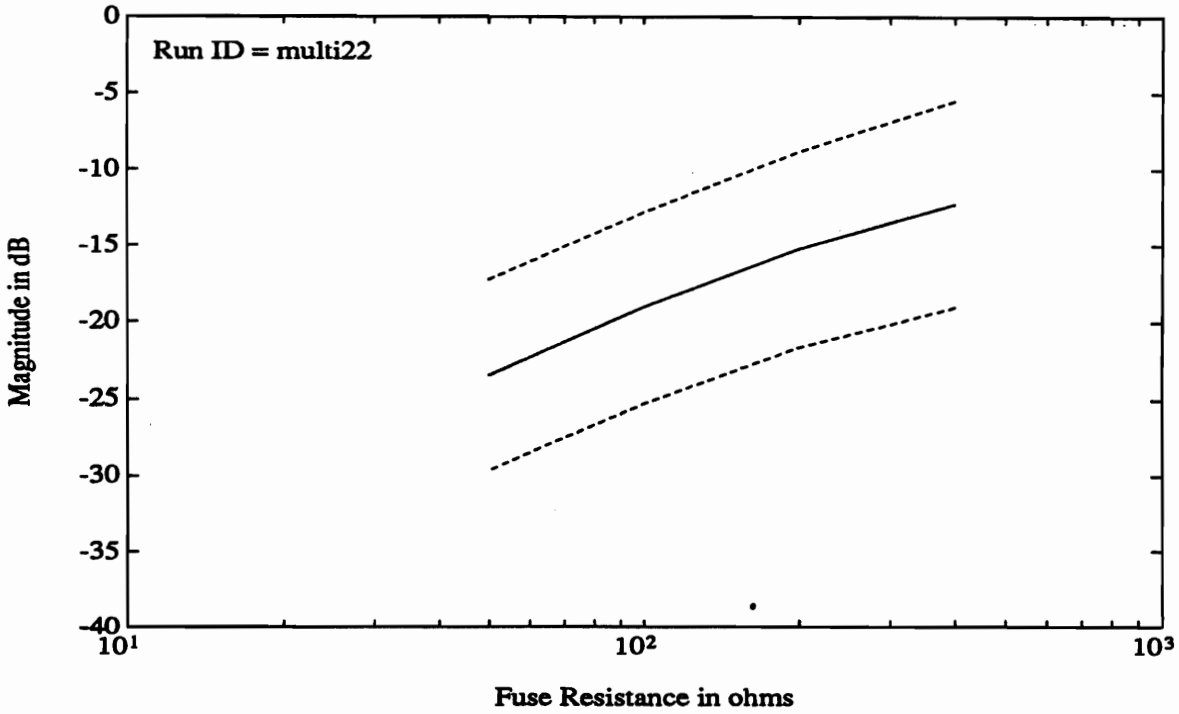

Figure 5.32 Mean and standard deviation of fuse loading for 50-wire cable.

The loading is apparently not directly proportional to the number of wires in a bundle. The mean values in Table 5.2 show only a 3 to 6 dB reduction from 50 wires to 12 wires. The L case for 25 wires shows no reduction from the 50 wire case and the S case for 25 wires shows only a 3 to 4 dB reduction. There is clearly a general trend in the data that shows the loading effect is reduced when the number of wires is reduced but the effect is small. This matches the results from the EMPTAC #7 tests where some of the results showed loading on a 6-wire cable to be as much as found on a 50-wire cable.

The effect of different load impedance is difficult to assess because there is such a large number of possibilities. The only calculations that relate to this are those made on the 25-wire cable. The data in Table 5.2 show that the mean values of loading differ by about 5 dB between the case L and the case S models. The change in load impedance might also be the reason that loading on the 12-wire case S cable was only about 2 dB below the 25-wire case S. This result is insufficient to draw any conclusions about loading based on termination impedance but is an indication that the variation could be large.

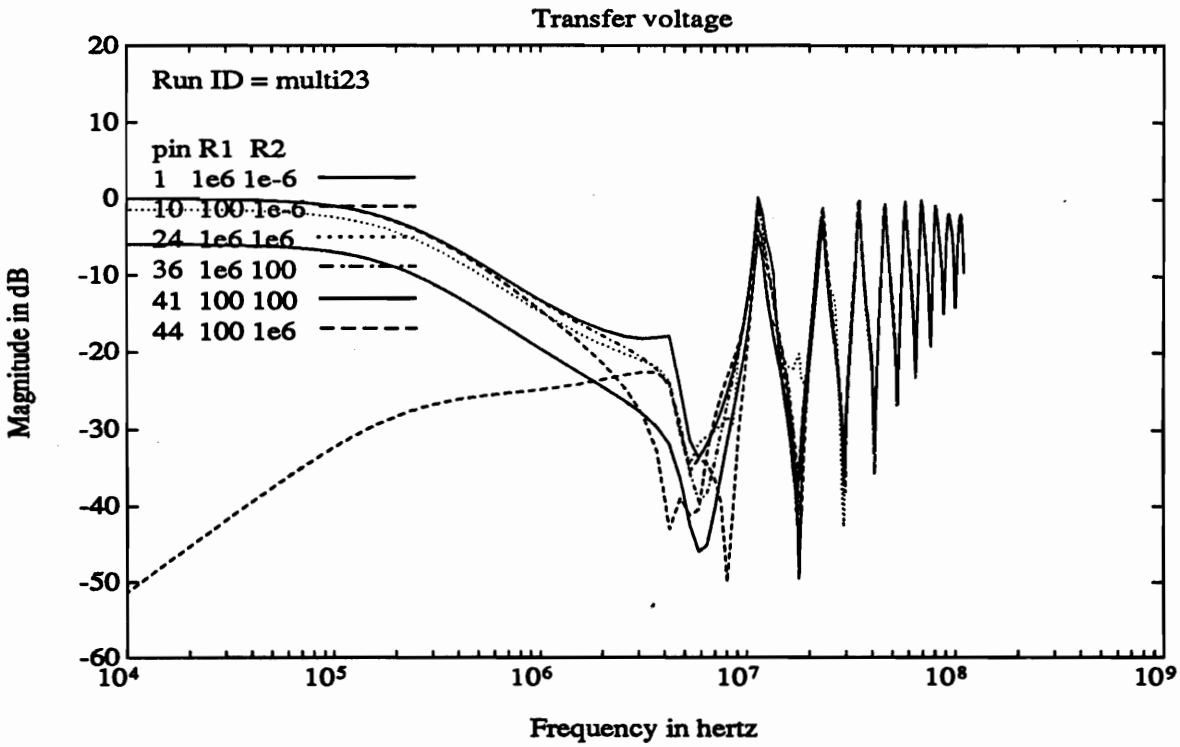

Figure 5.33 Transfer voltage for 50-wire cable with no fuses.

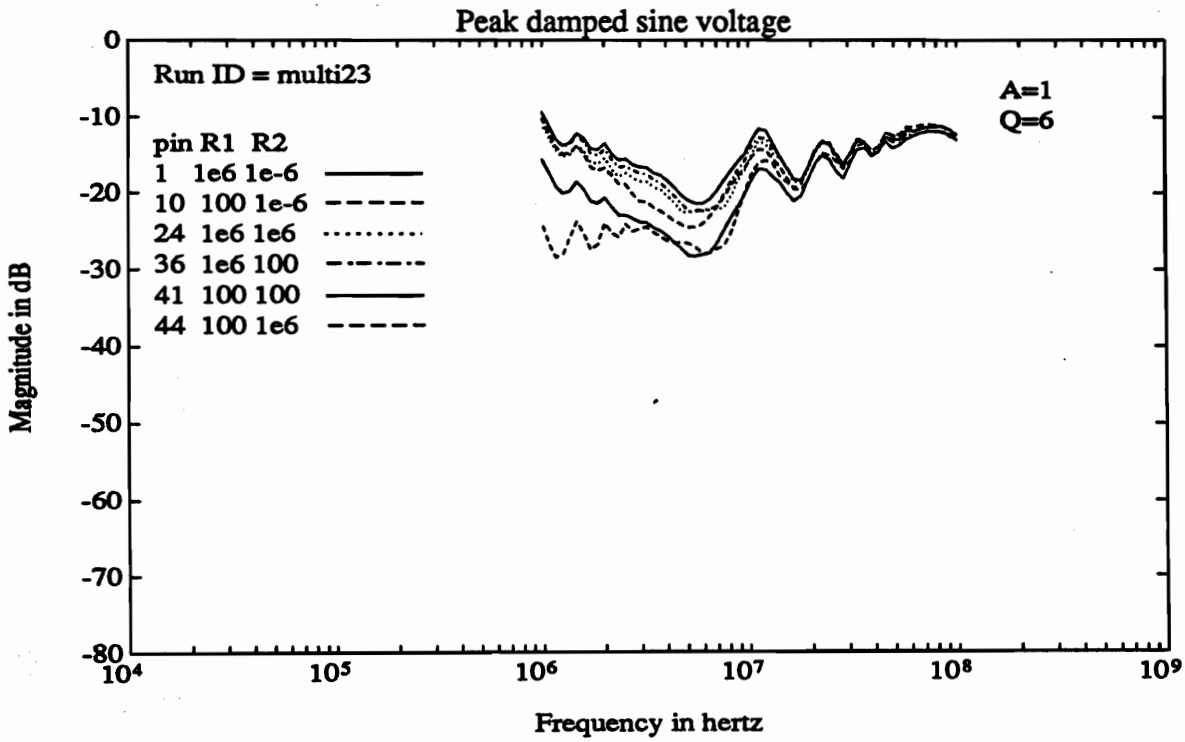

Figure 5.34 Peak damped-sine voltage response for 50-wire cable with no fuses.

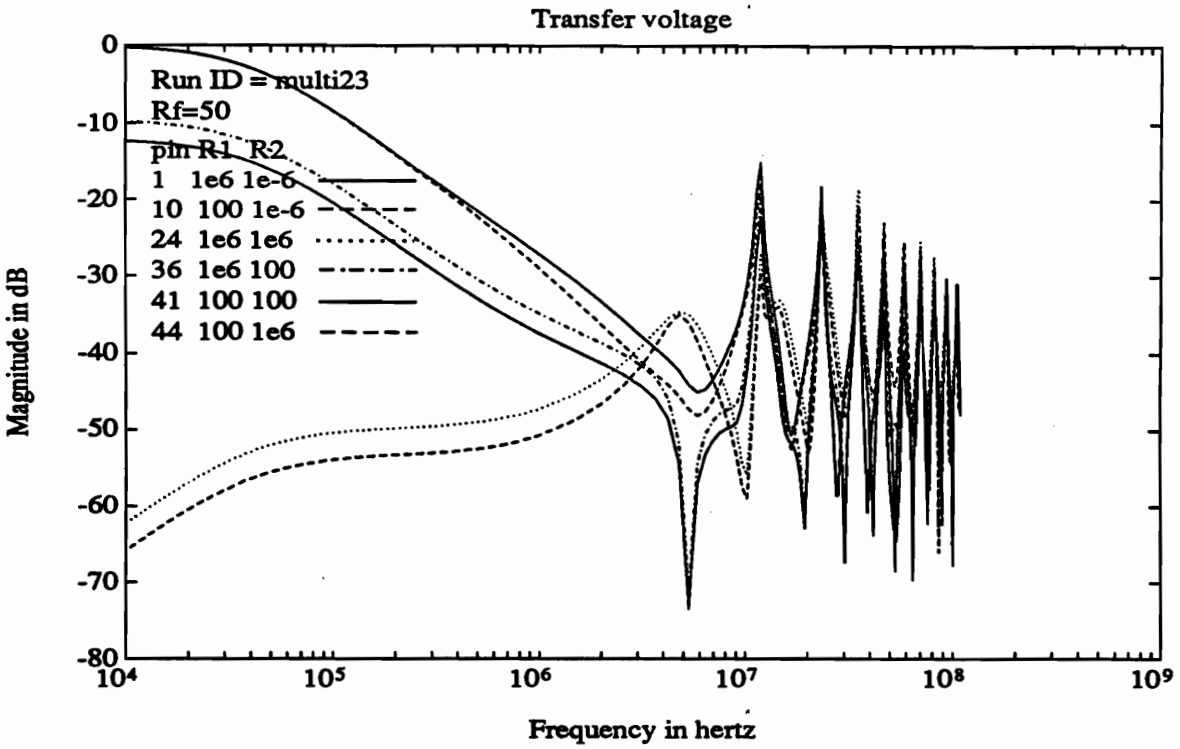

Figure 5.35 Transfer voltage for 50-wire cable with 50-ohm fuses.

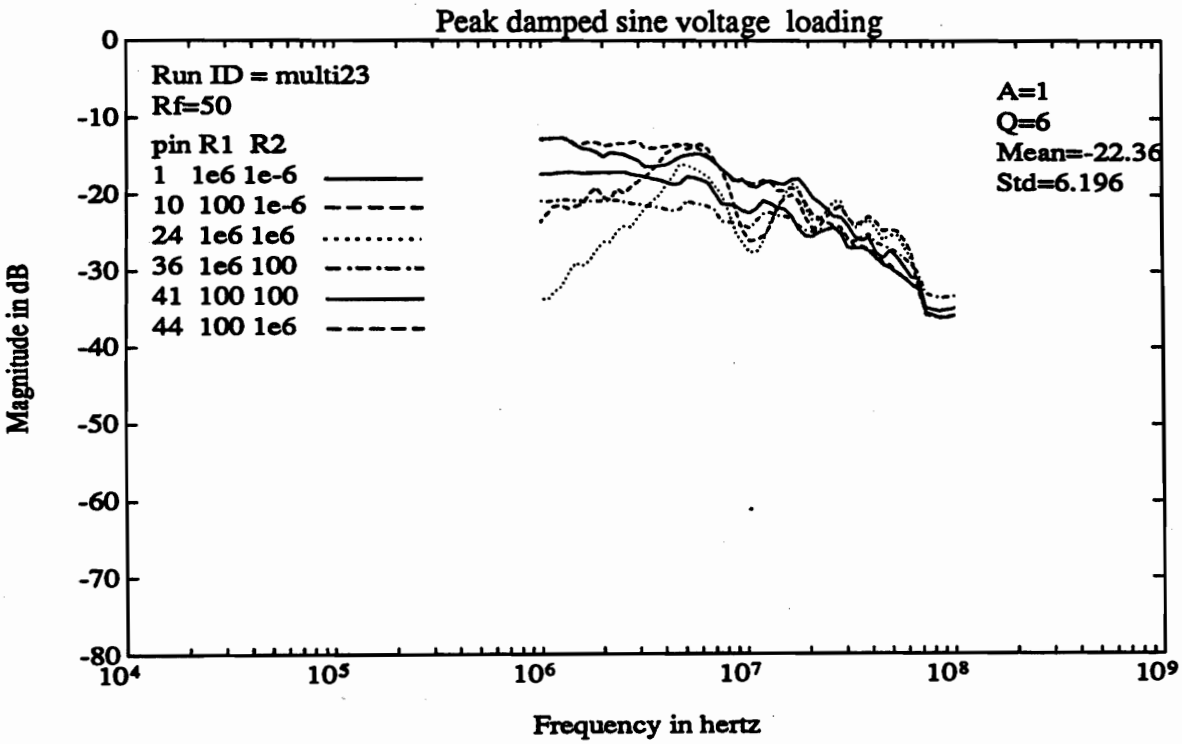

Figure 5.36 Peak damped-sine loading for 50-wire cable with 50-ohm fuses.

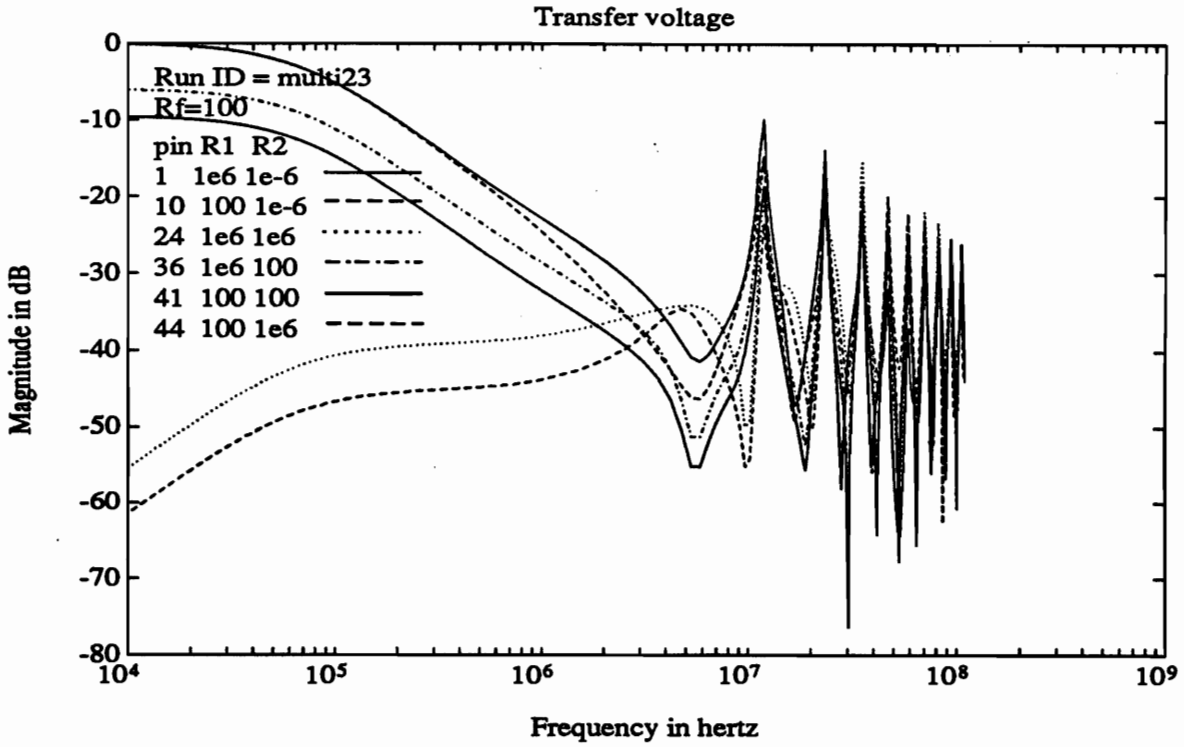

Figure 5.37 Transfer voltage for 50-wire cable with 100-ohm fuses.

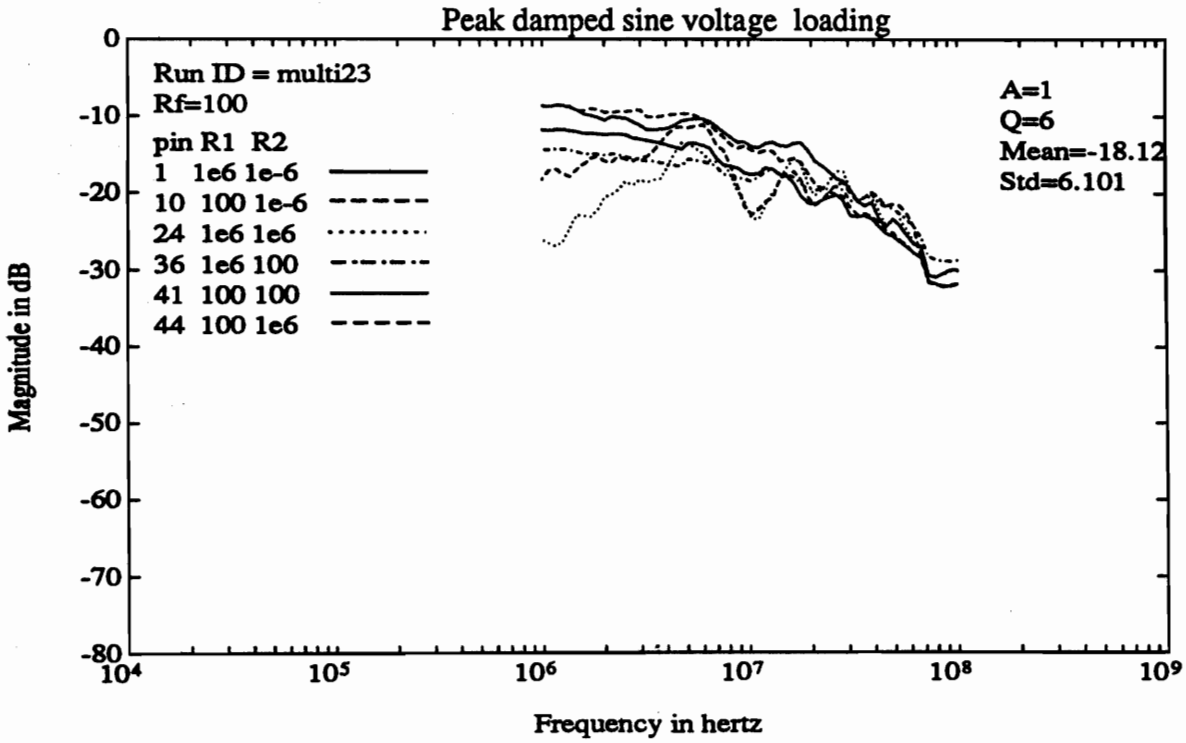

Figure 5.38 Peak damped-sine loading for 50-wire cable with 100-ohm fuses.

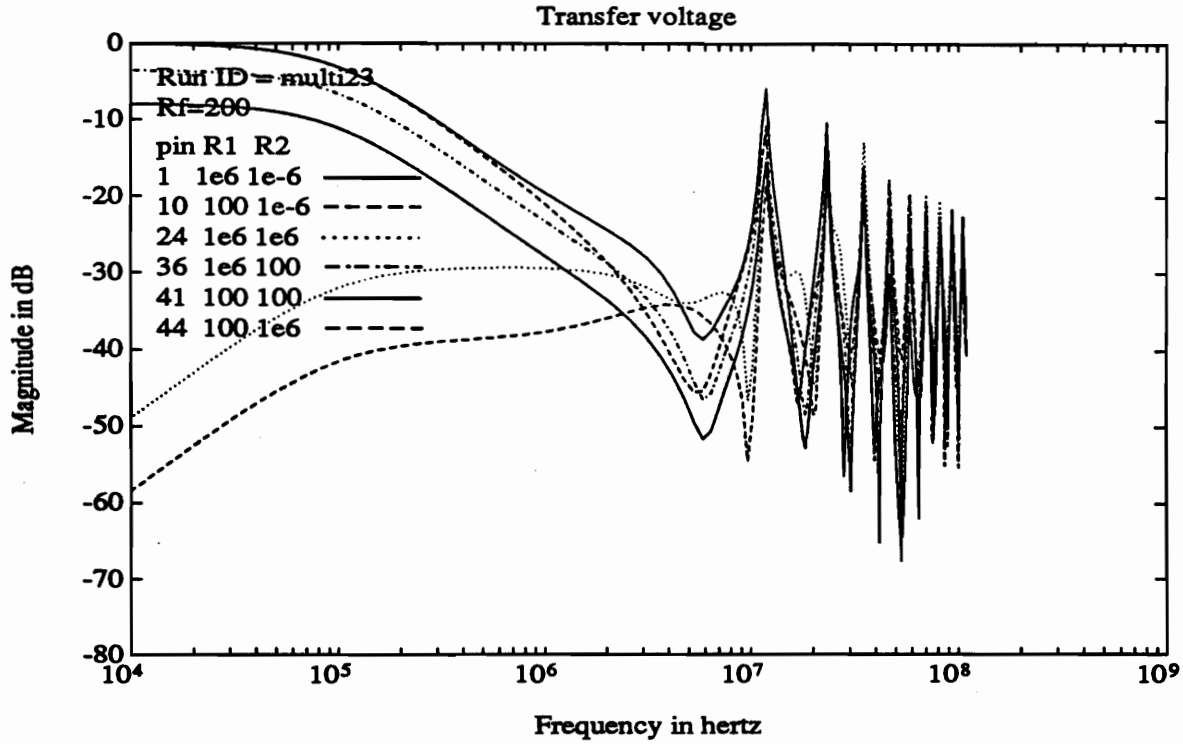

Figure 5.39 Transfer voltage for 50-wire cable with 200-ohm fuses.

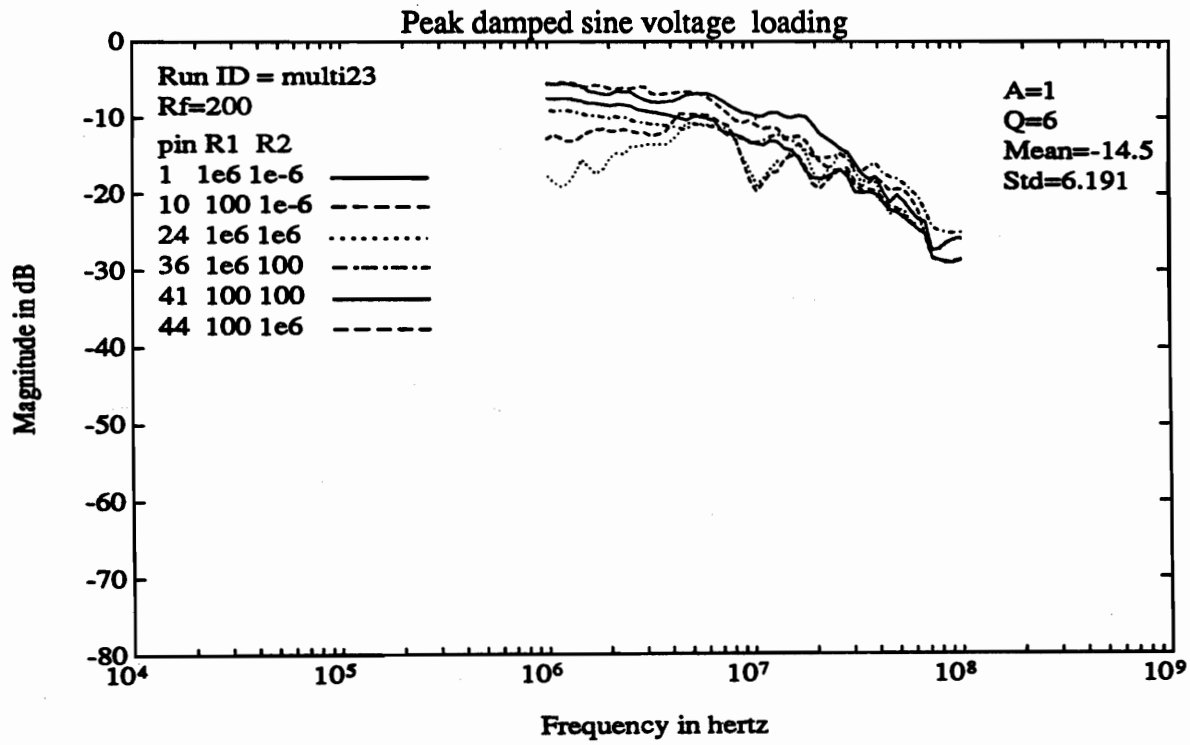

Figure 5.40 Peak damped-sine loading for 50-wire cable with 200-ohm fuses.

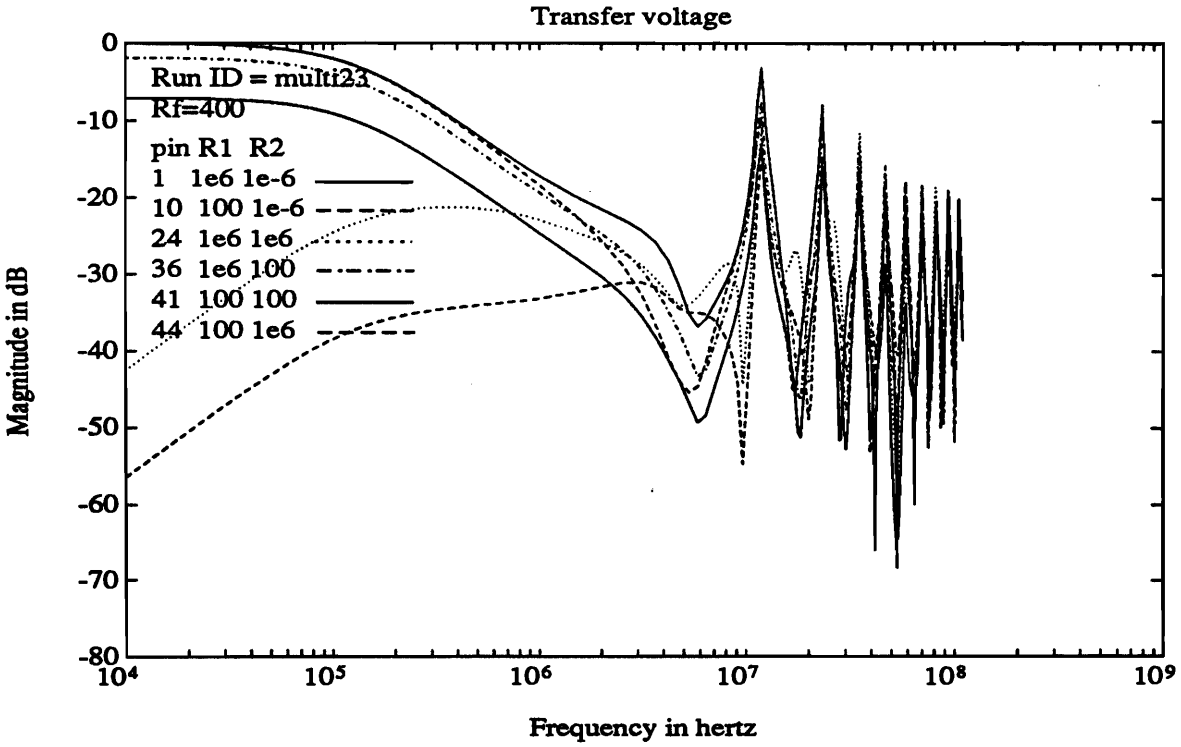

Figure 5.41 Transfer voltage for 50-wire cable with 400-ohm fuses.

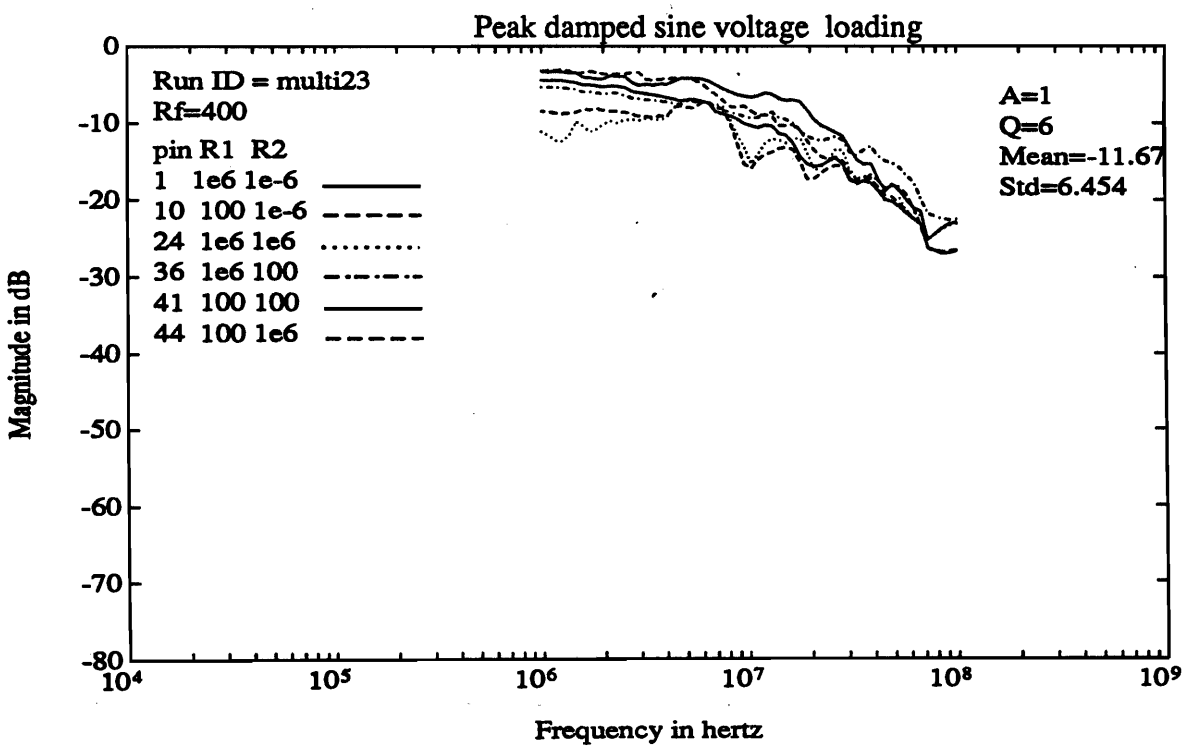

Figure 5.42 Peak damped-sine loading for 50-wire cable with 400-ohm fuses.

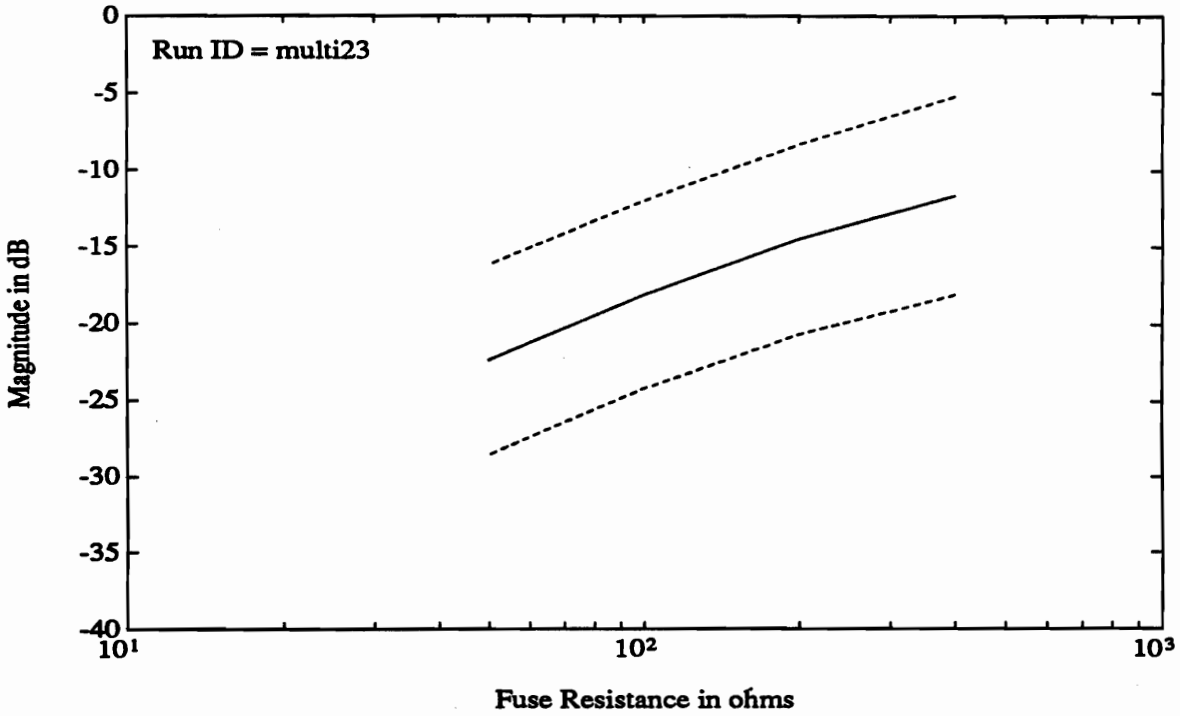

Figure 5.43 Mean and standard deviation of fuse loading for 50-wire cable.

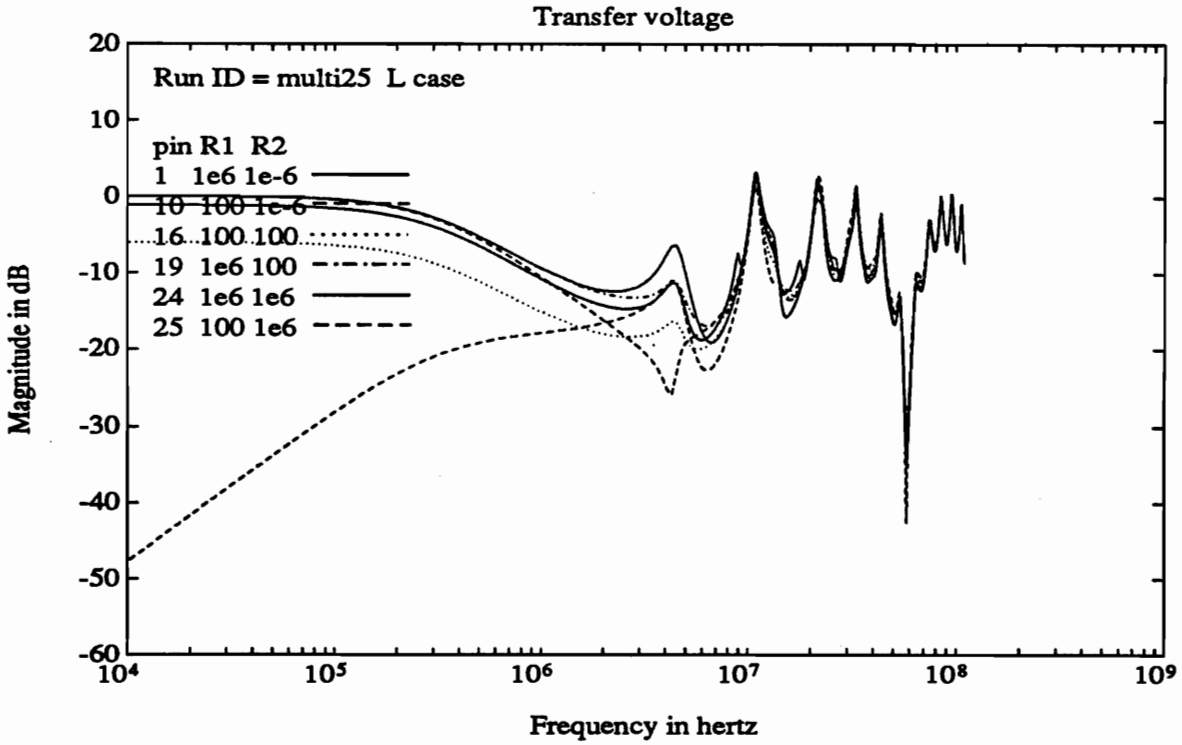

Figure 5.44 Transfer voltage for 25-wire cable with no fuses.

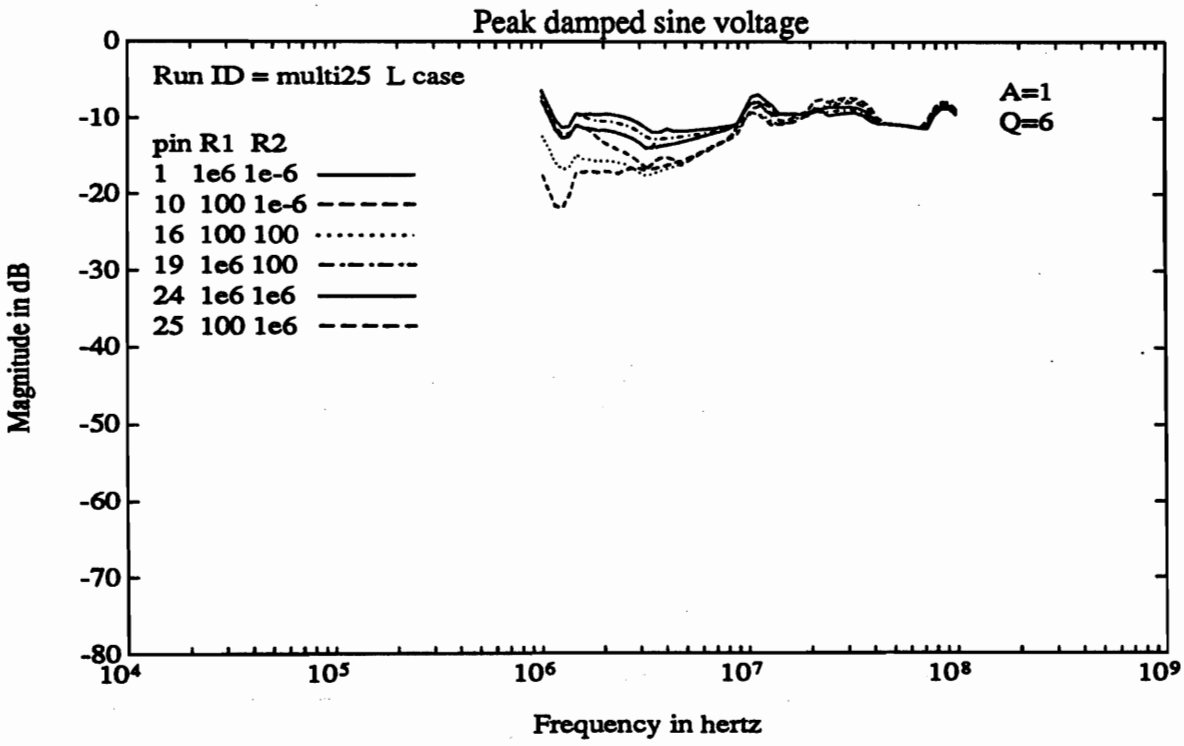

Figure 5.45 Peak damped-sine voltage response for 25-wire cable with no fuses.

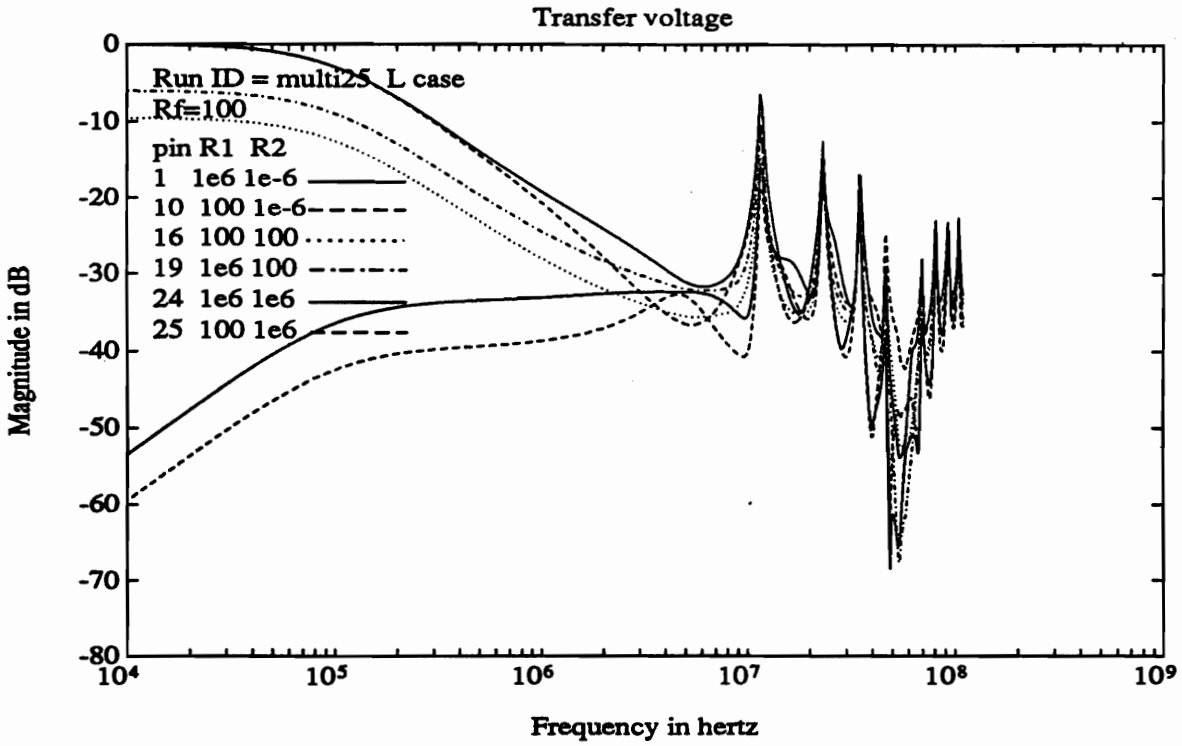

Figure 5.46 Transfer voltage for 25-wire cable with 100-ohm fuses.

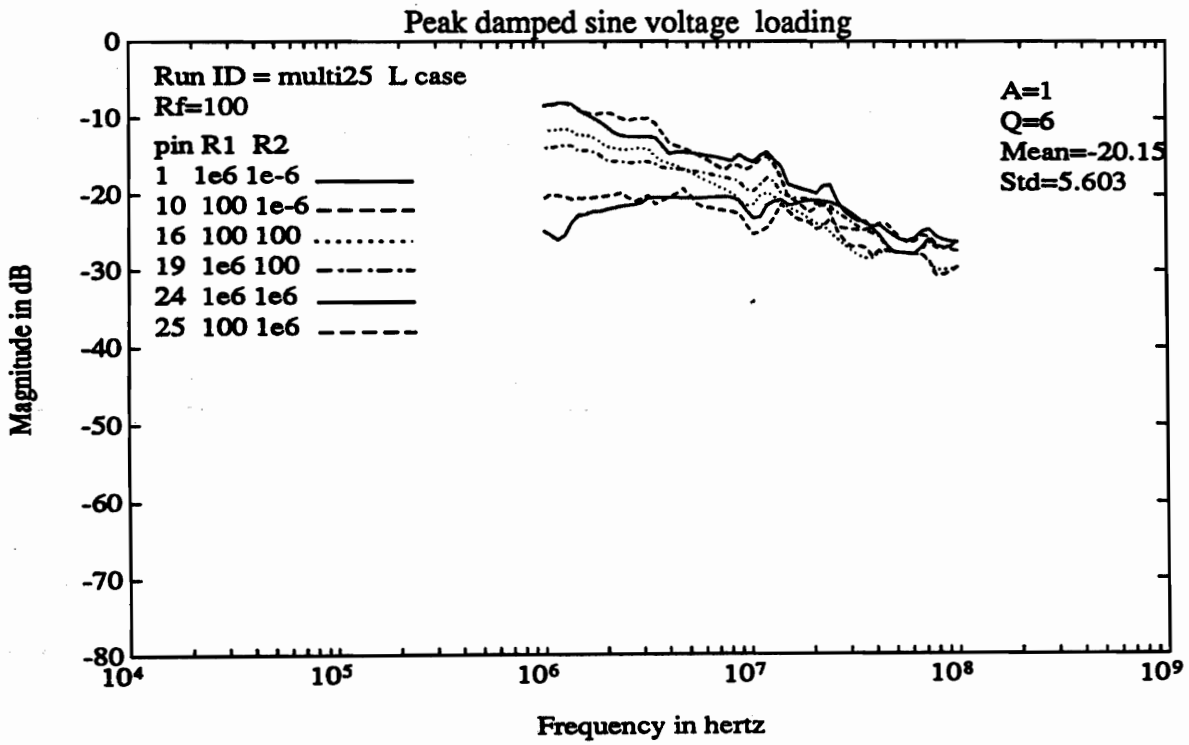

Figure 5.47 Peak damped-sine loading for 25-wire cable with 100-ohm fuses.

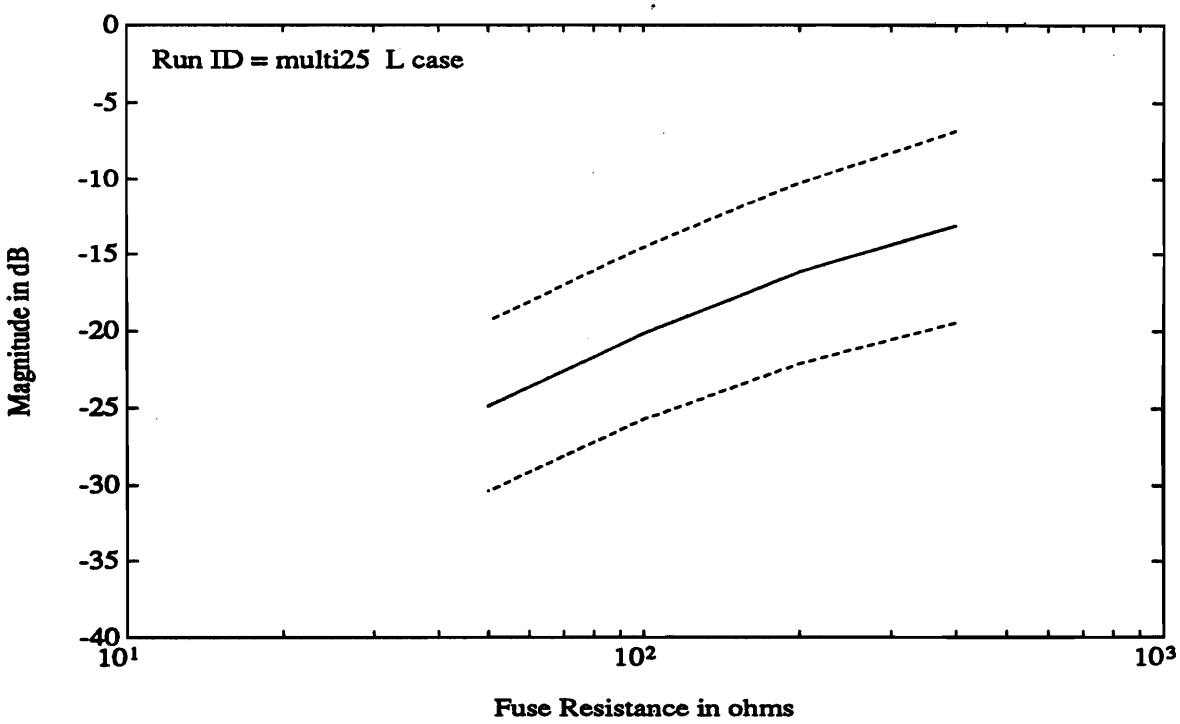

Figure 5.48 Mean and standard deviation of fuse loading for 25-wire cable.

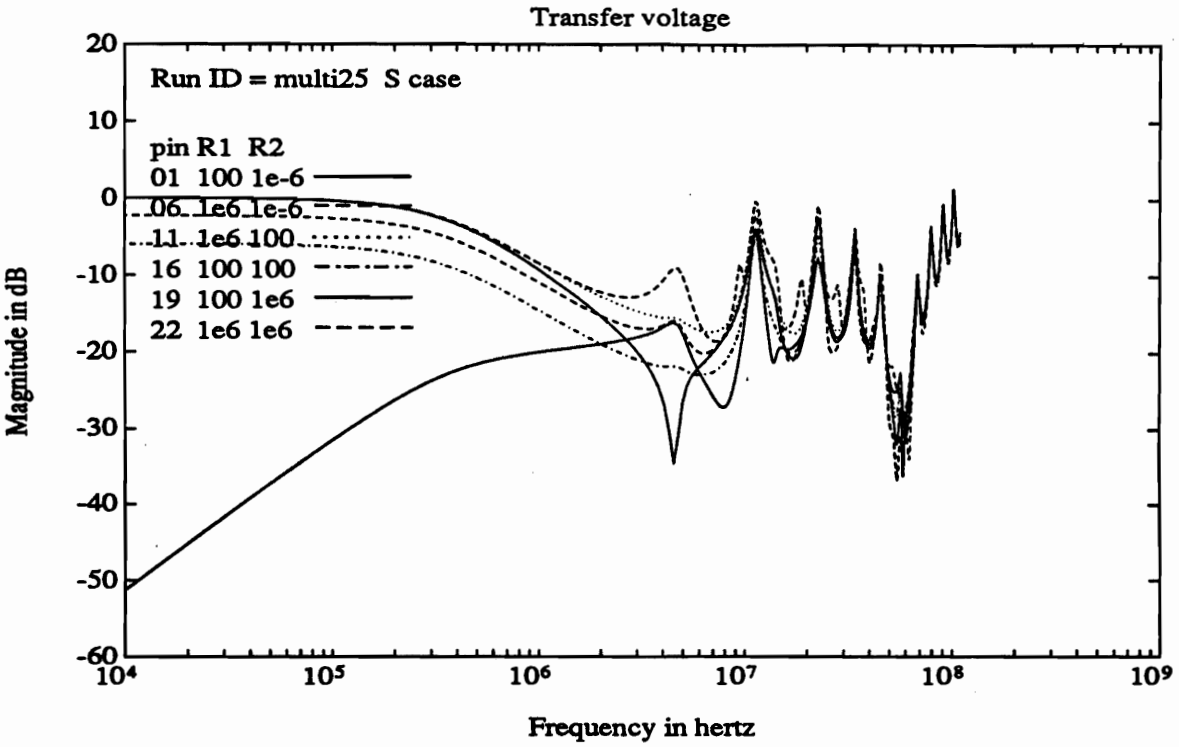

Figure 5.49 Transfer voltage for 25-wire cable with no fuses.

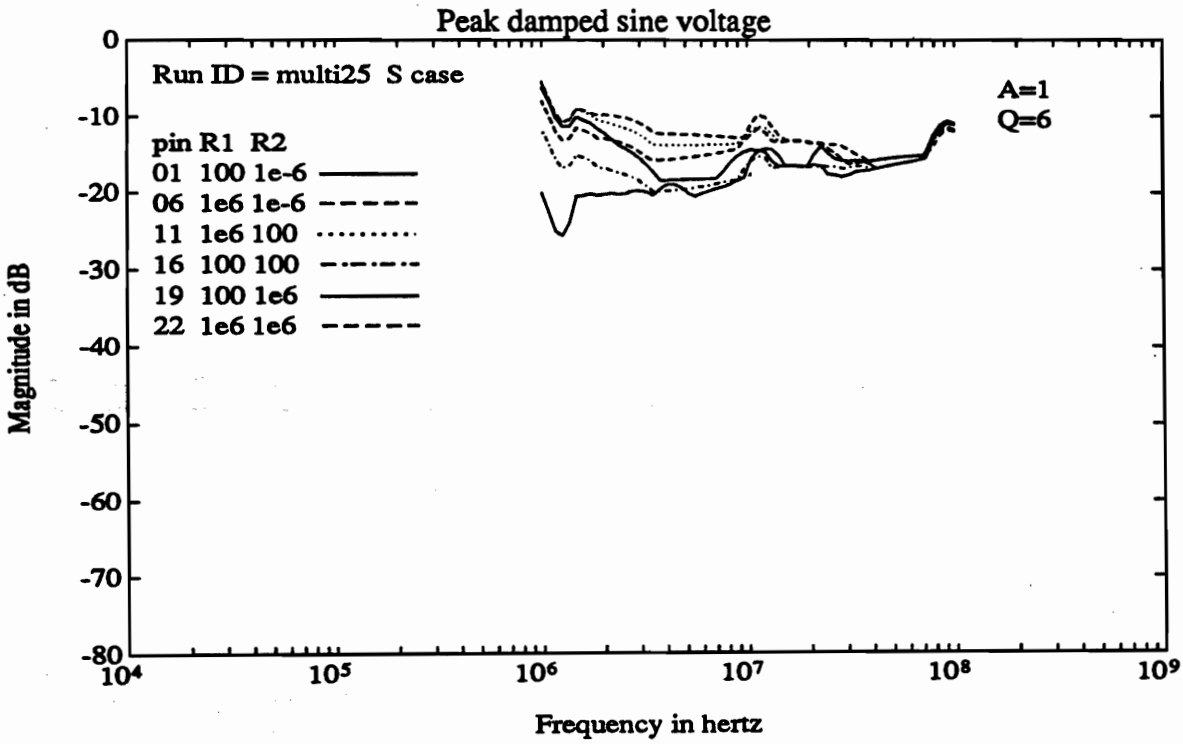

Figure 5.50 Peak damped-sine voltage response for 25-wire cable with no fuses.

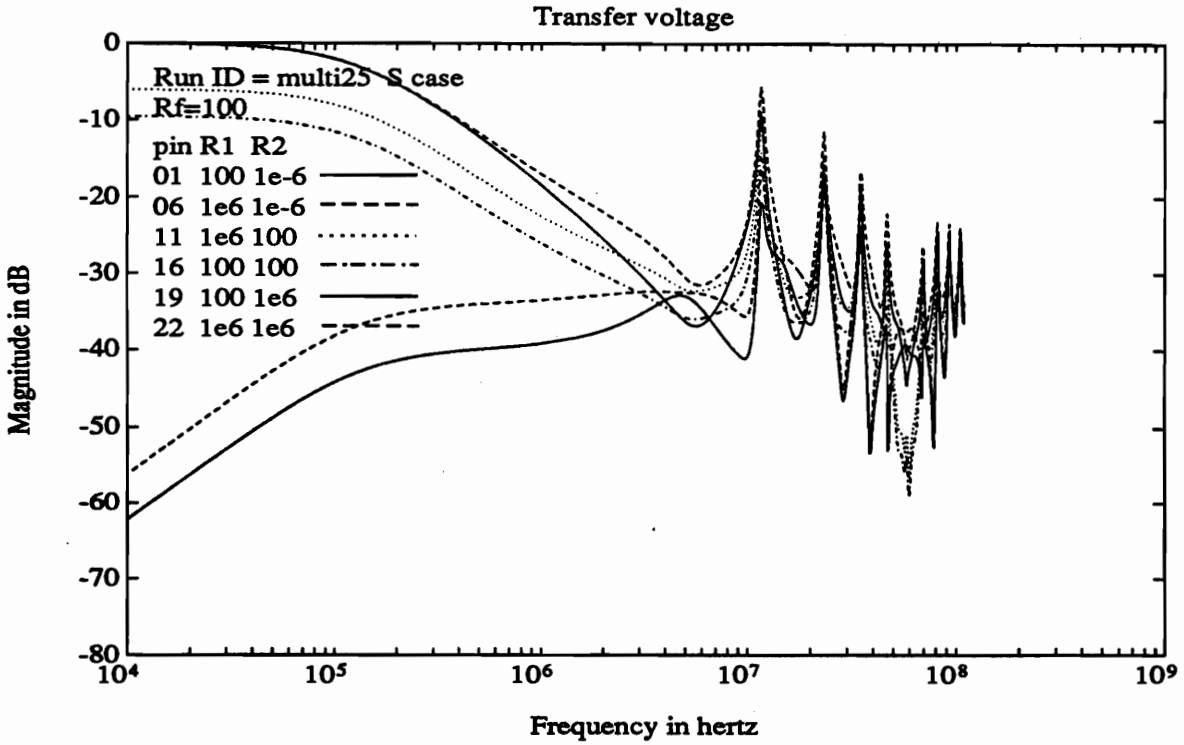

Figure 5.51 Transfer voltage for 25-wire cable with 100-ohm fuses.

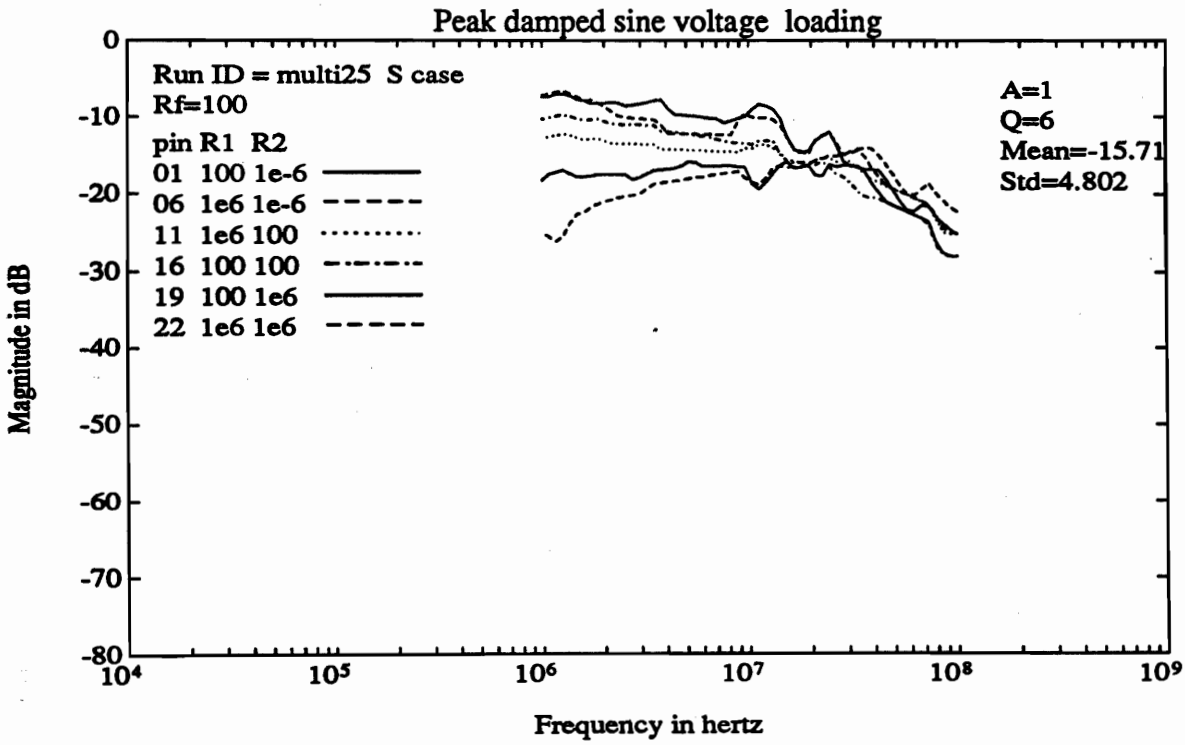

Figure 5.52 Peak damped-sine loading for 25-wire cable with 100-ohm fuses.

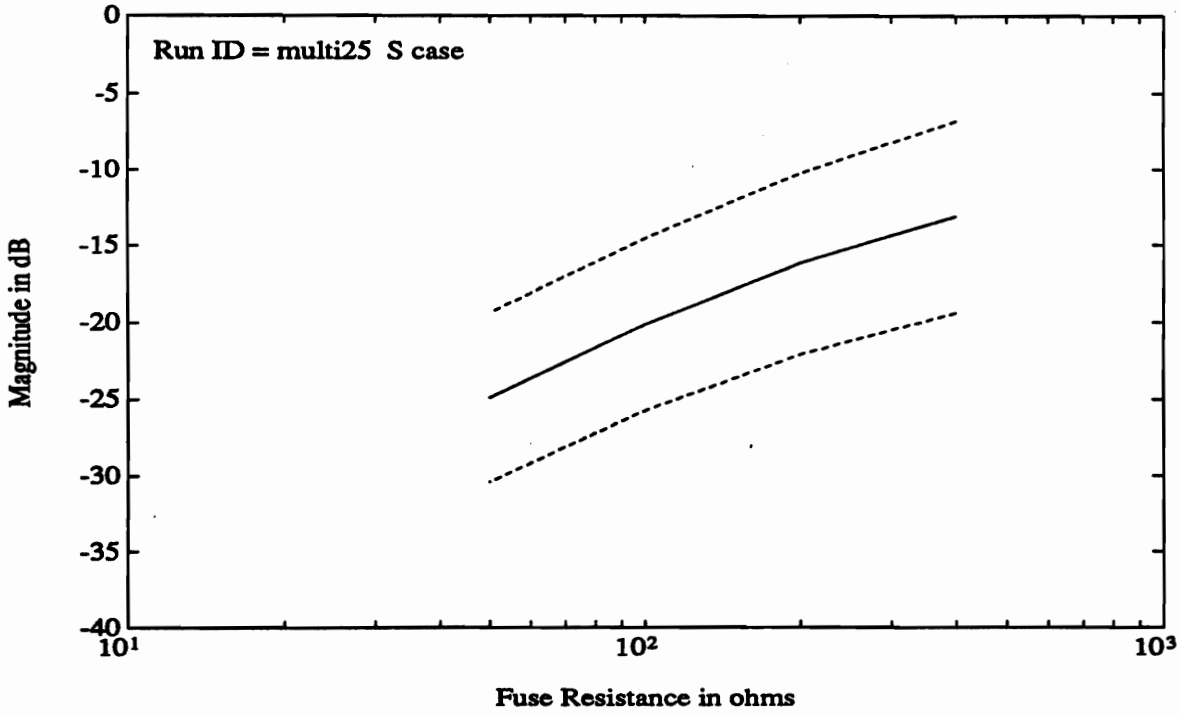

Figure 5.53 Mean and standard deviation of fuse loading for 25-wire cable.

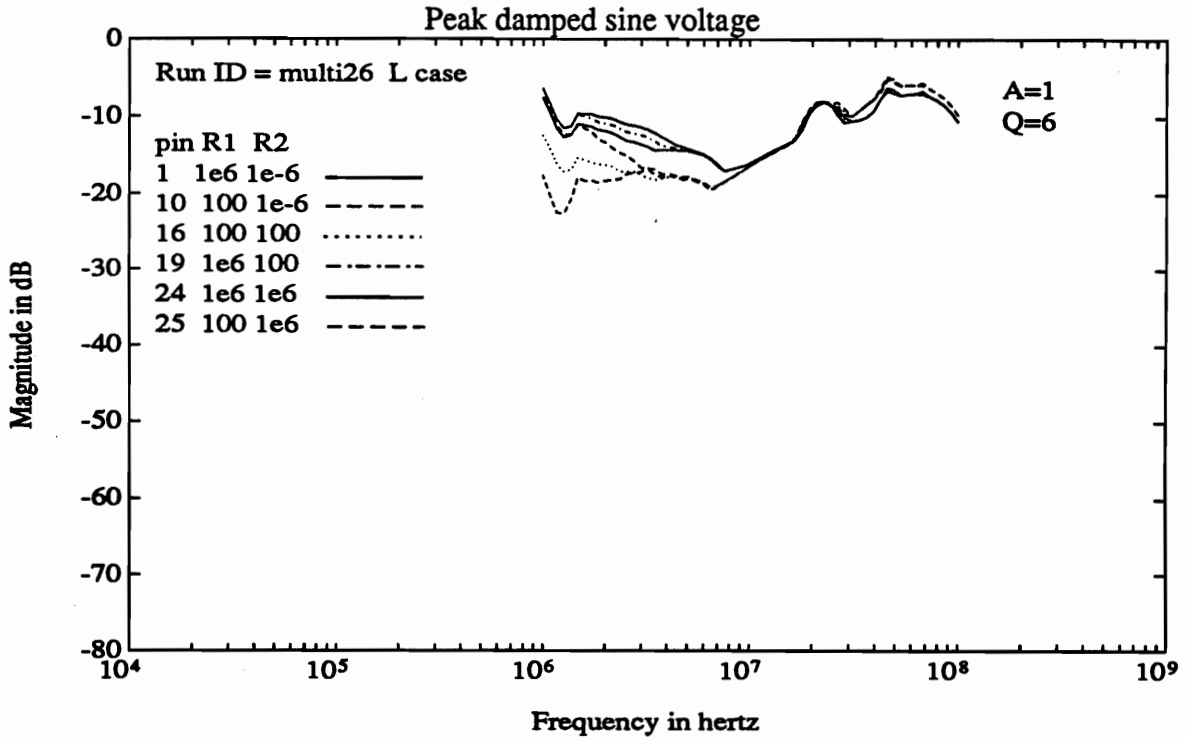

Figure 5.54 Peak damped-sine voltage response for 25-wire cable with no fuses.

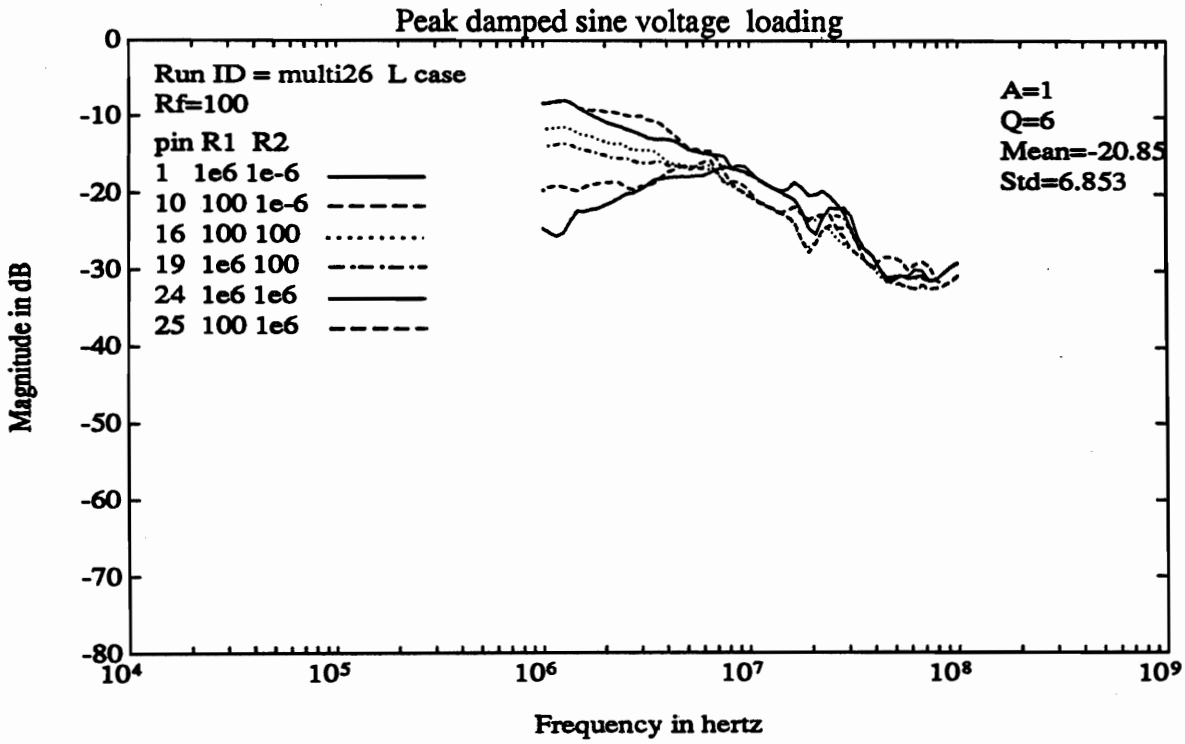

Figure 5.55 Peak damped-sine loading for 25-wire cable with 100-ohm fuses.

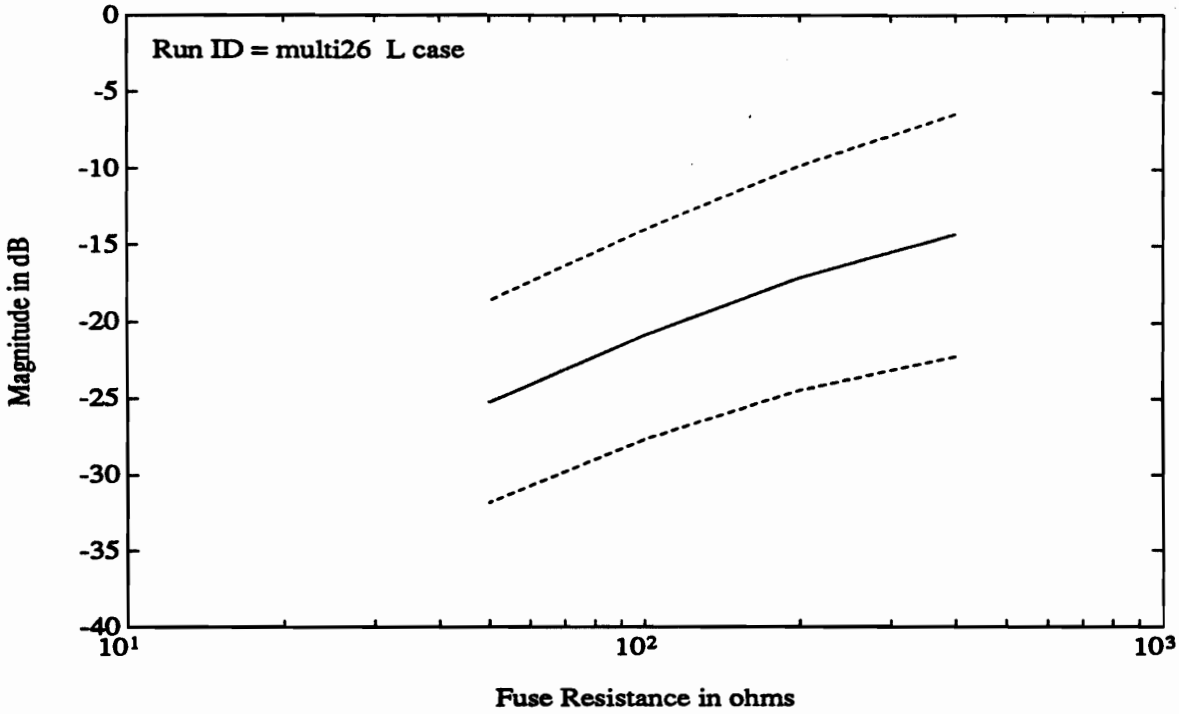

Figure 5.56 Mean and standard deviation of fuse loading for 25-wire cable.

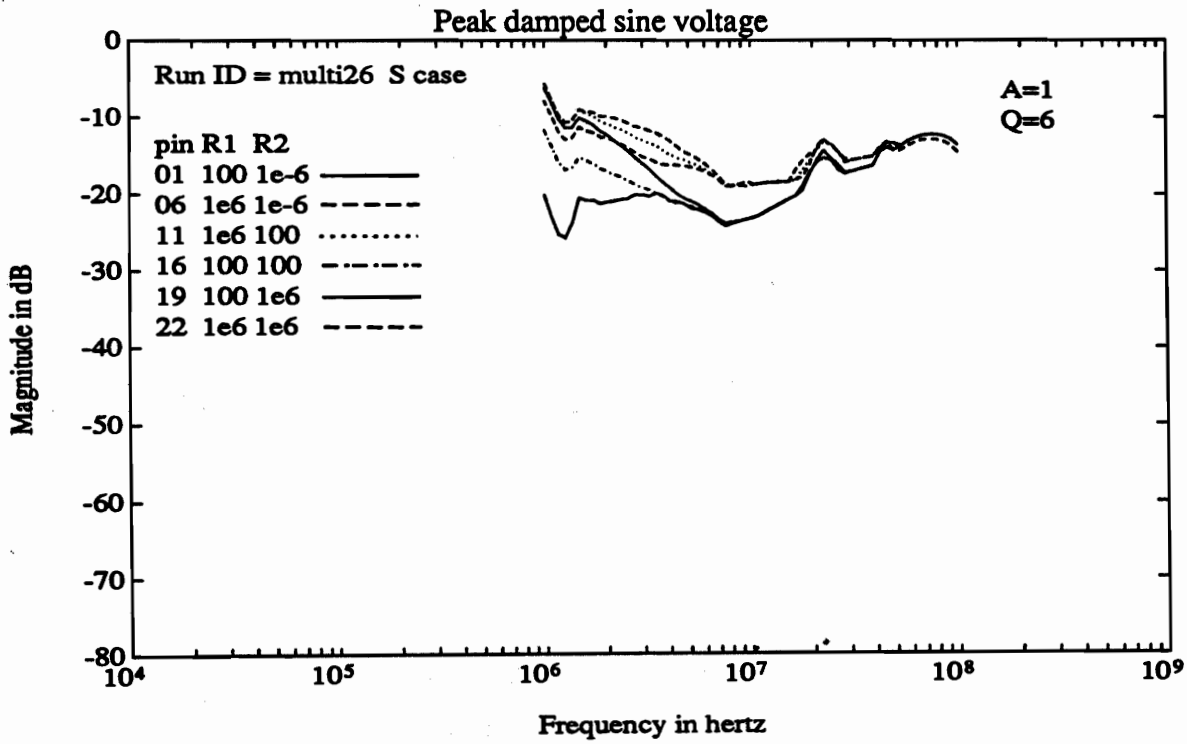

Figure 5.57 Peak damped-sine voltage response for 25-wire cable with no fuses.

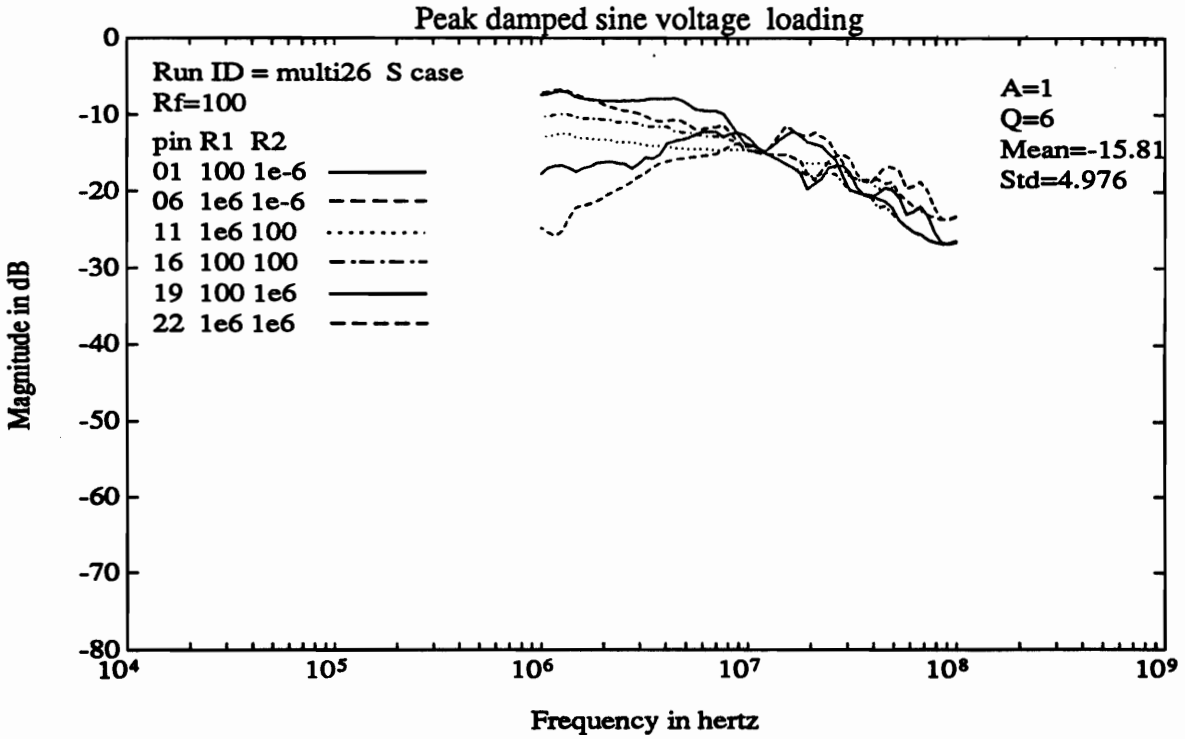

Figure 5.58 Peak damped-sine loading for 25-wire cable with 100-ohm fuses.

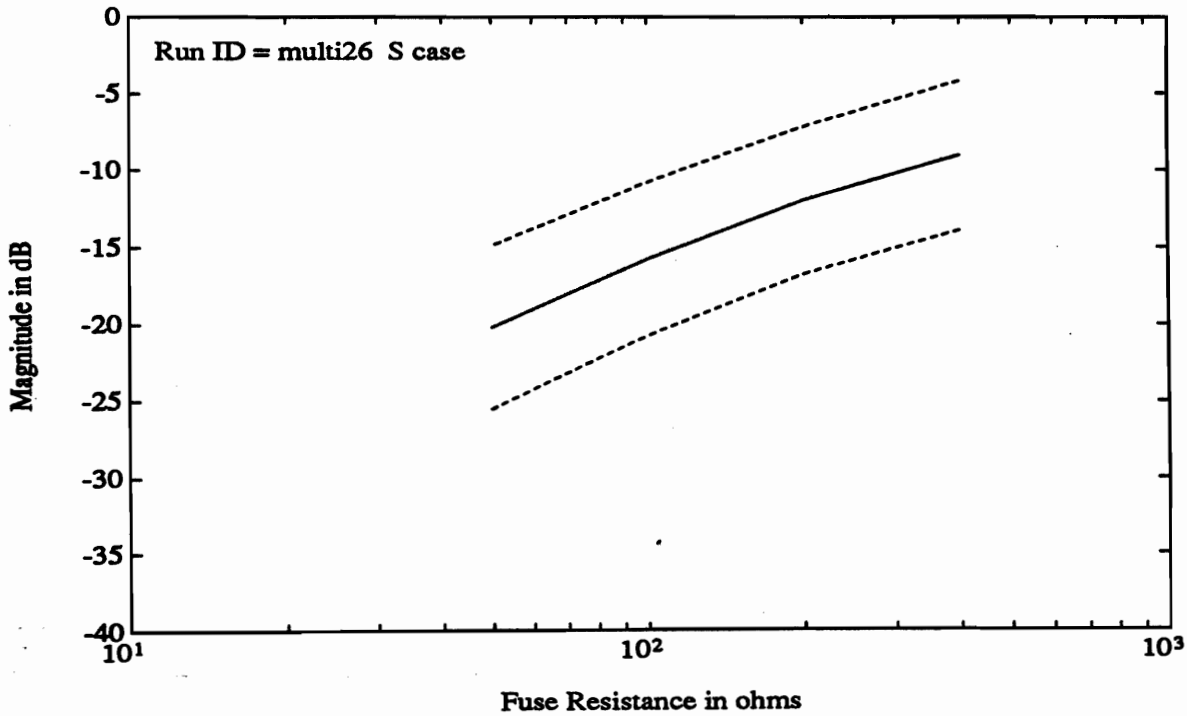

Figure 5.59 Mean and standard deviation of fuse loading for 25-wire cable.

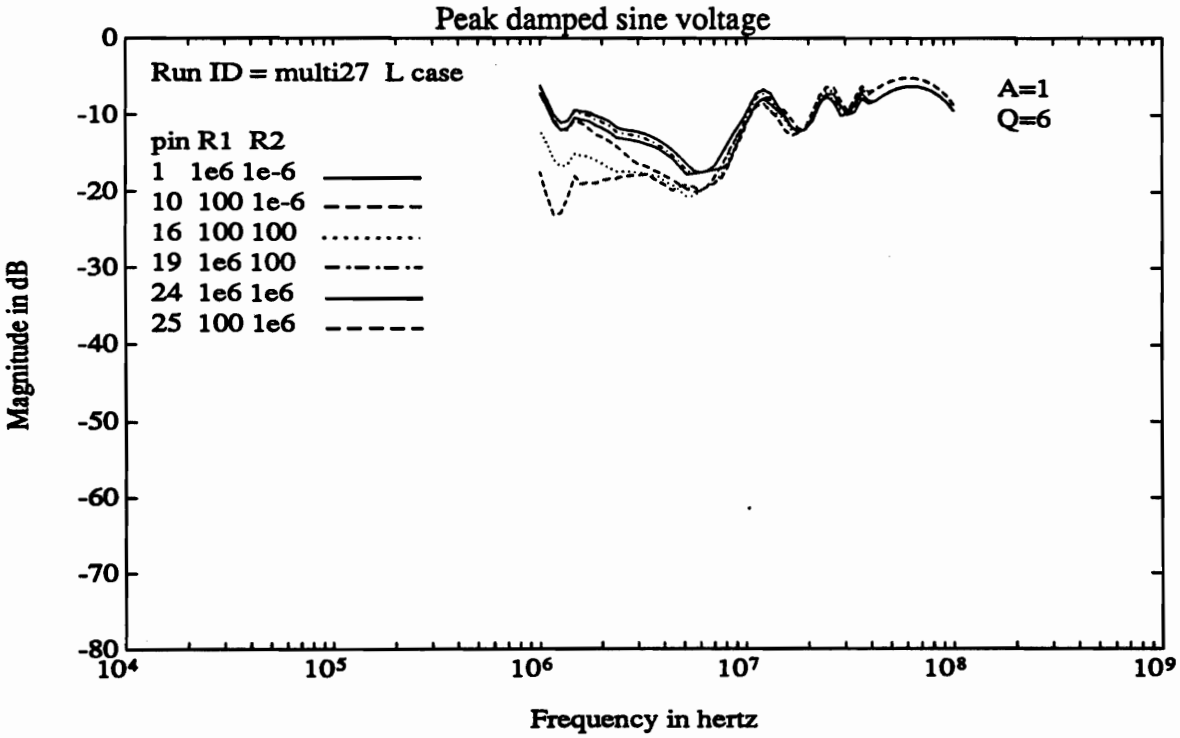

Figure 5.60 Peak damped-sine voltage response for 25-wire cable with no fuses.

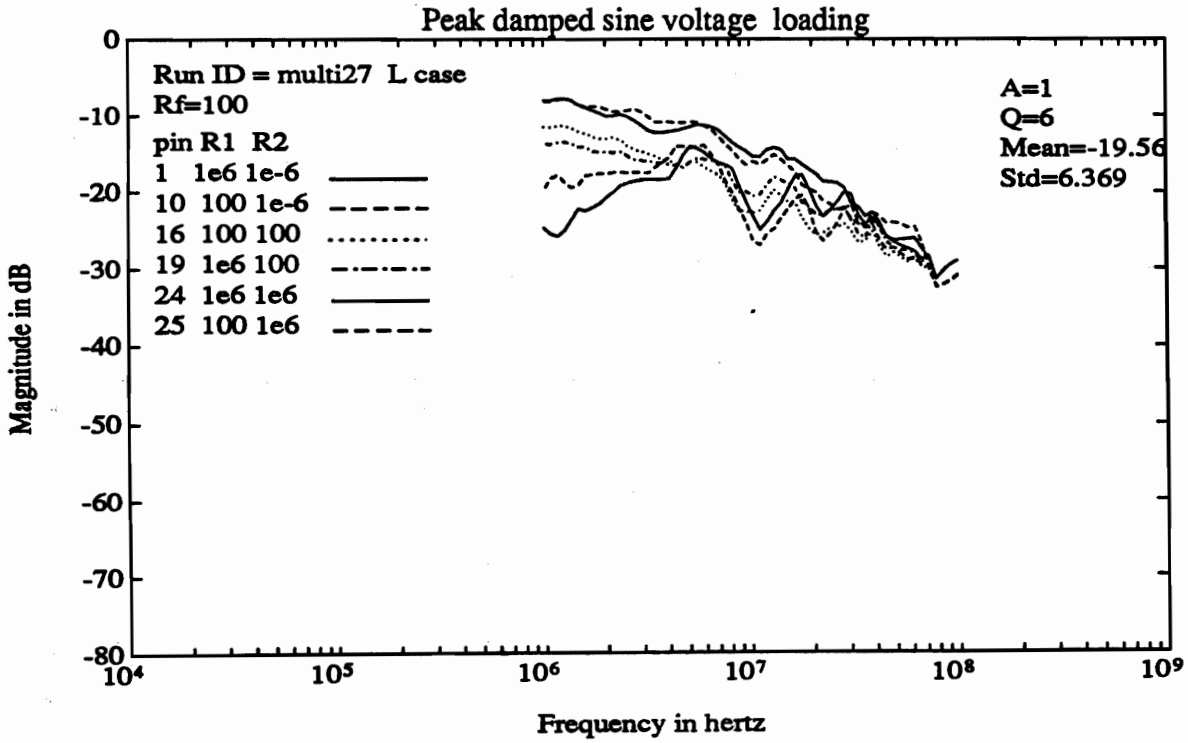

Figure 5.61 Peak damped-sine loading for 25-wire cable with 100-ohm fuses.

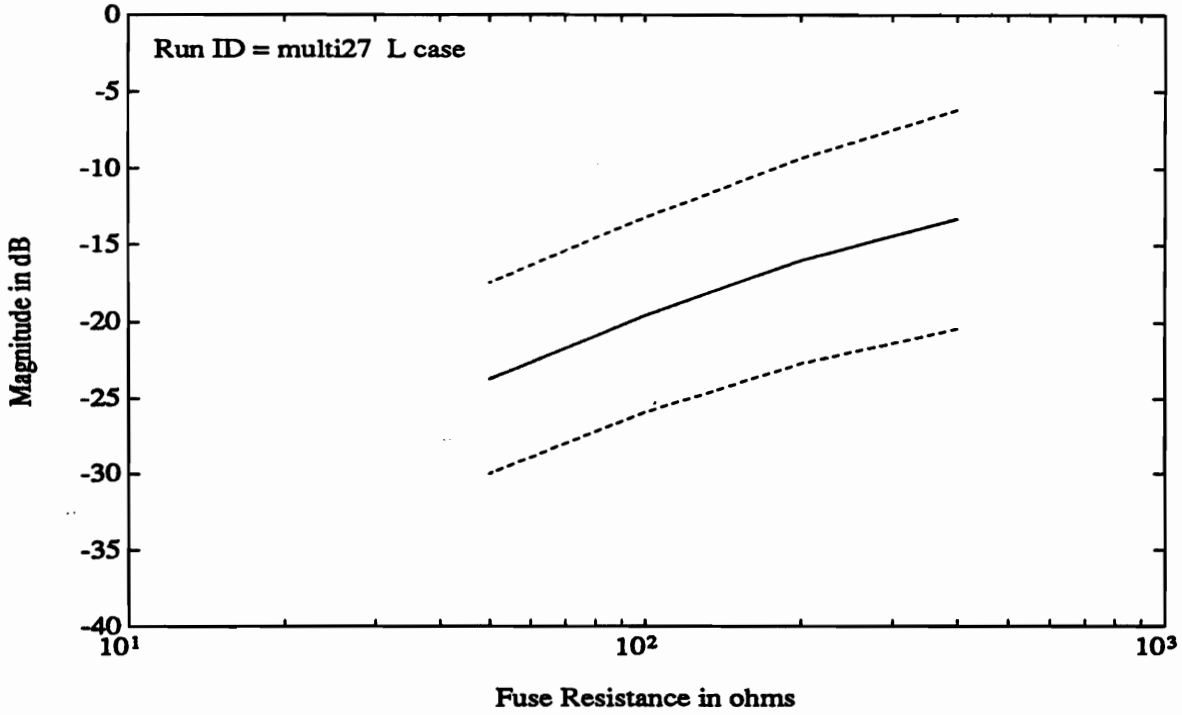

Figure 5.62 Mean and standard deviation of fuse loading for 25-wire cable.

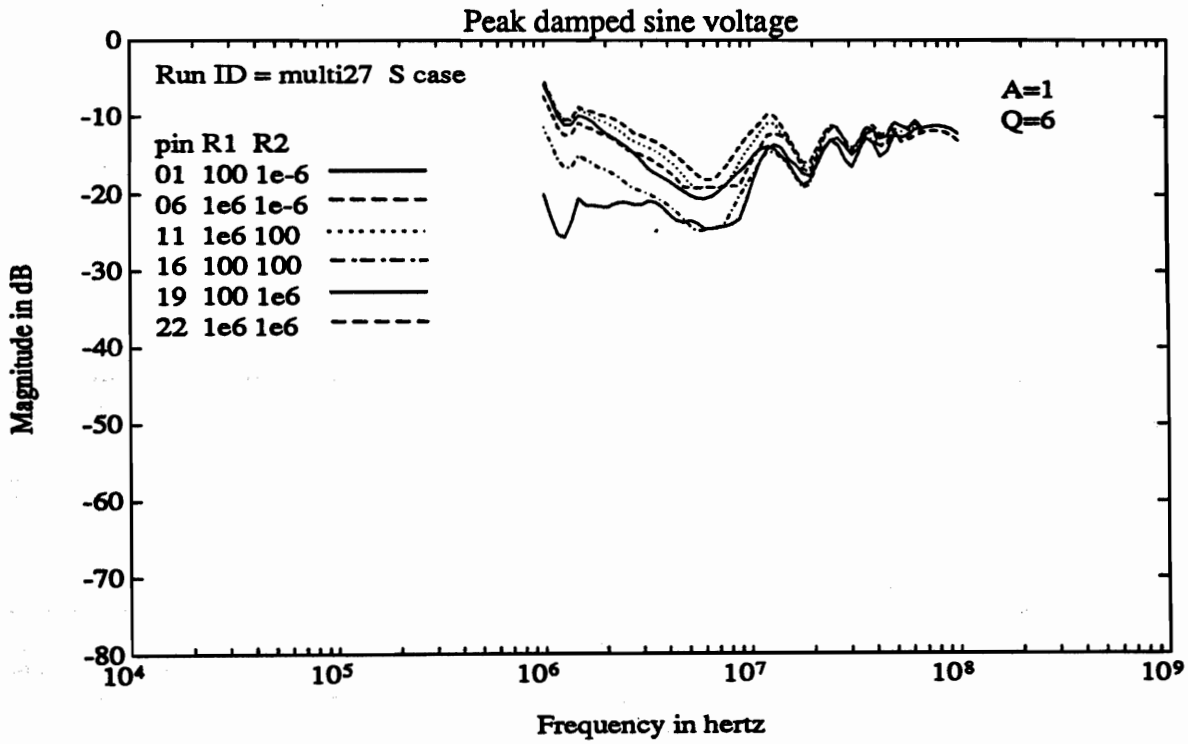

Figure 5.63 Peak damped-sine voltage response for 25-wire cable with no fuses.

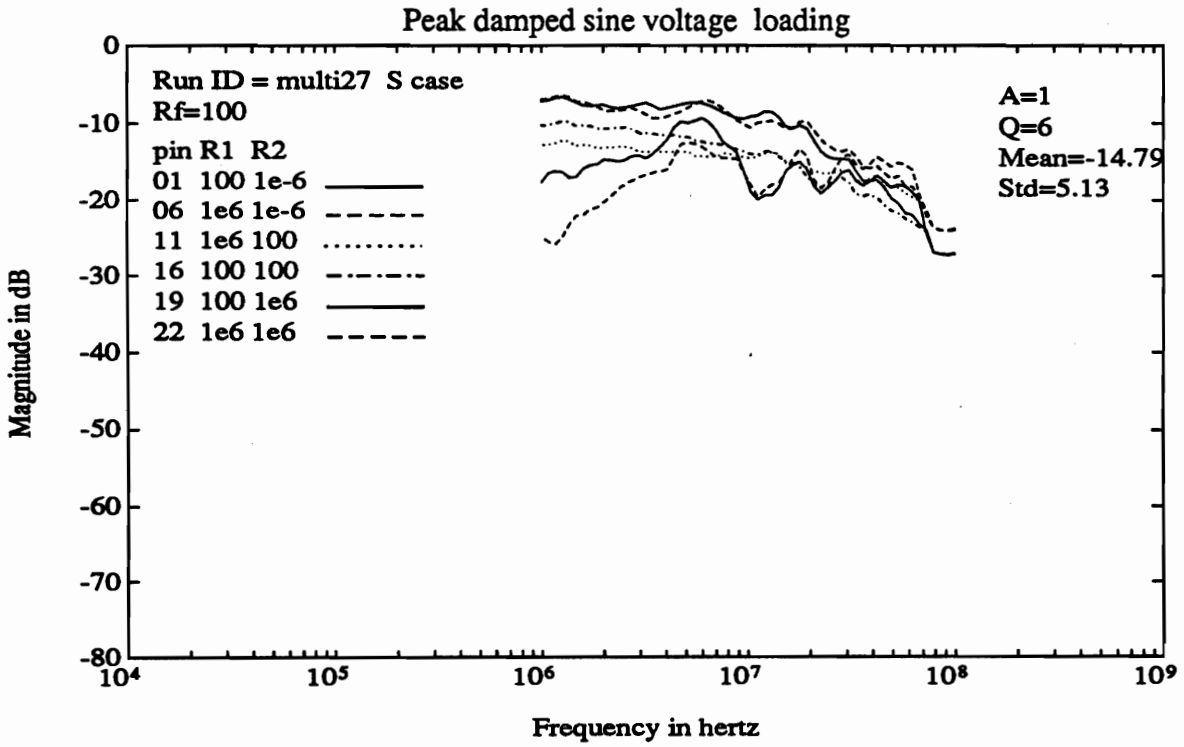

Figure 5.64 Peak damped-sine loading for 25-wire cable with 100-ohm fuses.

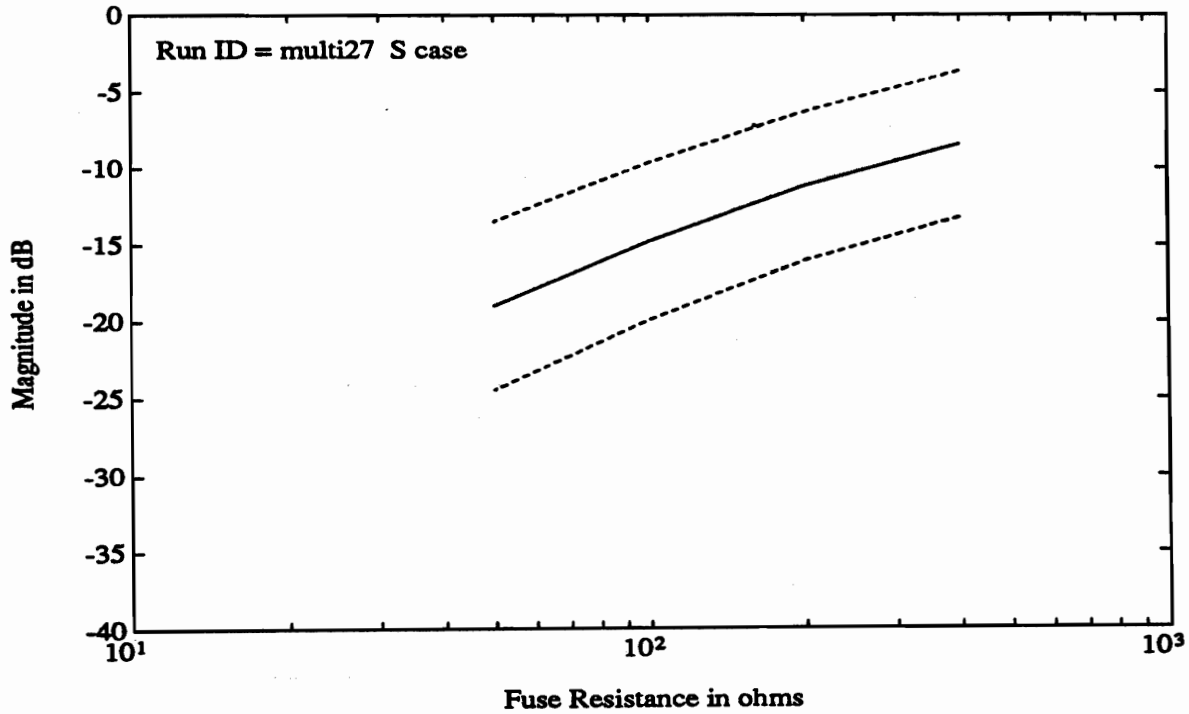

Figure 5.65 Mean and standard deviation of fuse loading for 25-wire cable.

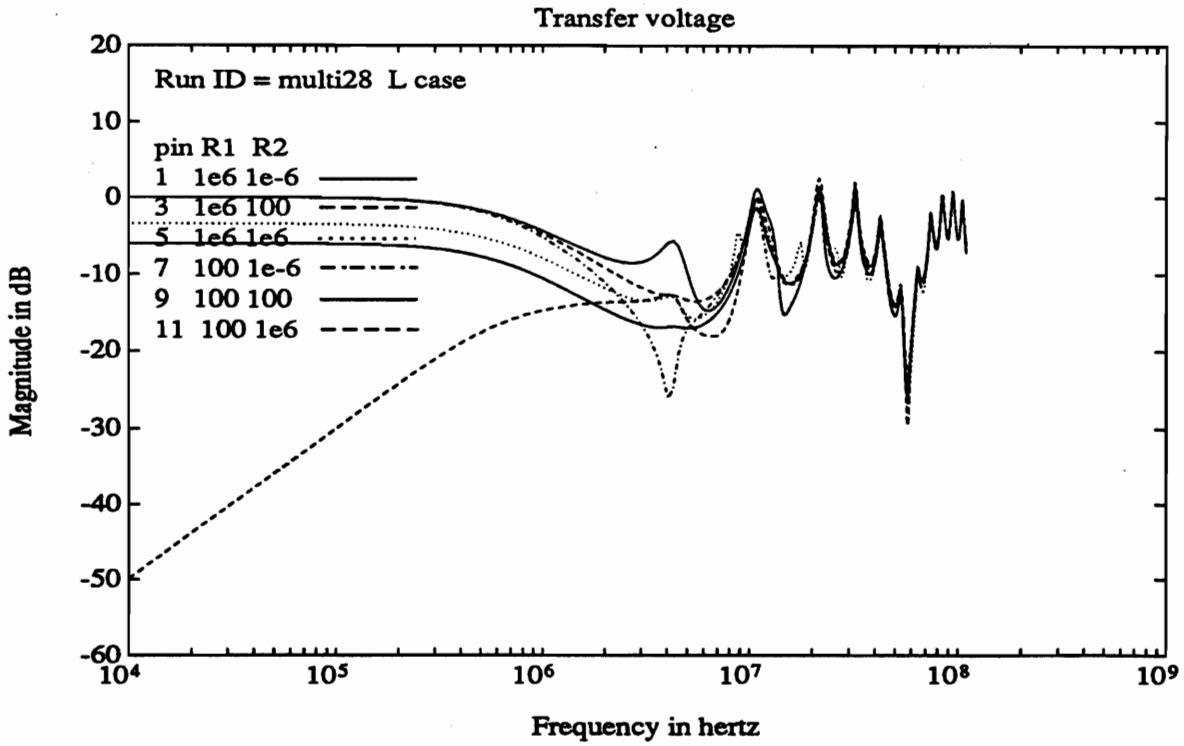

Figure 5.66 Transfer voltage for 12-wire cable with no fuses.

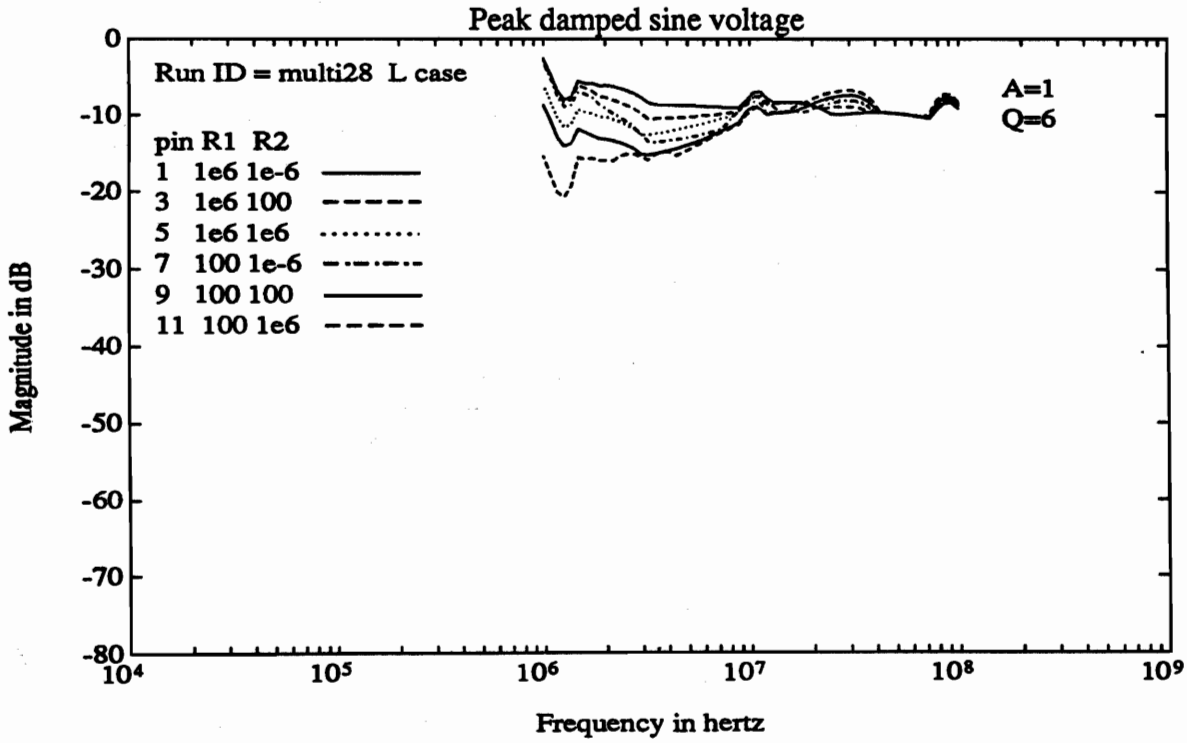

Figure 5.67 Peak damped-sine voltage response for 12-wire cable with no fuses.

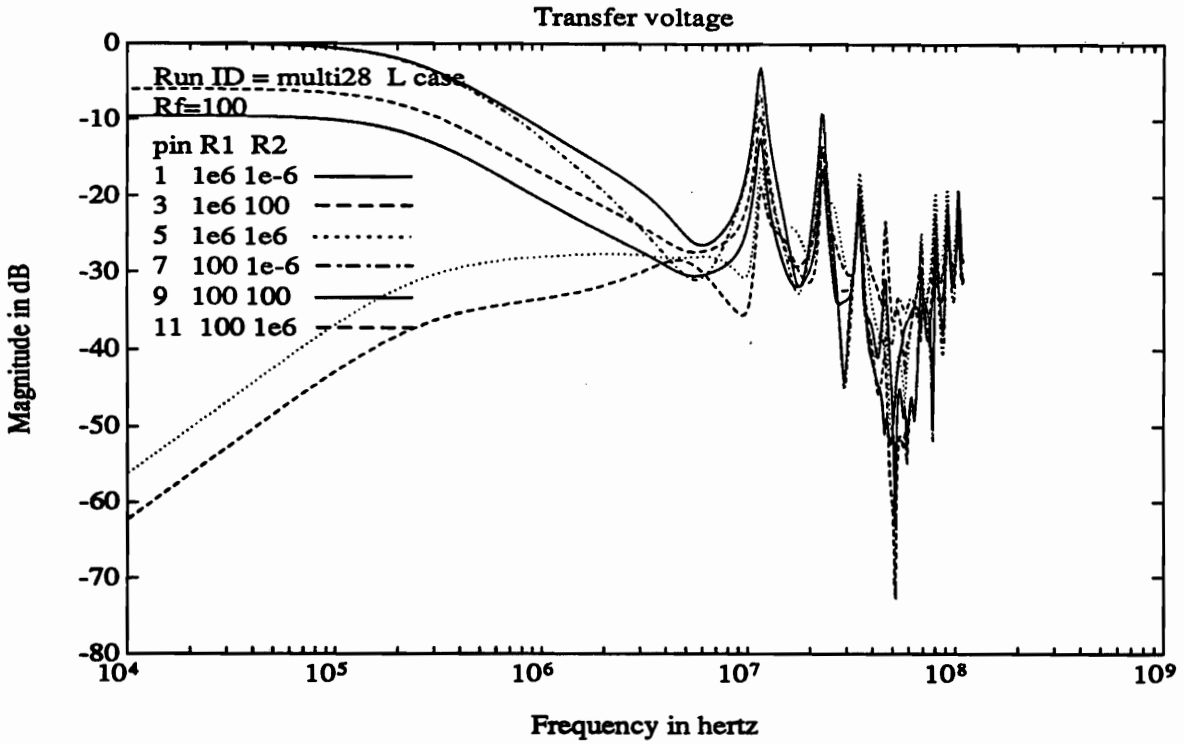

Figure 5.68 Transfer voltage for 12-wire cable with 100-ohm fuses.

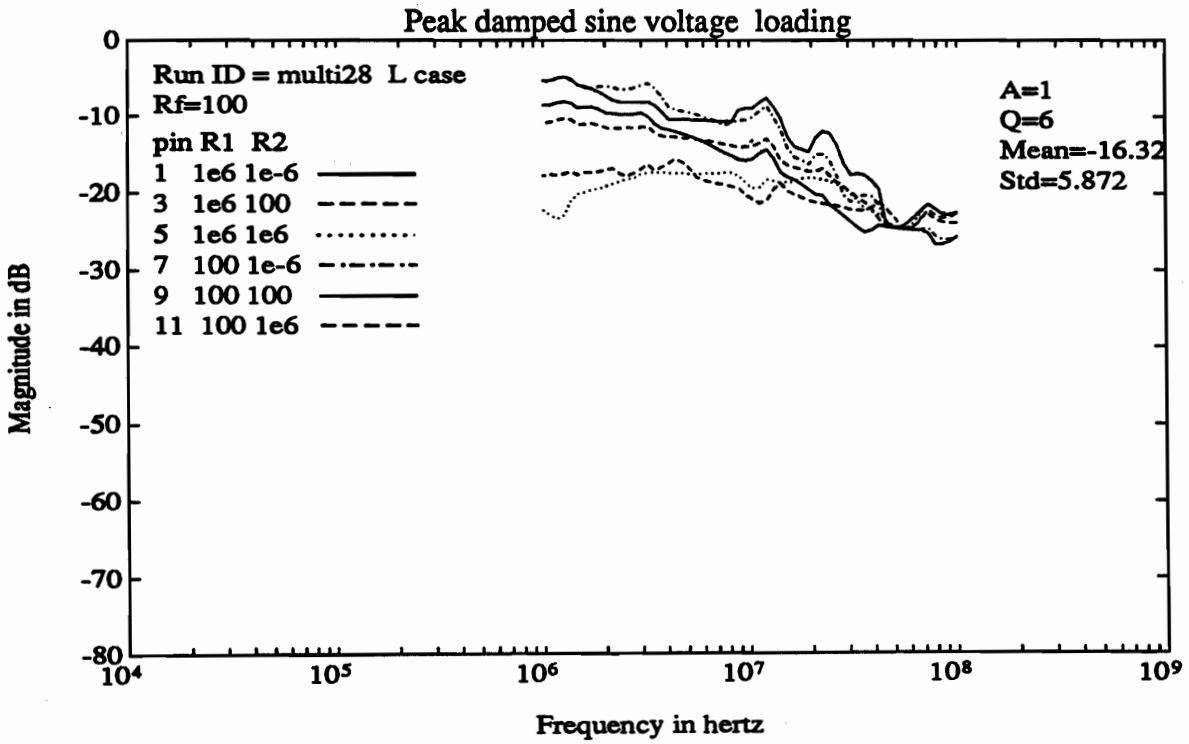

Figure 5.69 Peak damped sine loading for 12-wire cable with 100-ohm fuses.

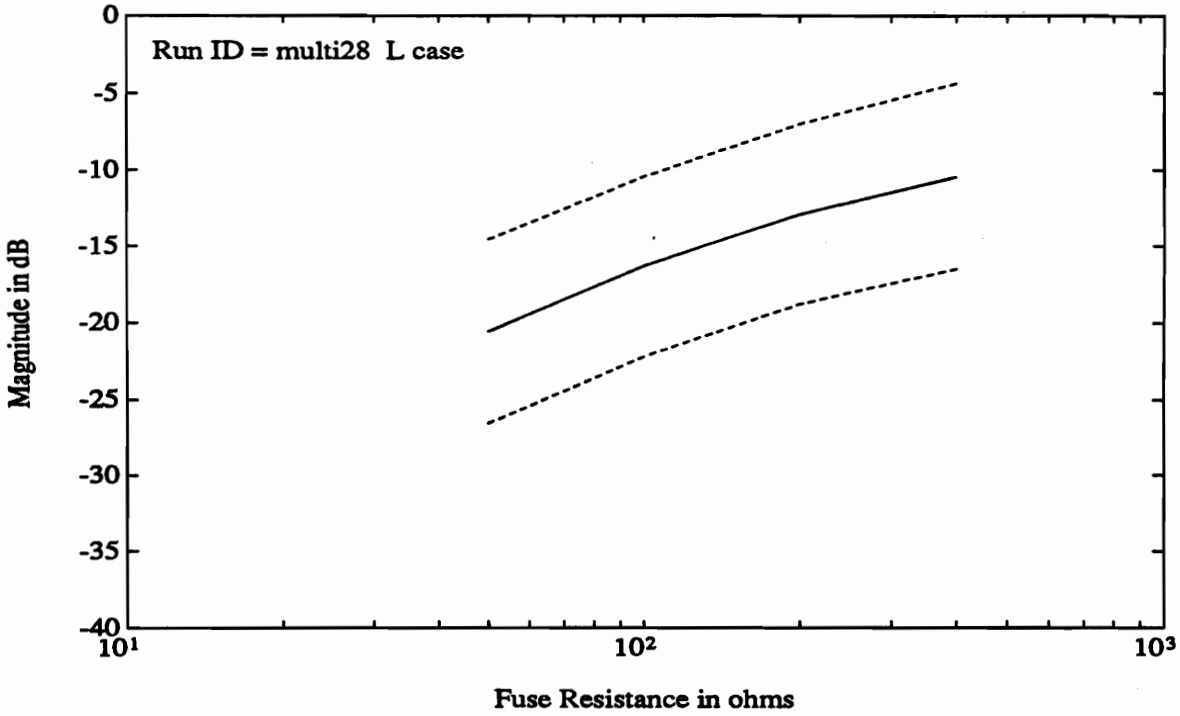

Figure 5.70 Mean and standard deviation of fuse loading for 12-wire cable.

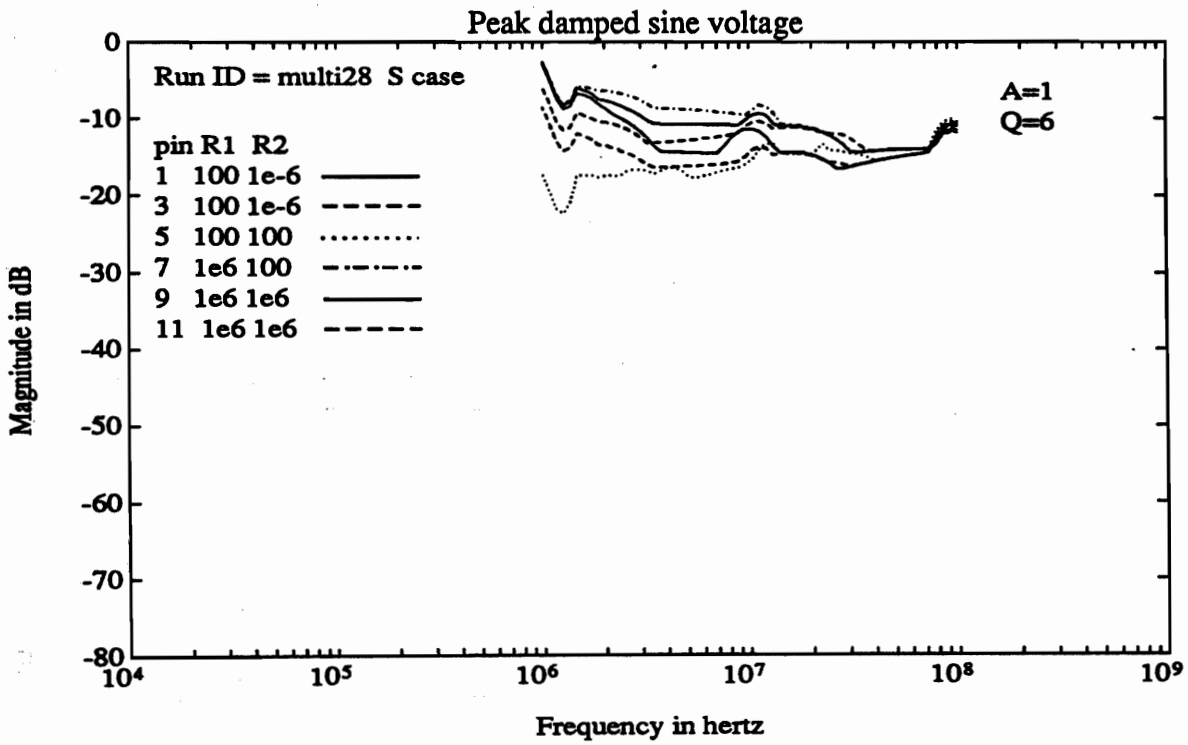

Figure 5.71 Peak damped sine voltage response for 12-wire cable with no fuses.

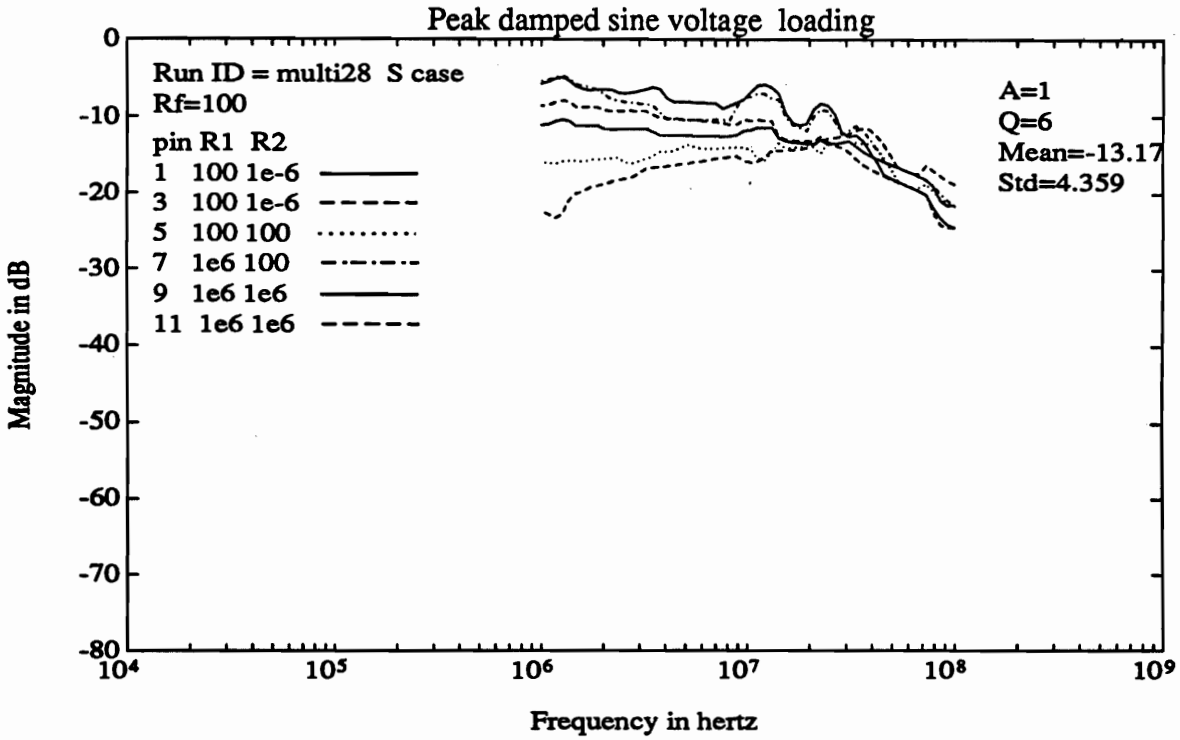

Figure 5.72 Peak damped sine loading for 12-wire cable with 100-ohm fuses.

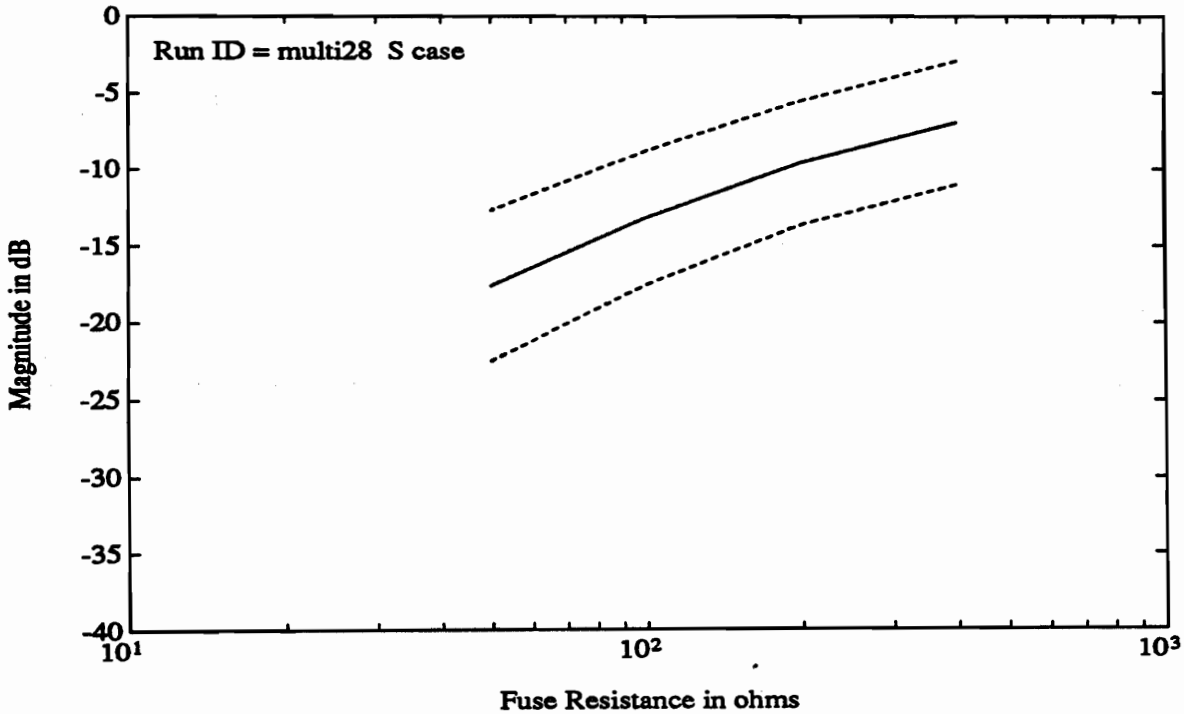

Figure 5.73 Mean and standard deviation of fuse loading for 12-wire cable.

References

1. Kevin Foreman, Paul Miller, "The μDISC Electrical Connector Circuit Wafer," *TRW Space & Defense Quest*, Winter 1991/1992.

2. Bruce D. Nordwall, "New Integrated Circuit Disc Allows No-Connection Monitoring," *Aviation Week & Space Technology*, April 20, 1992.

3. Pete Madel, "Fusible Sensors For System Level EMP Testing," Private communication about early research at TRW, Redondo Beach, CA.

4. Carl E. Baum, "Norm Detectors for Multiple Signals," Phillips Laboratory, Measurement Note 40, 8 October 1991.

5. D. F. Strawe, "Analysis of Uniform Multiwire Transmission Lines," Boeing document D2-26088-1, The Boeing Co., October 18, 1972.

Appendix A Calibrations

This appendix explains how calibration factors were obtained to account for the effects of voltage and current probes, test coaxes and adapters, and the network analyzer. Five steps (denoted as CAL0, CAL1, CAL2, CAL3, and CAL4) were needed to obtain all calibrations required in this test. Notation for the calibration details follows the general prescription in Table A-1.

Table A-1 Calibration Notation

A_{sub}	=	complex attenuation in a coax channel specified by *sub*
B_{sub}	=	$20\log A_{sub}$ (has a magnitude and a phase)
X_{sub}	=	20 log (Transfer function of the probe specified by *sub*
R_w	=	response, may be either current or voltage depending on choice of probe
M, R_n	=	measurements made with a network analyzer; have the form $20\log\left(\frac{V_{test}}{V_{ref}}\right)+\Delta_{NA}$
Δ_{NA}	=	network analyzer offset error

CAL0 Measurement of inherent network analyzer offset

The HP 3577B network analyzer, as most network analyzers, has a small fixed error of offset in amplitude and phase that can be corrected by the following calibration.

The measurement that corresponds to the setup of Figure A.1 is

$$C_o = 20\log\left(\frac{V_{test}}{V_{ref}}\right)+\Delta_{NA}$$

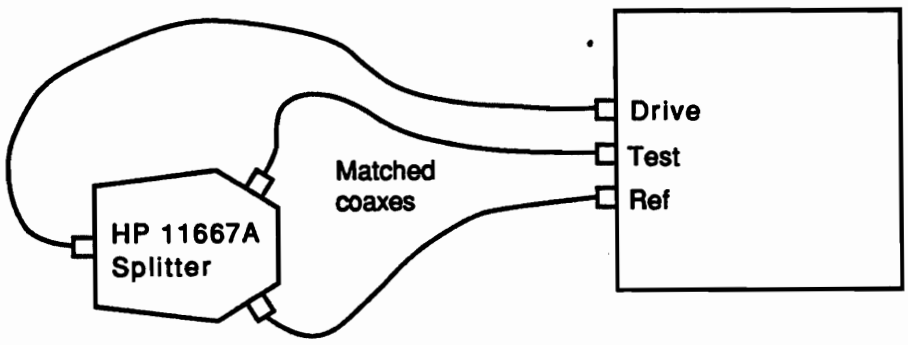

Figure A.1. Calibration for network analyzer offset.

The precision splitter and matched coaxes provide $V_{test} = V_{ref}$. (The channels can be interchanged for a check of this equality.) Thus,

$$C_o = \Delta_{NA} \tag{A.1}$$

CAL1 Calibration of Reference Channel CT-1 as a voltage sensing element

The CAL1 measurement is a step that obtains a factor to convert the voltage that is input to the reference channel connector of the network analyzer to the voltage that is induced in any loop through the drive coupler. CAL1 measures the net effect of the loop impedance, the transfer impedance of the CT-1, and the attenuation of the coaxes used in this channel during test. The calibration is made relative to the drive source and requires coax connections that must be balanced by subsequent steps.

The crucial choice in calibration run 1 is to connect the CT-1 to the *test* channel input with coax cables and fittings (as shown in Figure A.2) that are the same as will be used for connecting the CT-1 to the reference channel in the test measurements. In equation 3.3 of Section 3.0 the overall complex attenuation factor of these connections is denoted by A_{ref} and this attenuation will be measured here. The function of the calibration fixture is to carry the outer conductor of the test-channel coax around the outside of the 91550-2. Hence, the 91550-2 probe used as a coupler induces the same voltage, V_{test}, on the center conductor of the coax shown in the test channel and the small loop with 100-ohm load on which the CT-1 is installed. Thus, the equations that apply to the setup in Figure A.2 are

$$\begin{aligned} I_{loop} &= \frac{V_{loop}}{Z_{loop}} \\ V_{CT-1} &= Z'_{CT-1} I_{loop} = \frac{Z'_{CT-1}}{Z_{loop}} V_{loop} \\ V_{test} &= A_{ref} V_{CT-1} \end{aligned} \tag{A.2}$$

Here A_{ref} is the product of the attenuation in coaxes #20 and #30 and the required feed through fittings. The coax numbers shown in these figures are the identification numbers of the coaxes used in this test program.

The reference channel in CAL1 is a direct measurement of the coupler drive voltage. More precisely, the reference channel measures one half of the coupler drive voltage V_{loop} as attenuated by a relatively long pair of calibration reference coaxes. We denote the attenuation of the channel by A_{CRL} (cal-ref-long). Thus,

$$V_{ref} = \tfrac{1}{2} V_{loop} A_{CRL} \tag{A.3}$$

In our setup, the cal-ref-long coaxes were #26 and #15. Equations A.2 and A.3 yield

$$\frac{V_{test}}{V_{ref}} = \frac{Z'_{CT-1}}{Z_{loop}} \frac{A_{ref}}{\left(\frac{1}{2} A_{CRL}\right)} \tag{A.4}$$

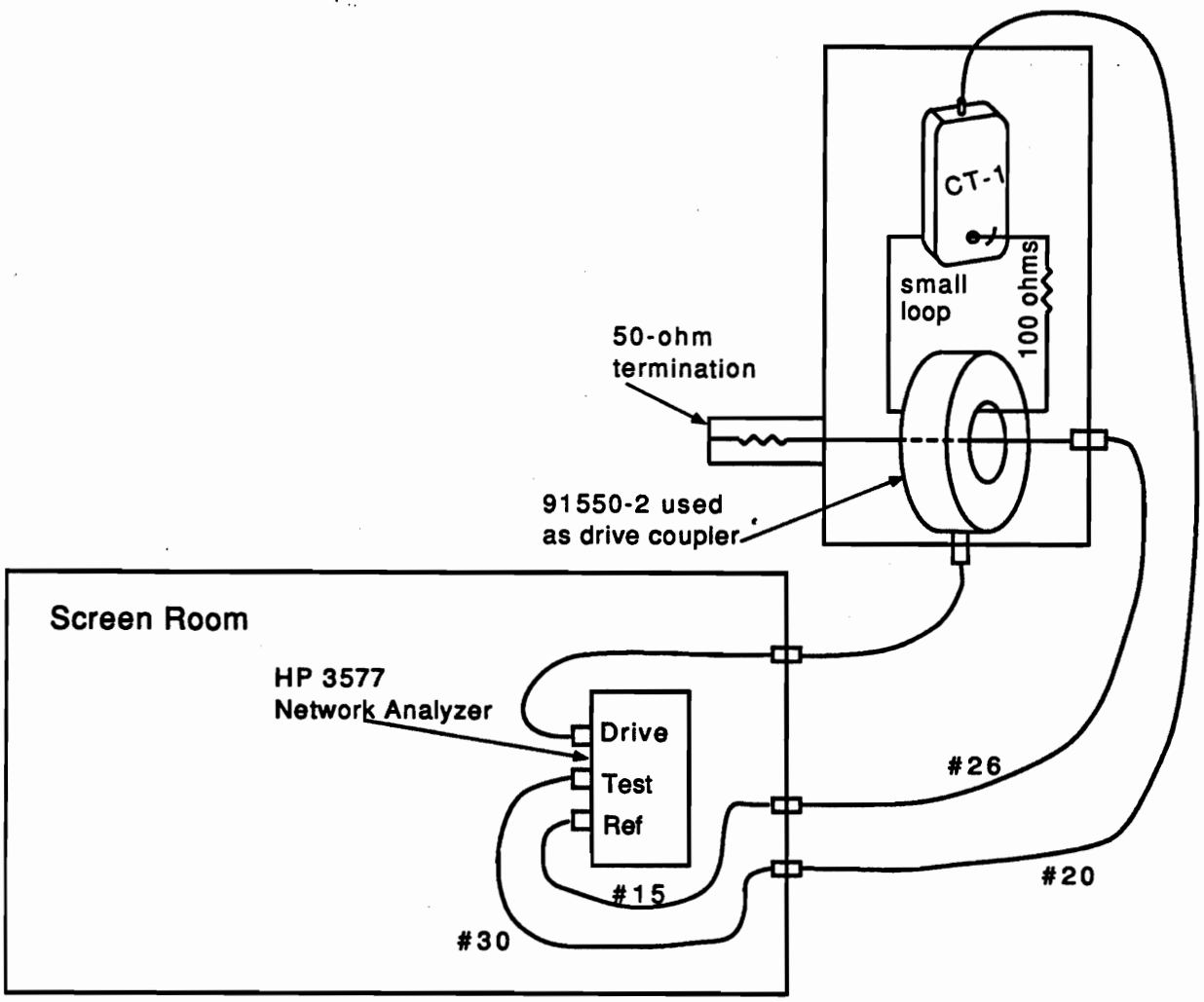

Figure A.2. Calibration of reference channel measurement of induced drive voltage.

Let $20\log\left(Z^{i}_{CT-1} / Z_{loop}\right) = X_d$. Then in dB the raw CAL1 measurement is

$$R_1 = X_d + B_{ref} - \left(B_{CRL} - 6\right) + \Delta_{NA}$$

where $B_{CRL} = 20\log A_{CRL}$. In this measurement acquisition, C_o is used as a calibration function (i.e., C_o is subtracted in the dB domain from R_1) and a mathematical correction is inserted for the 6-dB voltage division in the reference channel for the fact that half of the drive voltage is dropped in the 50-ohm load installed on the calibration fixture. Thus, the recorded CAL1 measurement becomes

$$C_1 = R_1 - 6 - \Delta_{NA} = R_1 - 6 - C_o = X_d + B_{ref} - B_{CRL} \qquad \text{(A.5)}$$

CAL2 Voltage probe calibration

This calibration measures a correction factor for the probe and the coaxial cables and adapters used in the test measurements. The measurement is made relative to the source by use of a splitter and reference channel coaxes that are chosen to be the same as in CAL1. Thus, when the net difference

calibration is constructed, it is directly applicable to a test measurement.

The crucial aspects of connecting the voltage probe for calibration are to

(a) connect the balun to the network analyzer test channel with the same coax and adapters to be used in test measurements

(b) use the same cal-ref-long coaxes from the splitter to the reference channel of the network analyzer as used for the reference channel of CAL1.

The coax numbers as used in this test are indicated in Figure A.3. Also, two extra type-N barrel fittings were used in the reference channel as shown to balance the delay in the probe adapter that is attached to the test channel output of the splitter. The Miletus probe is an active differential probe with high-impedance inputs (nominally 1 megohm paralleled by 3 pF) at both tips.

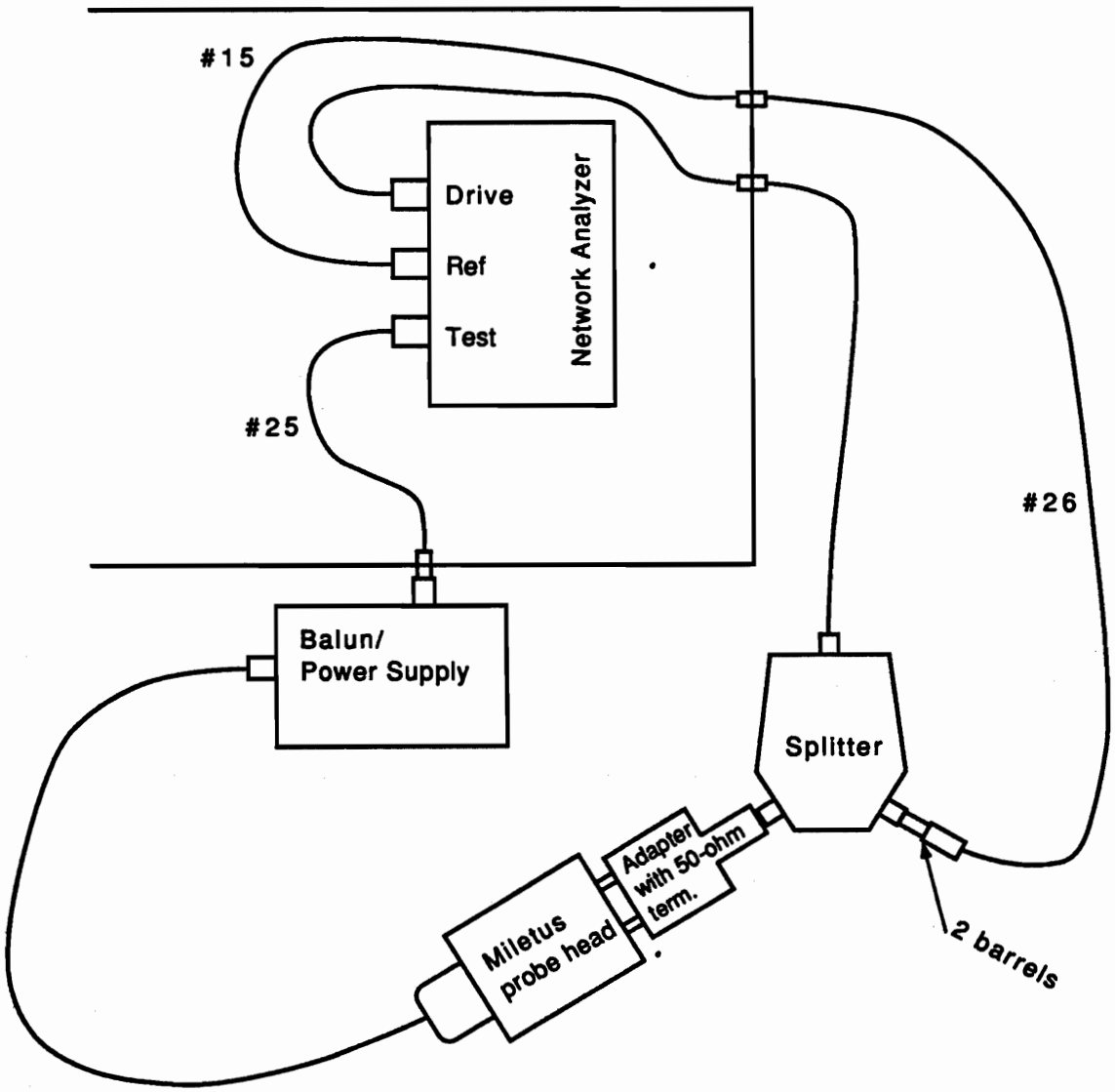

Figure A.3. Setup for calibration of load voltage measurement with Miletus probe.

For the setup of Figure A.3

$$V_{test} = G_P A_{VP} V_s$$
$$V_{ref} = A_{CRL} V_s \qquad \text{(A.6)}$$

where G_P is the gain of the Miletus probe (i.e., represents the transfer function of this sensor in the general terminology of equation 3.2), A_{VP} is the attenuation of the coax and feed through used to connect the output of the voltage probe to the network analyzer, and V_s is the voltage out of the splitter. From this pair of equations

$$\frac{V_{test}}{V_{ref}} = \frac{G_P A_{VP}}{A_{CRL}} \qquad \text{(A.7)}$$

In dB the raw measurement is given by

$$R_2 = 20\log G_P + 20\log A_{VP} - 20\log A_{CRL} + \Delta_{NA}$$
$$= X_P + B_{VP} - B_{CRL} + \Delta_{NA}$$

where $X_P = 20\log G_P$ and $B_{VP} = 20\log A_{VP}$. For this measurement C_1 is used as the calibration function. The recorded calibration is then

$$C_2 = R_2 - C_1 = X_P + B_{VP} - \left(X_d + B_{ref}\right) + \Delta_{NA} \qquad \text{(A.8)}$$

This voltage probe calibration has the desired form of equation 3.8 and is used for voltage measurements.

CAL3 Current probe calibration

This calibration step is used to measure an overall factor for the current probe and its associated coaxial cabling. The reference channel coaxes differ from those used in the step labeled CAL1. Therefore, an addition step, CAL4, is required to determine the net calibration factor for current measurements in this test program.

Two configurations were calibrated to allow use of different coax connections from the CT-2 measurement probe to the test channel. The configuration shown in Figure A.4 is used for measurements within the load box. For measurements in a breakout box, the connection to coax #11 was extended with another coax, labeled #31, and then a short RG174 was used to connect from #31 to the CT-2 probe. In both cases the length of RG174 was less than 8 inches. The sequence of measurements and processing described in CAL3 and CAL4 was repeated for the second set of current probe connecting coaxes.

A critical point of CAL3 is to use short (essentially as short as possible, about 2 feet total in this calibration) coaxes from the probe calibration fixture back to the reference channel of the network analyzer. The attenuation in this reference channel set is denoted as A_{CRS} (cal-ref-short). The short coax is required to eliminate reflection mismatch from the calibration fixture source to the network analyzer load within the 150-MHz band of the measurements.

Figure A.4 shows the setup for CAL3.

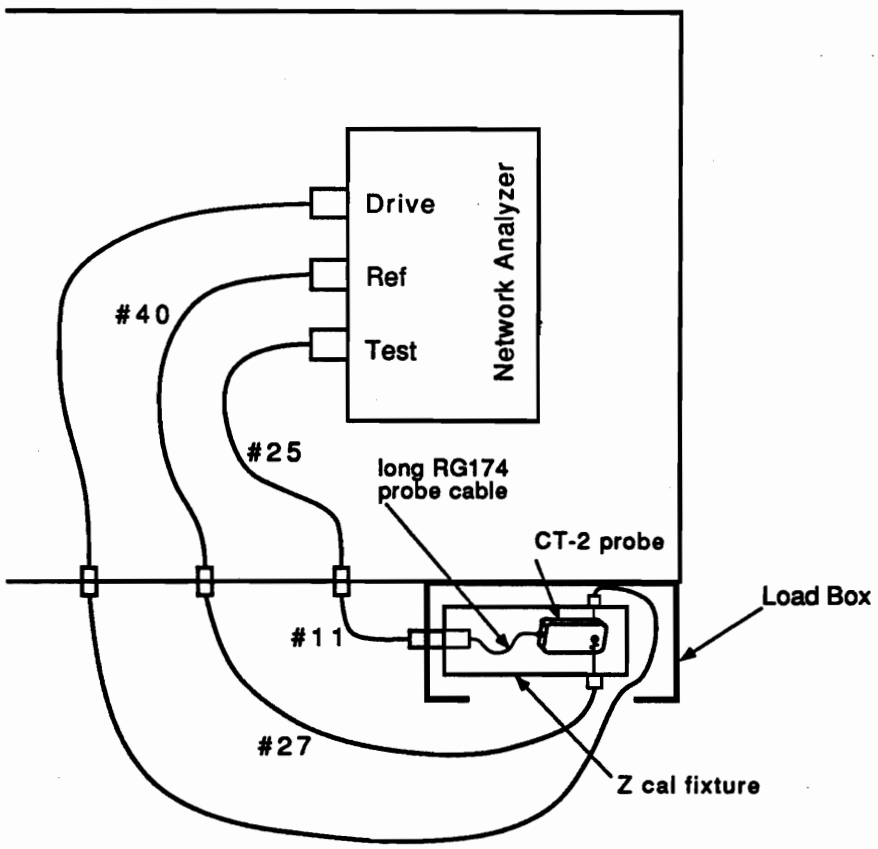

Figure A.4. Setup for calibration of current probe with short reference channel coaxes.

In this setup

$$V_{test} = Z^{t}_{CT-2}\left(\frac{V_{dr}}{50}\right)A_{CP} \qquad \text{(A.9)}$$

where the transfer function of the current probe is given by the conventional transfer impedance Z^{t}_{CT-2} and A_{CP} represents the attenuation in the test channel for the particular current probe hookup (shown as the long RG174 coax plus coaxes #11 and #25 and required feedthrough fittings in Figure A.4). The reference channel equation for this setup is

$$V_{ref} = V_{dr}A_{CRS} \qquad \text{(A.10)}$$

The ratio of equation A.9 to equation A.10 yields

$$\frac{V_{test}}{V_{ref}} = \frac{Z^{t}_{CT-2}}{50}\frac{A_{CP}}{A_{CRS}} \qquad \text{(A.11)}$$

The raw calibration measurement in dB is then

$$R_3 = 20\log Z^{t}_{CT-2} - 33.9794 + B_{CP} - B_{CRS} + \Delta_{NA}$$

where $B_{CP} = 20\log A_{CP}$ and $B_{CRS} = 20\log A_{CRS}$.

The recorded calibration for the current probe uses C_1 as a calibration function for this third calibration run denoted as C_3 and adds the constant $20\log 50 = 33.9794$ numerically to give

$$\begin{aligned} C_3 &= R_3 + 33.9794 - C_1 \\ &= X_{CT-2} + B_{CP} - B_{CRS} - \left(X_d + B_{ref} - B_{CRL}\right) + \Delta_{NA} \\ &= X_{CT-2} + B_{CP} - \left(X_d + B_{ref}\right) + \left(B_{CRL} - B_{CRS}\right) + \Delta_{NA} \end{aligned} \tag{20}$$

CAL4 Calibration for different lengths of calibration reference (long vs. short)

This calibration of the difference in two coaxial paths used only in calibration reference channels is necessary because of requirements of the current probe calibration in CAL3 and physical length constraints in the test setup. It is needed only for current response measurements.

The setup is connected as shown in Figure A.5. In this case

$$\frac{V_{test}}{V_{ref}} = \frac{A_{CRL}}{A_{CRS}}$$

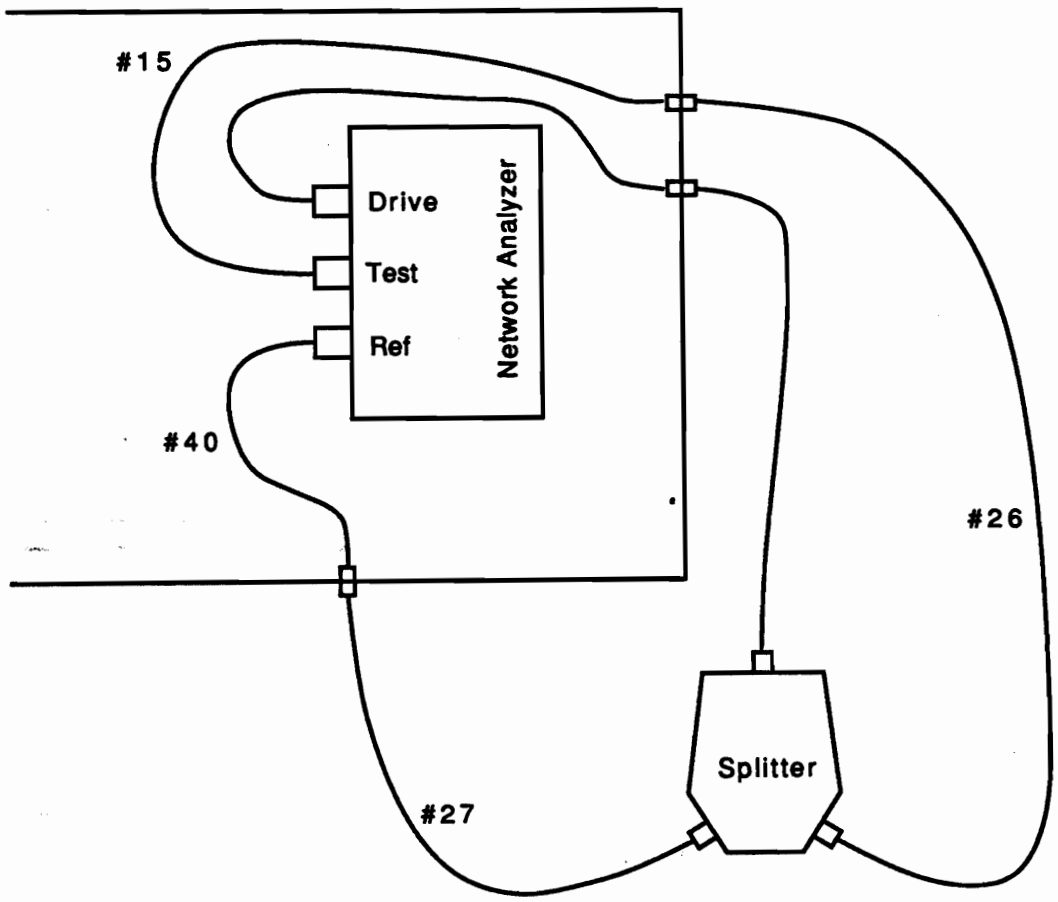

Figure A.5. Setup for calibration of attenuation difference in short and long coax paths used for cal reference channel.

The raw measurement is

$$R_4 = B_{CRL} - B_{CRS} + \Delta_{NA}$$

The recorded measurement uses CAL0 as a calibration function to obtain

$$C_4 = R_4 - C_o = B_{CRL} - B_{CRS} \tag{A.13}$$

The last step in constructing the calibration function for a current probe measurement is to compute (i.e., at each frequency to subtract the amplitudes in dB and the phase angles)

$$\begin{aligned} C_5 &= C_3 - C_4 \\ &= X_{CT-2} + B_{CP} - \left(X_d + B_{ref}\right) + \Delta_{NA} \end{aligned} \tag{A.14}$$